Measuring Ionic Concentrations in Sweat

using cyclic voltammetry

T. S. Kolukisaoglu

Technische Universiteit Delft

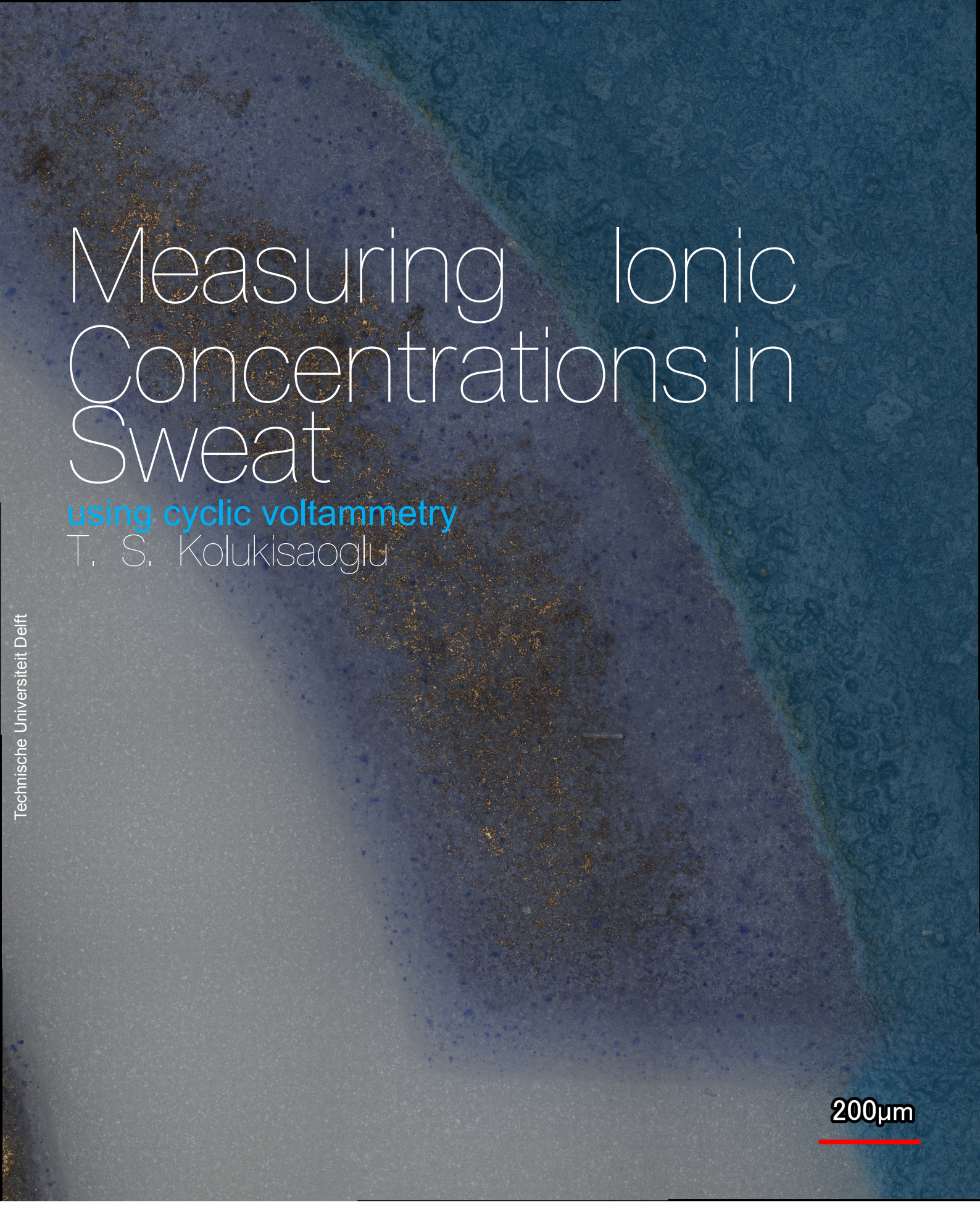

TU Delft

Measuring Ionic Concentrations in Sweat

using cyclic voltammetry

by

Tom S. Kolukisaoglu

to obtain the degree of Master of Science
at the Delft University of Technology,
to be defended publicly on Monday August 22, 2022 at 10:30 AM.

Student number:	5280745	
Project duration:	December 1 2021 – August 22 2022	
Thesis committee:	Dr. ir. A. Bossche,	TU Delft, supervisor
	Prof. P. J. French,	TU Delft
	Dr. ir. T. L. M. da Costa,	TU Delft
	Ing. J. Bastemeijer,	TU Delft
	Ir. A. S. M. Steijlen,	TU Delft

An electronic version of this thesis is available at http://repository.tudelft.nl/.

Abstract

This report presents a proof-of-concept for a sensor measuring the ionic concentrations in sweat using cyclic voltammetry. Development is focused on feasibility of the sensor. Theoretical evaluations of voltammetry as a working principle and its physical and electrochemical foundations are guiding principles of the design. The sensor is then implemented using commercial components. Experiments show that the sensor has good sensitivity and linearity for single ions in the physiological range. For the measurement of multiple ions the voltammogram is characterized in-depth. A matrix of different ionic fluids with multiple ions is prepared and two independent parameters for the concentration of two ions (sodium and potassium) are found, proving the concept of the sensor for more complex solutions. The usability of the sensor is verified using a sweat sample. Different influencing factors are researched and their impact characterized. Varying electrode materials are evaluated considering durability and sensitivity. Conclusions are drawn and an outlook for future research on this type of sensor is given. The concept of the sensor is proven to work within certain limitations.

Preface

Since the beginning of my academical and professional career I have been interested in biomedical and medical technology applications. My previous work has shown me that this is a diverse field with nearly endless opportunities. Working on a project that improves health and healthcare induces a uniquely satisfying feeling.

While the project took a lot of sweat to complete (pun intended) the exploratory aspect of it reinvigorated my scientific urge that can so often get lost in the small details of technical discussions. Thus my first thanks goes to my supervisors Andre Bossche, Annemarijn Steijlen and Jeroen Bastemeijer for giving me the freedom to explore the topic with sometimes unusual methods. I would also like to thank them for their guidance with the many questions and discussions that came up during this process. These discussions often extended into our weekly meetings and the input I received from them and other members of the group was invaluable. Thus I would like to extend my gratitude also to Paddy French, Zybrand van der Zwaag, Pim, Zakaria and Adam.

Samhitha, Öykü and Rocco thank you for your constant friendship and companionship. Studying for a masters degree at this university can be rough and 2020 was a rougher year yet to start it - you made this town feel like home. I look forward to many more dinners yet to come.

Lastly to my family, Mum, Dad, Niklas, Nathalie and Tori I cannot express my gratitude in words alone. Thank you for being there for me, always.

Dear reader, I hope you enjoy reading this thesis as much as I did producing it.

Tom S. Kolukisaoglu
Delft, July 2022

Contents

List of Figures

List of Tables

1 Introduction

Sweating is a function unique to mammals and crucial to the evolutionary success of humans. It has been hypothesized that our superior ability for thermoregulation via sweating was developed when humans emigrated from forest biomes into warmer dry-lands. Thermoregulatory sweating allowed humans to run longer distances. Our higher endurance allowed for both more successful hunting and escape from predators. The ability to sweat additionally allowed humans to inhabit different climates diversifying their chances for survival [1].

In the modern day and age sweating is, while still a necessary feature for survival, no longer an important evolutionary edge we exploit. Moreover sweating in daily situations is regularly associated with anxiety, nervousness and insecurity. We often take measures to prevent sweating and hide the traces of sweat. New clothing is developed breathable which indicates we still recognize its importance.

In sports however sweating retains its importance. Athletes in sports that include extensive cardiovascular activity experience sweating as our ancestors did, benefiting from the thermoregulatory effect. Given the degree of optimization that is being reached in many sports ever more indicators for improvement are being explored. Sweat is one of the aspects being considered. Between the sweat rate and the composition of sweat a wide range of information on the status of an athlete can be extracted from it.

A few key technological developments allow for extraction of useful information from sweat. Firstly miniaturization of electronics in the past decades has allowed for smaller sensors. Where previously bulky tabletop devices were necessary for any measurements of concentrations in aqueous solutions nowadays many of these measurements can be performed by wearable devices. Secondly, these wearable devices have sophisticated collection mechanisms that are mostly based on micro-manufacturing techniques. This smart collections circumvents the issues posed by more arduous conventional techniques such as patches or whole body washdown. Lastly our deeper understanding of the underlying physiological mechanisms has allowed us to tune our sensors to the adequate substances and relate changes in concentration more meaningfully to fatigue.

Sweat measurement is complex. The proof-of-concept presented within this thesis will demonstrate an as of yet untested approach using cyclic voltammetry. This technique aims to elucidate information on the concentration of all ions and charged particles within the solution in a single voltage sweep. While the potential advantages of such a measurement are evident - a complete essay in a single sweep, only simple material required and potential re-usability of electrodes - some major challenges stand in the way of implementation. These will be tackled in the course of the project

This thesis consists of three major parts. The first part is literature research. In these chapters (ch. 2-4) the pertinent theoretical foundation is discussed including physiology of sweat, state of the art sweat measurement and basics of voltammetry. Subsequently the theoretical foundation is translated into a sensor design and implementation (ch. 5-6) before experiments are performed, analysed, conclusions on the sensor are drawn and an outlook for future research is given (ch. 7-8).

2

Physiological principles of sweat secretion

This chapter will explore the physiological mechanisms underlying sweat secretion as they pertain to the measurement of sweat. The focus will be put on the quantifiable factors such as the concentrations of the species, their temporal and inter-individual variations as well as their relation to other physiological fluids. This summary should help the reader understand what insights can be gathered from sweat analysis.

2.1. Sweat as a physiological fluid

The healthy human body consists of 50-60 % water [2]. This water is evidently not found in pure form but rather as physiological fluids. These fluids range from blood needed for the circulation of nutrients and oxygen, bile required for digestion in the small intestine to tears secreted to clean and lubricate the eye. One of these physiological fluids is sweat. Sweat is a generally clear, hypotonic aqueous solution [3]. It is often used as a marker for fluid loss and thermoregulatory function of the body. Sweat is secreted onto the skin via sweat glands. Once secreted the sweat evaporates drawing the required energy from the heat of the body. This evaporation leads to a cooling of the body [4]. The amount of sweat that is secreted depends on the region of the body, the physical status of the individual, gender, age, ambient temperature and a variety of other factors. Generally full body sweating rate ranges from $0.5 - 3.0 \frac{l}{h}$ [3].

Sweat itself is derived from interstitial fluid which in turn is a filtration of blood plasma [3]. This indicates a relationship between sweat and blood concentrations of species such as electrolytes or metabolites. The nature of this relationship is still the subject of debate in literature [5], [6]. Notwithstanding this debate on the correlation between sweat and blood concentrations, sweat is gaining in importance as a physiological fluid independently, which is accentuated by the growing sensing capabilities that allow for the detection of species with lower concentration such as glucose, lactate or urea [7]. Measurement of sweat is preferred in certain scenarios over blood since it can be sampled non-invasively and monitored continuously.

2.2. Sweat secretion

To understand sweat secretion one has to acknowledge that there is different types of sweat glands and resulting sweat compositions [8]. In this thesis the focus is put on eccrine sweat glands. These glands are mainly present in hairy regions of the body excluding the pubic and perianal region, eyelids, aerola and auxilliary fossa [9] where apoeccrine glands dominate. Eccrine sweat glands are mainly responsible for thermoregulation and secrete the highest volume of sweat leading to a loss of electrolytes [9], [3], [8]. The focus is put on eccrine sweat since it can possibly serve as the indicator for acute fatigue and fluid / electrolyte loss in athletes - the aim of this research. Fatigue for the purposes of this thesis is defined in terms of a sports-context. Fatigue is an acute condition marked by a lack of energy and extreme tiredness [10]. Fatigue leads to the inability of continuing physical activity and

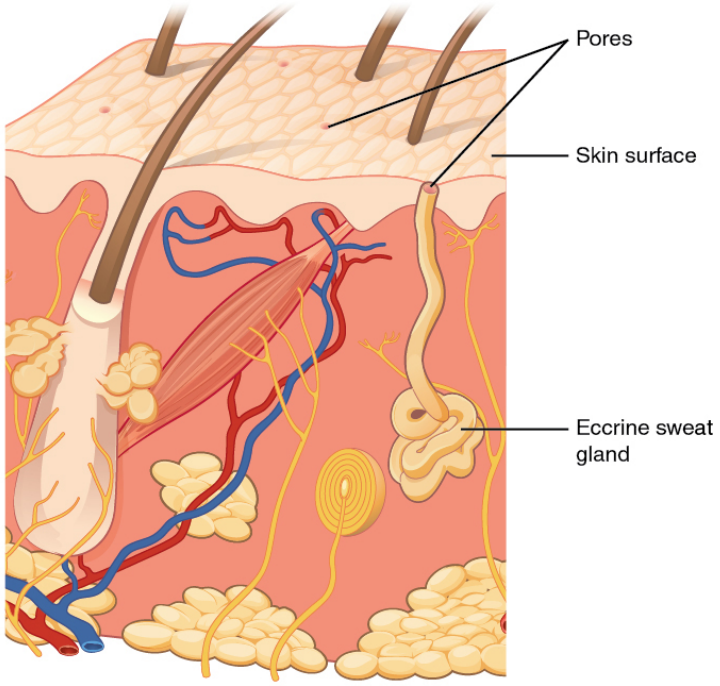

Figure 2.1: Eccrine sweat gland with coil and duct/pore in a cross section of skin [11], reproduced under creative commons license 4.0

increases the chance of injury. The anatomy of the eccrine sweat gland can be seen in fig. 2.1 [11].

Sweat is a hypotonic filtration of blood as initially hypothesized by [12] later supported by [13] and [14] and generally accepted in literature today [3], [15]. This filtration is also called primary sweat. It is filtrated into the sweat gland. The primary sweat then flows through the duct onto the skin surface. The main function of the duct appears to be resorption of chloride and sodium [13], [8]. The body utilizes this resorption to avoid excessive electrolyte loss. The underlying mechanisms determining the final concentrations of certain species are complex and deeply involved with the physiological and anatomical mechanisms [3]. Taking the concentration of sweat sodium as an example influencing factors on the secretion include: sweat rate [16], [17], heat acclimatisation [18], dietary salt intake [19] and many more. This variation leads to physiological tests often being inconclusive or marred with inaccuracies [3]. The secretion mechanisms and their variations call for a sensor with reasonable accuracy that is able to provide measurement results with high stability over a longer period of time. A voltammetric sensor might provide such stability.

2.3. Sweat composition

Sweat is a aqueous fluid containing 99 % water [15], [3]. The remaining 1 % are made up of different classes of solutes:

- electrolytes
- micronutrients
- metabolites
- cytokines
- cortisol

All references below relate to the changes in concentration during active sweating (due to exercise). Note that some of these changes are significantly different when observing passive sweating due to either heat or medication.

2.3.1. Electrolytes

Electrolytes are the most abundant species in sweat. The main electrolytes in sweat are :

- sodium (Na^+)
- chloride (Cl^-)
- potassium (K^+)

The main role of these electrolytes is to facilitate the secretion of the sweat by providing the necessary osmotic pressure. While the blood concentrations of both chloride and sodium are considerably higher than the sweat concentration (owing to the resorption of these electrolytes in the duct) this does not hold true for potassium. For typical concentrations of all species refer to table A.1. The relatively high concentrations of these electrolytes (in the $\frac{mmol}{l}$ range) allows for detection with differing techniques (see chapter 3 'Technology state of the art'). These ions have simple one electron reduction / oxidation reactions that can be elucidated via voltammetry.
Electrolytes and electrolyte loss are important to the health and performance of athletes. A homeostatic balance of electrolytes is important for the efficiency of transport processes in the body. [20] showed that supplementing athletes with electrolytes they lost during exercise increased their endurance significantly. If electrolyte loss could be monitored in real time the re-intake of electrolytes could be controlled better and endurance of athletes improved. [20] additionally showed that blood-lactate-levels, a common marker for fatigue, were reduced when electrolytes were supplemented. It is evident that electrolyte loss is an important marker for fatigue.

2.3.2. Micronutrients

Micronutrients include organic and inorganic species that the body requires, cannot produce itself and does not use mainly as an electrolyte. These include:

- iron (protein bound)
- copper (protein bound)
- zinc (protein bound)
- magnesium (Mg^{2+})
- calcium (Ca^{2+})

Little research has been performed on the secretion and concentration of micronutrients in sweat. The introduction of radioisotopes in blood suggests only a very limited transport and secretion in sweat of these components not exceeding 5 % of the blood concentration [21]. This is compounded by many micronutrients being protein bound and thus not being readily filtrated into the sweat gland [22]. Altogether while crucial to the overall health of the body it is not expected that measuring sweat micronutrient content is an efficient monitoring technique for fatigue. As such, few devices exist to monitor micronutrients in sweat. This deficiency is entrenched by micronutrients appearing in sweat only in $\frac{\mu mol}{l}$ concentration range, thus making measurement more difficult for commercialized devices and requiring specific techniques.

2.3.3. Metabolites

Metabolites, typically small molecules, are the byproduct of metabolic reactions such as cellular breathing, digestion etc. They are usually end-products that are of no further use to the body. The main metabolites contained in sweat are:

- glucose ($C_6H_{12}O_6$)
- lactate ($C_3H_6O_3$)
- ammonia (NH_3)
- urea (CH_4N_2O)
- bicarbonate (HCO_3^-)
- amino acids (variety)
- ethanol (C_2H_5OH)

Metabolites are of specific interest when observing fatigue in athletes or monitoring the health status of patients. For example lactate in sweat might be a marker for muscle fatigue while a high sweat glucose level might indicate intake of insulin to a diabetic patient.
While the relation between the levels in blood and sweat of the previously discussed substances was relatively straightforward the picture is more complex when observing metabolites.
Glucose transports from the systemic circuit into sweat via a complicated mass transport model. The concentration is highly dependent on the sweat rate with a positive correlation [23].
Lactate in blood is a ”byproduct of glycolysis and accumulates when there is either an absolute or relative lack of oxygen” [24, p. 1]. As such it can be used as a marker for muscle fatigue (since muscles start anaerobic function once all the stored glycogen and oxygen are used up). However the correlation between blood and sweat concentrations is low [24], [6]. It is expected that lactate in sweat is a poor indicator for muscle fatigue. Current research suggests that the bulk of lactate in sweat is not filtrated in via the blood but rather secreted by the sweat gland itself. In this course [25] reported a shift in the sweat lactate curves with a faster peak and faster resorption if the athlete is fatigued. While no consensus yet exists whether sweat lactate is a usable marker for fatigue it remains, for the time being, an important molecule to consider in any sports-focused sweat-sensing application.
Ammonia is a waste-product in the amino acid metabolism. While most of it is metabolised to urea some of it is secreted directly via sweat and urine [15]. Ammonia might thus be a good marker for fatigue although again the relationship between blood and sweat concentration is contested [6]. It is however well established that blood is the source of sweat ammonia [26] and even given a complex relationship using it as a biomarker in sweat seems feasible. Given the higher concentration in sweat [3] and the polarity of the molecule many detection techniques including voltammetry are feasible.
Urea is the final product for many metabolic processes and is used by the human body to rid itself of nitrogen. Hyperuremic conditions have been well established to be damaging to muscles among other side effects [15]. Urea sweat levels were found to be elevated during exercise and directly linked to protein catabolism [27]. Its relatively high sweat concentration allows for measurement with differing techniques.
Bicarbonate (chemically: hydrogencarbonate) is a main actor in keeping the bodies acid-base balance. Bicarbonate in sweat might thus suggest an imbalance caused by stress or fatigue. Additionally bicarbonate has been identified to be one of the main transport methods for carbondioxide in blood. Thus higher concentrations in sweat might indicate an increase in cellular breathing and muscle activity overall. Little research exists on the mechanisms of transport. Measurement with voltammetry appears feasible given the ionic nature of the compound.
Different amino acids are present in sweat. Their concentration is minuscule and the transport mechanism is little researched.
Ethanol can be excreted via sweat. Given that ethanol is almost exclusively taken in via alcoholic drinks, methods already exist for non-invasive monitoring (breathalyzer) and this research is aimed at observing the health status of athletes no further focus is put on sweat ethanol.

2.3.4. Cytokines and cortisol

Cytokines are a group of substances that the body secretes as a reaction to foreign bodies. They can indicate inflammation. While technically of interest to the issue at hand the concentration is too low to be measured reliably without very specialized procedures.

Cortisol, produced by the adrenal cortex, is the hormone mainly responsible for converting proteins to glucose [15]. Cortisol in sweat might thus indicate a higher fatigue in muscles given it is likely exchanged from the blood content [3]. However detection is specialized, concentrations are low and thus of little relevance as an easily accessible biomarker in sweat measurement.

Sweat as a physiological fluid has potential to supplement other measurements to ascertain the physical status of an athlete. Of the measured species the electrolytes and some of the metabolites including ammonia, lactate, urea and bicarbonate appear to best reflect fatigue. Measurement of these ions or polar molecules via voltammetry might open a thusfar unexplored avenue of broad yet accurate analysis. Challenges in the measurement include the low concentration of some of these substances and limitations imposed by water as a carrying medium.

3

Technology state of the art

In this chapter the current state of the art of sweat analysis will be explored. The focus is put on wearable and miniaturized platforms. The analysis aims to explore the advantages and pitfalls of the different measurement principles and learn lessons to be applied in the device to be developed.

3.1. Collection of sweat samples

Before sweat can be analyzed it needs to be collected. A collection system for sweat should be non-intrusive, not affect the concentrations and ideally allow for real time monitoring.
The most accurate technique for the collection of sweat is whole body washdown. It allows for the whole body sweat to be collected. However it is an arduous technique requiring laboratory equipment and not allowing for temporal resolution. Similarly the measurement of nude body mass is often employed to measure sweat rate. Both are discarded for the project at hand given their lacking applicability to real time measurements. They do however form a reference point that can help determine the accuracy of the collection technique [3], [28].
Classically sweat is collected in an absorbent patch. The patch is applied to the skin and soaks up the sweat. To make sure that the result is not skewed by residual salt and other substances it is necessary to clean the skin thoroughly before the patch is applied [3]. Typically this cleaning is done using alcohol, followed by pure water and then drying it of. Patches only allow for a relatively low temporal resolution since the patch has to soak before the sweat might be analysed [3]. To analyse the sweat from an absorbant patch it is necessary to centrifuge it at a low temperature so the fluid can be separated from the patch again. Neither this process, nor cold temperature storage appear to affect the composition of the sweat significantly [29]. Similarly filter paper can be used to collect the sweat. Studies have shown a reasonable compliance between sweat rate and electrolyte content when comparing these localized techniques to the whole body washdown [28], [30]. It should be however noted that the intra-process-variability is high. Sweat pouches as were often used in the 20th century have been found to significantly alter the local sweat rate and are thus no longer in use for most academical purposes [28].
Similarly to absorbent patches [31] used absorbent sportswear with a biologically inspired fractal structure to capture the sweat. The usage of the sportswear has the advantage of not altering the local sweat rate significantly. This is due to the lower flow resistance of the material relative to an absorbant patch. The fractal geometry was used to avoid an overflow of the sensor.
Researchers at Lausanne [32] developed a passive micro-pump for the collection of sweat. The pump slows the flow of sweat to allow for reliable real time measurements. Their application demonstrates the capabilities of using MEMS fabrication techniques for the collection of sweat. Other applications utilize this technique [33].
The final technique for collection of sweat are microfluidics platforms [34], [35], [36], [37]. Most are fabricated as layers of laser cut polymers while some utilize photoresist as their material. [36] presents a platform that can collects samples in separate reservoirs for later analysis. [37] shows a platform tailored to real time measurements. Overall the diversity and possibility for adaption and iteration make microfluidics platforms the most versatile choice. They are also useful in particular when planning to perform real time measurements. Challenges of microfluidics platforms include flow-control of the sen-

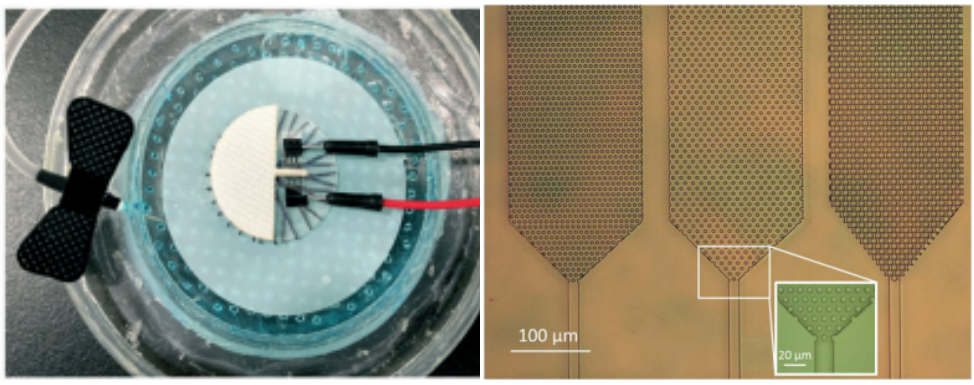

Figure 3.1: Different state of the art sweat collection mechanisms, left: fractal textiles emulating sweat patches [31], right: passive micro-pumps [32]

sor (both to allow for accurate measurements and prevent overflow), channel geometry influencing flow and material choices for ease of manufacturing and durability. Using these platforms with voltammetry can be tricky as shown by [38]. Care needs to be taken to ensure that the flow-rate is set in such a way as to ensure the response of the sensor is not limited by convection. If these challenges can be addressed, a microfluidics platform appears to be the prime candidate for sweat collection in a wearable device.

3.2. Preparation of sweat samples

While most real time measurements such as the one planned within this project, cannot use preparation methods a short overview of the possibilities is given here. This should aid to show some of the issues that are anticipated in using voltammetry.
Any preparation of sweat samples is necessarily a chemical alteration of the fluid. The most common addition are enzymes to measure certain cytokines or micronutrients with high accuracy or buffers to increase the conductivity of the sweat. This can allow for acceleration in the measurement for certain principles. Additionally a buffer can be introduces to change the pH value of the sweat and thus move the voltage window which can be applied without electrolysing the water.
All of these buffers could find application in a voltammetric sweat sensor. An introductions of a buffer in real time would complicate the sensor since it necessitates an additional control system.

3.3. Measurement principles applied

To analyze the chemical composition of a fluid a wide variety of techniques can be employed. This section will focus on the most prevalent ones recently presented in literature.

3.3.1. Colorimetric Sensors

Colorimetric sensors use decoloration of a reacting agent in presence of a species to be analyzed as their working principle. The sensors generally have the advantage of the result being visually easily accessible. However quantifying concentrations from this colorimetric essay is more arduous than for other measurement principles.
The simplest application of a colorimetric sensor is the detection of pH as applied to sweat by [39]. They find a mostly linear correlation between sodium concentration and pH-value. However the variance of the measurement is relatively high and the correlation low. In this paper the colorimetric measurement was implemented using a smartphone application allowing for a convenient point of care. Many subsequent papers utilize a pH sensor in some form to relate their analyses [40], [41], [42].
Colorimetric sensors have been developed for many sweat components. They all utilize a camera application either laboratory based or smartphone based for the analysis of the color displayed. The sweat is (mostly) taken into microfluidics platforms and then delivered to the reacting agents. Some designs even allow for a degree of temporal resolution [43], [44], [40], [45], [39]. This temporal resolution is mainly achieved by different distances between the opening of the sensor and the reacting agents [44] or the implementation of different chambers via micro-valves [45].

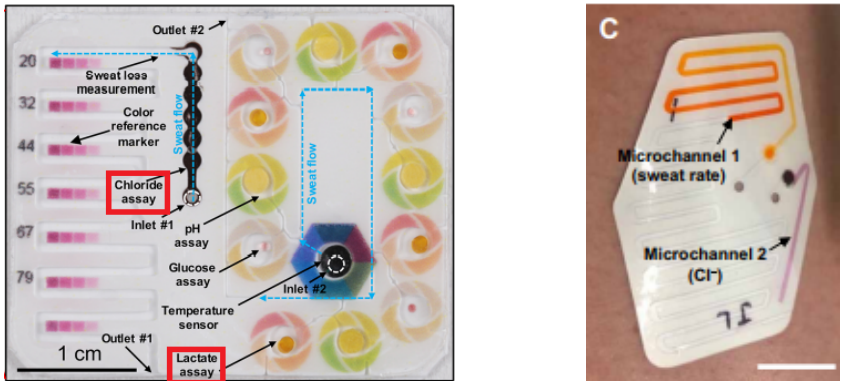

Figure 3.2: Different state of the art colorimetric sensors, left: full assay with the markers for fatigue highlighted, adapted from [40], right: collection system and colorimetric patch for Cl^--measurement [46]

Sensors were developed for glucose [43], [44], [40], chloride [42], [46], [45], sodium [39], lactate [33], [40], [47], micronutrients [48], [49] and cortisol [50].
The accuracy achieved by these sensors varies widely mainly depending on the quality of the camera used to measure the color of the patch, the method used for collection, the adherence to the good practice of experiment preparation and the correct choice of reacting agent. Overall while the patches show potential their disposable nature, high variance results and low temporal resolution stand in the way of their broad acceptance. On the other hand their specificity to certain low concentration substances is remarkable and the sensors can achieve a higher flexibility than most based on electronics. Stability of the sensors over time can come up as an issue and should be taken as a lesson learned for the design at hand.

3.3.2. Ionophores and ion selective electrodes [ISE]

A second principle of measurement works via electrochemical transduction. This method relies on turning the concentration of certain species into an electrical potential. The measurement relies on ion selective membranes or electrodes. These membranes bind with the respective ions or charged particles establishing a stable potential. This potential, called the Nernst-potential, can be related to the concentration of the species of interest via the Nernst-equation. An obvious advantage of this technology is the relatively simple measurement of ions in the fluid without the need to apply any external voltage [51]. By applying one electrode for each species of interest a chemical assay can be performed. This however shows an inherent disadvantage of the technology - an electrode can only ever be used for one ion or molecule and cross-sensitivity can be an issue. Furthermore the Nernst-potential is influenced by factors such as temperature and pH necessitating a correction of any measurement results. [51] presents an overview of ion-selective electrodes with the accompanying substrates, their accuracy and stability. Most sensors listed were used to detect Chloride, sodium, potassium, ammonium or sweat pH. This is owed to the higher concentration of these species. While the electrode material used is invariably gold [Au], platinum [Pt] or carbon nanotubes [CNT] the membranes and ion-transducers used vary widely. Au, Pt and CNT appear to perform equally well in these potentiometric applications. Most reference electrodes recently presented used CNT or Ag/AgCl.
Sodium has received particular attention in potentiometric applications. The relatively high concentration paired with the physiological relevance for electrolyte loss leads to many projects tackling this ion in their research in this relatively immature field. [52] related their measurements with analysis using flame photometry. While their measurements were performed in a laboratory setting and not real time, the results showed the feasibility of using ISE for sweat analysis. [53] follows up on this study and provides proof that measurements using ISE can meet the standards set by 'standard' laboratory equipment (i.e. tabletop equipment used for broad measurement of ionic contents in fluid). In the past decade and specifically in the last three years new developments have advanced the sensing capabilities of sodium sensors. With the development of all solid-state carbon electrodes that can be screen printed [54], major steps towards miniaturization with good characterization were taken. The ability to MEMS-manufacture these electrodes in combination with the collection system is crucial to the adoption of wearable platforms. Recovery rate and sensitivity of the sensor presented by [54] were high and

show promise for both temporal and magnitude accuracy of the measurements. [55] put their focus on the adherence of their measurement to the expected nernstian behavior and a low cross sensitivity. They found good linearity of their Na^+ and K^+ ionophores as well as of their pH-sensor with an undesirable cross-sensitivity between the two ISE. Additionally they found the connection of their electrodes and collection system to lead to high noise levels during movement of the subject. The application [55] shows the potential of ISE for the analysis of sweat while at the same time demonstrating some of the short-comings:

- to achieve Nernstian behaviour full flow over the ionophores needs to be steadily ensured
- ISE are susceptible to a number of influencing factors including sweat pH and struggle linearity over a higher dynamic range
- cross-sensitivity remains an issue even with careful ISE selection

Closing the section on sodium ISE sensing the work of [56] is of note, introducing sensing based on textile organic electrochemical transistors. In this technique the selective membrane as well as the electrodes are printed directly onto the fabric of sports clothing. This allows for even less invasive sensing at the cost of some accuracy and selectivity. Further work will be necessary on these specific sensors to achieve a close to Nernstian response. The trade-off of this non-invasiveness vs. a good fit and accurate measurements becomes clear when observing results obtained by [57] who use gold-nanowires to achieve good contact and report accurate results.
Analogous to the sodium sensing, applications exist for potassium and chloride (sometimes multiplexed with each other). [58] present a textile based sensor for both chloride and pH with good selectivity but struggling with linearity. Generally the sensitivity is a smaller issue for the measurement of Cl^- given that it dominates all other anions in concentration (see: tab. A.1). These issues are overcome by [59] who use a specific ionophore (Tripodal Squaramide Derivative) for their more efficient H^+ donation to the chloride anions. This results in a Nernstian behavior with good selectivity and a low detection limit. This specific choice of ionophore demonstrates the capability of ISE to sense components of low concentrations effectively. This is further demonstrated by the detection of ammonium [60], glucose and ethanol [61]. Ethanol and glucose were measured in an experiment additionally including an iontophoretic platform to induce the sweating without the need for exercise (this might significantly alter the sweat concentration of various components which needs to be taken into account [3]). The Prussian blue based membrane was supplemented with enzyme based receptors and an amperometric system at a voltage of -0.2 V to provoke a response. While the system demonstrates the capabilities for accurate measurement of low concentration metabolites it trades off for a rather narrow scope. [60] discusses in detail ammonium sensing using ISE. They explore the fact that cross-sensitivity is the harshest issue facing the ISE-sensing of this species. Finding the correct ionophore remains a big challenge to potentiometry using ISE.
Another challenge facing ISE is biofouling. Biofouling is the degradation of a surface in contact with the human body due to chemical or biological processes. Generally biofouling can affect any wearable sensor given the close contact between device and body. The speed of this biofouling depends strongly on the choice of material [62]. ISE are specifically susceptible due to the thin layer that is typically applied [51]. Quantifying the effect of biofouling has proven difficult. Minimizing this effect is an important issue in modern devices [62], [51]. This is in line with the current development of medical device regulations focusing on the durability of devices and instrumentation.
ISE potentiometry together with colorimetric analysis today makes up the lions share of devices presented. ISE show promise for portable, easy-to-use, point-of-care solutions if issues with cross-sensitivity, linearity and a large number of influencing factors can be properly accounted for. One issue that is inherent to ISE and might call for the exploration of different technologies is the fact that for a complete essay of the sweat requires an ionophore and electrode for each species to be analysed. Additionally ISE can suffer from degradation over time, not allowing for a re-usability of sensors.

3.3.3. Stripping voltammetry

Stripping voltammetry is another commonly used technique for the analysis of sweat and/or blood. Depending on whether the ion of interest is positively or negatively charged the technique is called cathodic or anodic stripping voltammetry. The technique relies on carefully pre-treating the analyte.

Usually the analyte is diluted with acidic or basic substances as necessary to achieve a desired conductivity and pH value. Additionally a ligand is added to bind to the species of interest. Subsequently a potential is applied that allows for the species to be adsorbed into the working electrode. Following this the potential range is swept with distinctive peaks for the respective substances of interest. The sensitivity and specificity of the system depends strongly on several influencing factors such as pH, accumulation potential, choice of ligand, choice of electrode material and shape, etc. The technique is often applied to find trace amounts of minerals [63], [64].
[63] describe a determination of copper in human blood with a detection limit as low as $0.001\ \frac{ng}{ml}$ that is sensitive to all factors mentioned above. It is noteworthy that the required potentials are far lower than would be required for the measurement of the Redox-behaviour of copper on its own. The low detection limit and high linearity of the finding by [63] show the potential of the technique while the necessity to prepare the sample very carefully (i.e. deoxygenating the sample with argon gas, keeping the pH value under close control and deal with the liquidity of the mercury drop electrode) shows its limitations. Both portability and real time measurements seem unfeasible with this amount of preparation and precision necessary. Furthermore the necessity to use a mercury electrode has adverse environmental implications that are ever more important in today's society.
Another advantage of the technique is demonstrated by [64]. They show that the detection of molecules is not restricted to polar molecules and ions. If a substance has a suitable ligand and the surface of the sensing electrode can be prepared properly sensing of e.g. ethanol becomes possible using voltammetry. Again the selectivity of the method allows only for sensing of a single species. Similarly sensing of other ultra-low concentration, nonpolar biomarkers was possible e.g. cysteine [65], norepinephrine [66] or antioxidants [67]. This was greatly aided by the implantation of specific antibodies or nanoparticles into the electrode.
While all cases presented above were first demonstrated in blood an equivalent approach for sweat seems feasible. Overall, while the principle is powerful in the detection of low concentration species its focus on single components paired with the intense preparation necessary restrict its use-cases and likely does not allow for the adoption in wearable devices.

3.3.4. Laboratory equipment for measurement

Additionally to the innovative and mostly miniaturized techniques presented above, traditional tools exist to determine the concentration of species in fluid. These tools were developed multi-purpose and thus while mostly superior to the approaches above in accuracy are costlier, more arduous in the sample preparation and non-portable. They are reported here since many researchers refer their results back to these methods as a kind of standard.
[68] compares the most common laboratory methods and analyses their inter-method variability as well as deviation against each other. Of the methods discussed above both a direct ion-selective electrode (without membrane) and indirect ion-selective electrode (using ionophore) were included. Additionally flame photometry (measuring the color of a flame using a mix of air, fuel and the sample to burn), electrical impedance spectroscopy (sweeping the electrical impedance over the frequency spectrum) and ion chromatography (exchange of ions respective to their functional groups) were tested. Ion chromatography was set as the standard. All principles showed similar in-method variability while they showed significant differences between the methods. Sodium levels, which were used as the species to compare the methods, show high variability between the methods up to discrepancies of 12 % relative difference. While the standard deviation of the methods was low the systematic error appears to be significant. To establish consistency results should be referenced to standardized measurements. Ion chromatography appears to be the most reliable choice as a standard.

4

Voltammetry

Voltammetry is an electrochemical analysis method. In this method the voltage is swept over the sample via electrodes and the current recorded during the sweep. The method was chosen to be explored in this thesis due to its potential for accurate results on the ionic concentrations as well as the possibility to measure several species in a singles sweep.
There exist several different methods of voltammetry. The method chosen to be explored within this thesis is cyclic voltammetry in which the voltage is swept bi-directional at the same speed. This has the advantage of making reactions taking place in solution reversible while still maintaining the advantages mentioned above. Other methods, such as the previously discussed stripping voltammetry, do either not fulfil the requirement of being able to distinguish multiple ions or are to intensive in preparation of the sample. Voltammetry is chosen over the analogous amperometry since implementing a potentiostat is easier than a constant current source in the environment of this electrochemical cell [69].

4.1. General principle

Voltammetry relies on the usage of an electrochemical cell. This cell typically consists of three electrodes submerged in the analyte. The three electrodes are the working electrode [WE], counter electrode [CE] and reference electrode [RE]. In voltammetry a voltage difference is applied between CE and WE. The potential on each electrode to induce this voltage difference is referred to the RE. Once the voltage between CE and WE reaches a certain threshold the desired chemical reactions take place in the cell. These reactions are typically simple one electron redox reactions but can be more complex, include several components and multiple oxidation/reduction states. The current induced by these reactions is called the ionic current. The strength of the ionic current is proportional to the concentration of the species of interest and peaks at its reaction voltage [70]. The ionic current can be estimated using the formula:

$$I_p = 0.446 * nFAC^0 * \sqrt{\frac{nF\nu D_0}{RT}} \tag{4.1}$$

Equation 4.1 [70] shows the influencing factors on the ionic current to be measured. Table 4.1 lists the factors of the formula and their values or typical ranges. The following section will explore the different factors and explore their variations to evaluate the accuracy that this technique can achieve. Note that 4.1 (called the Randles-Sevcik equation) indicates the maximum current. The current decreases exponentially with absolute difference of the potential from the reaction voltage.

4.2. Influencing factors on ionic current

4.2.1. Natural Constants

Easiest to evaluate in the list of influencing factors are the natural constants. Both the universal gas constant R and Faraday's constant F are invariable. They are not subject to temporal or other changes

Symbol	Parameter	Value / Range
n	state of charge	in sweat, typically: 1-3 (unitless)
F	Faraday's constant	$9.65 * 10^4 \ \frac{C}{mol}$
A	area of the electrode	for wearable application: mm^2 - range
C^0	concentration of species in question	depending on ion; $\frac{mmol}{l}$ - range for ions of interest
v	sweep rate	variable; typically kept between $50 - 5000 \ \frac{mV}{s}$
D_0	diffusion coefficient	varies between species; typically $10^{-9} \ \frac{m^2}{s}$
R	gas constant	$8.31 \ \frac{J}{K*mol}$
T	absolute temperature	in application relatively constant $306 - 309 \ K$

Table 4.1: Parameters and constants influencing ionic current

and can thus be neglected when evaluating variations in the ionic current. The same holds (with slight differences between species) for the diffusion coefficient D_0. Regardless, they are necessary to acquire a baseline evaluation of the ionic current.

4.2.2. Charge state of ion

Molecules expressing a net electrical charge are called ions. Ions can have different charge states. The charge state of an ion is defined as the number of electrons missing from (or added to) the atoms original state. The ions contained in sweat either have a charge state of I (Na^+, Cl^-, HCO_3^- and K^+) or II (Ca^{2+} and Mg^{2+}).
For charged molecules the charge state is not immediately evident given that the complexes formed do not have a net electrical charge. Looking at ammonia (NH_3) as an example we can observe that the natural charge state of H is $+I$ while N has a charge state of $-III$. Balancing the charge within the molecule we observe no net electrical charge.
Thus to relate what change in charge takes place when the species is oxidized / reduced and subsequently relate the ionic current which is induced we need to look at the reactions taking place in the solution. In an alkaline solution ammonia is evolved to nitrogen gas and water:

$$2\ NH_3 + 6\ OH^- \xrightarrow{-0.06V} N_2 + 6\ H_2O + 6\ e^- \tag{4.2}$$

Balancing equation 4.2 three electrons are released for each ammonia molecule [71]. The charge state of ammonia for the calculation of ionic current is III. For other charged molecules similar reactions take place allowing for the derivation of charge states.
The strength of the ionic current depends on the charge state to the power 1.5. This is important for range considerations of the sensor. Considering that the species which are in highest concentration (Na^+ and Cl^-) have a charge state of I while those of lower concentrations commonly have higher charge states is favorable for range. The ionic current depends on the charge state of the ion or molecule since the energy required for certain reactions is higher or lower depending on the charge state.

4.2.3. Electrode Area

The strength of the ionic current depends linearly on the electrode area A [m^2]. This can easily be visualized by realizing that reactions can only take place on the electrode surface. While the calculation of surface area is a simple exercise it is complicated by the surface structure of the electrode. A rougher electrode surface can lead to a higher effective area, while a smoother surface diminishes the surface area reducing sensitivity of the sensor. This effect should be observed in the temporal domain. Screen printed electrodes, such as the one used for this proof-of-concept, often have porous structure leading

to a relatively high initial surface roughness. Initial surface roughness can be influenced by a variety of factors including roughness of the substrate and number of layers printed [72]. Over several uses of the electrode roughness is conjectured to reduce. This is due to the surface imperfections being filled by species in the solution. Comparison of surface roughness measurements between a factory-new and extensively used electrode will be able to quantify this reduction in effective area and sensitivity.

4.2.4. Species Concentration

The ionic current depends linearly on the species concentration C_0 $[\frac{mol}{l}]$. This linear dependence is the relation that is exploited to relate the concentration to the ionic current. While this linear relationship is true in the initial condition, in which all ions are present in their charged state, the transfer-coefficient dependent relation (also called the Butler-Volmer-equation) can be expressed as [73]:

$$j = j_0 \cdot \left\{ \exp\left[\frac{\alpha_a n F \eta}{RT}\right] - \exp\left[-\frac{\alpha_c n F \eta}{RT}\right] \right\} \tag{4.3}$$

where α_c and α_a are the cathodic and anodic transfer coefficients [unitless] while η $[V]$ is the overpotential of the cell above the reaction voltage of that species [73]. j_0 $[\frac{A}{m^2}]$ is the current density in a solution with only oxidized species, F is Faraday's constant, R the universal gas constant and T the absolute temperature. The transfer coefficients in turn are dependent on the relative concentrations of reduced and oxidized species in solution. As such it can also be interpreted as relating the ionic current to time during the experiment, since the concentration of species changes once voltammetry and the associated reactions take place. To still achieve a linear current the change in concentration induced by a single voltammetric cycle ΔC should observe $\Delta C << C_0$. This does not need to be satisfied for non-reversible reactions since one of the transfer coefficients in these reactions will be $\alpha_c/\alpha_a = 0$.

4.2.5. Sweep rate

Different waveforms for voltammetry exist as will be explored later in this chapter. Common to these waveforms is the necessity to sweep the voltage. The speed at which this voltage is swept is called sweep rate $v = \frac{V}{t}$ $[\frac{V}{s}]$. The ionic current scales with $v^{0.5}$. This scaling can be exploited. By increasing the sweep rate the sensitivity of the sensor can be increased. This however comes with drawbacks. Increasing the sweep rate leads to a further separation of peaks for the reaction and respective reverse reaction. This separation leads to residual reactant remaining in solution after the sweep is done altering its composition. This can again be mainly neglected when the reaction is irreversible. Regardless of the reversibility the sweep rate is also capped by the hardware being used. Excessive sweep rate can lead to the rising current exceeding the slew rate of the system, clipping the resulting current. Sweep rate does not need to be constant over time. Variations in sweep rate can be used to improve the sensitivity of the sensor at the cost of more complexity.

4.2.6. Temperature

Temperature T $[K]$ influences the ionic current. With rising temperature the ionic current falls with a factor $T^{-0.5}$. The temperature in laboratory environments can be well controlled. As such for the proof-of-concept sensor the temperature as an influencing factor can be neglected. It should be noted that the relevant temperature in application is human skin temperature. Research shows that the skin temperature drops during exercise by around $3 - 5\ K$ [74], [75]. This relative drop of $1 - 1.6\ \%$ leads to a total error in the result of less than $1\ \%$.

4.3. Sample preparation

Sample preparation is often used to improve the performance of voltammetry. In general, sample preparation is more complex in a system measuring a physiological fluid in real time. Adding a substance dynamically to a sample being measured is possible but would call for a relatively complex control system. Thus to keep the resulting sensor close to the principle being explored sample preparation is not treated at length in this thesis. There are three main ways of preparing the sample for voltammetry:

- buffering solution

- supporting electrolyte
- pH-adjustment

4.3.1. Buffering solution

Buffering solution is added to increase the potential window in which voltammetry can be used as well as increase the sensitivity of measurements. The buffer is chosen with respect to the solvent and can boost linearity of measurements greatly as well as improve signal strength [76]. Additionally the buffer can be used to shift the reaction voltage of compounds [77]. In this manner species previously not measurable can be evaluated. While buffering the solution of interest has distinct advantages it also narrows down the spectrum of species that can be measured analogous to a fluid ISE. Buffering in a real-time application increases the complexity of post-measurement-processing given that the sensitivity of the measurement depends (either linearly or non-linearly) on the buffer-concentration. A correction for the addition of buffer in real-time would complicate the measurement substantially.

4.3.2. Supporting Electrolyte

Typically samples to be analyzed are supported with electrolytes. These electrolytes serve several roles including to ensure low ohmic drop, sufficient mass transport and reduction of ramping in the voltammogram [38]. Research including numerical modelling and experimental results show that the amount of excess supporting electrolyte, the flow rate and the scan rate have a significant influence on the behaviour of the species of interest [38]. A high flow rate paired with a low sweep rate might lead to convection of the fluid becoming the dominating mode of mass transport instead of the desired redox-reactions. The lesson for the thesis at hand is to adjust sweep and flow rate to achieve a proper diffusion and mass transport behaviour.
The amount of supporting electrolyte necessary to achieve a diffusion only behaviour depends on the charge state of the electrolyte used, the amount of charge transferred, the diffusion coefficients and the voltage sweep rate [78]. Some guidance has been given on this issue by numerical simulations, but experiments with the actual application will be necessary. There is evidence that diffusion only behaviour can be achieved even without supporting electrolyte although only at microelectrodes [79]. Thus microfluidics designs should be modelled using a finite element solver to establish whether diffusion models apply or corrections are necessary. The average conductivity of sweat samples (modelled in chapter 5) indicates supporting electrolyte might not be necessary to achieve diffusion only behaviour considering the findings on minimum conductivity by [78].

4.3.3. pH-adjustment

The pH of sweat is correlated with the sweat rate. With increasing sweat rate the pH of sweat becomes more alkaline [80]. This was hypothesized to be due to the lower concentration of lactic acid at higher sweat rates. This variation in sweat pH poses issues to methods that are sensitive to it (e.g. ionophores or colorimetric measurements). Changes in pH can become relevant in voltammetry since they shift the so-called water window, altering the voltages at which water is reduced or oxidized. Thus many voltammetric applications use a pH-buffer (nonreactive acid or base) to shift this window. Commonly water based applications avoid extreme pH-values as to not shift the conductivity of the solution unnecessarily. [81] found a significant difference in the sensitivity of their ZnO based glucose sensor when shifting the pH of the sample from slightly acidic ($pH = 6$ to slightly alkaline ($pH = 8$).
Given the variation over sweat rate this adjustment would need to be dynamic for the application at hand. Given this complexity a real-time adjustment seems unfeasible. It should however be noted that this negligence of the pH-adjustment will lead to alterations of the electrolysis-currents induced. These variations should however be able to be accounted for given a well-characterizable slope of this current. The variations in pH will complicate the measurements.

4.4. Types of voltammetry

There are different types of voltammetry. The different types of voltammetry are mainly differentiated by the waveform used to excite the voltammetric behaviour. Different waveforms with more sophisticated control mechanisms have become more commonplace recently owing mainly to advances in micro-

controllers allowing for easier control [82], [83], [71]. A visualization of the most common waveforms can be found in fig. 4.1.

4.4.1. Linear Sweep Voltammetry

Linear sweep voltammetry [LSV] is the simplest form of voltammetry. In LSV the cell is excited using a linear sweep of constant sweep rate in both anodic and cathodic direction. LSV is the easiest form of voltammetry to implement. It is thus often used as a reference point. Additionally LSV is used in characterization measurements and the acquisition of calibration curves since the sweep rate is well defined at all points. These calibration curves can then be used during other waveforms to relate the results. Variations are taken in LSV by altering the sweep rate and the duty cycle of the waveform, that is which portion of time is active measurement. Especially in in-vivo measurements this duty-cycle needs to be taken into account considering the possible damage to tissue via heating.

4.4.2. Fast Scan Cyclic Voltammetry

Fast scan cyclic voltammetry [FSCV] is similar to LSV. FSCV however has a faster sweep rate. There is no fixed value differentiating the two methods but sweeps faster than $50\,\frac{V}{s}$ are typically called FSCV. This method is mainly used for constituents with a small concentration such as dopamine [83] or other hormones. As eluded to earlier in this chapter the sensitivity of the voltammetric sensor scales with the square root of the sweep rate. Thus increasing v by several orders of magnitude can decrease the detection limit. This increase in speed does not come without drawbacks. Generally electronics for FSCV need to be more sophisticated. This is owed to the fact that the faster sweep rate necessitates faster recording electronics. Additionally for low concentration components overlaid on a relatively high baseline background current a significant dynamic range is necessary. The background current is higher in FSCV since the faradaic effects are excacerbated at higher frequencies. Applications with a sweep rate of $100 - 1000\,\frac{V}{s}$ are not uncommon. While most FSCV applications still utilize the traditional sawtooth waveform more specialized applications have trended towards using adapted sweeps. The reasons for using these differing waveforms are manifold and range from preventing fouling of electrodes in in-vivo applications, adapting the hold-voltages and times to the exact electrochemical processes and reducing background current [83].
Modifications to the waveform mainly include holding patterns and variations in sweep rate over the sweep. For FSCV these patterns are often asymmetric given that reversibility is less of a concern in these applications. Modifications of the waveform require expert knowledge of the reactions as well as the electrodes.

4.4.3. Differential Pulse Voltammetry

Differential pulse voltammetry [DPV] has a waveform fundamentally different from LSV. DPV, as the name suggests, uses differential pulses to elucidate a response instead of a linear sweep. This has the advantage of being more sensitive and also allowing for less faradaic current as charging of the system is reduced [84]. The differential pulses are overlaid over a linear sweep. The current is not measured continuously but rather at the beginning and end of each pulse. The difference between the two currents is (mostly) equivalent to the peak current in cyclic voltammetry. LSV and DPV are often used in tandem, LSV for more general exploration and DPV for the more detailed analysis.

4.4.4. Square Wave voltammetry

Square wave voltammetry [SWV] uses a series of square pulses with a potential of ΔE both above and below a potential E_{base} that is being stepped up and down. The ionic current is determined by the difference in current ΔI after each half period. This method is even more resilient to capacitive currents than DPV and has a higher sensitivity. As such it is the state of the art for purely voltammetric detection of low concentration components and characterization of electrodes.

4.4.5. Stripping Voltammetry

Stripping voltammetry is another form of voltammetry. It was discussed in detail in the previous chapter on state of the art analysis methods. It is not usable for sweeps of multiple species due to the restrictions given by the requirement to use a ligand.

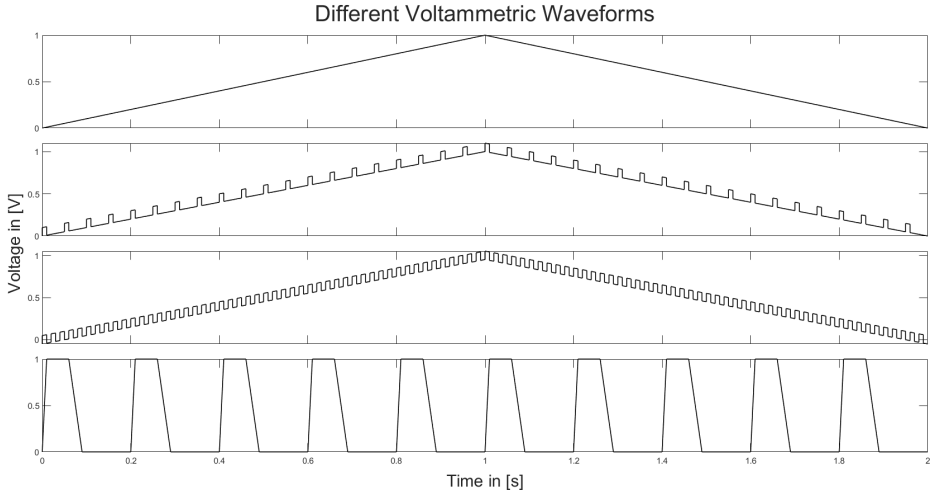

Figure 4.1: Different voltammetric waveforms sweeping from 0 to 1 V; from top to bottom: linear sweep voltammetry [LSV], differential pulse voltammetry [DPV], square wave voltammetry [SWV] and fast scan cyclic voltammetry [FSCV]

4.5. Electrolysis as a challenge

When performing voltammetry there is typically a potential window in which the technique can best be used [70]. This potential window is influenced by different factors including buffer solution, supporting electrolyte, electrode material, pH of the sample and temperature. The window is due to chemical restrictions. Outside of the potential window the evolution of the solvent takes place. When analyzing sweat the solvent is water. At the anode water is oxidized:

$$2\,H_2O \xrightarrow{+1.23V} O_2 + 4\,H^+ + 4\,e^- \tag{4.4}$$

At the cathode the corresponding reduction half reaction takes place:

$$2\,H^+ + 2\,e^- \xrightarrow{0.00V} H_2 \tag{4.5}$$

The full reaction, the electrolysis of water, thus balances at:

$$2\,H_2O \rightarrow 2\,H_2 + O_2 \tag{4.6}$$

The reaction described by equations 4.4, 4.5 and 4.6 is irreversible [85]. While the voltage difference between the anodic and cathodic reactions remains constant the individual values vary with the pH of the solution. The current induced by this reaction can be found to depend exponentially on the overvoltage above the half-cell-voltage induced [86]. This dependency indicates that once a certain overvoltage has been induced the electrolysis is no longer limited by the voltage but rather by the mass transport of the oxygen and hydrogen produced. How strong this current will be is difficult to predict. If the current is magnitudes higher than the one induced by the ionic reactions (due to the much higher concentration of the solvent) than it might mask any analytic value of the process beyond that potential window of 1.23 V. The data on this interference is slim and thus tests will show what potential window can reliably be used for analysis.

4.6. Reaction voltages for the components

The different species in solution have specific reaction voltages. These reaction voltages correspond with the peaks in ionic currents that are induced during the voltammetry [70]. These reaction voltages depend on the reaction energy necessary to overcome the tendency of the species to remain in its ionic state. They can be modelled using the Marcus-Hush-model by utilizing the Gibbs-energy of the oxidized and reduced states of the molecule [73]. The reaction voltages for the ions/charged particles most common in sweat (at $T = 300\,K$) are:

Species	Reaction Voltage	Source
Sodium (Na^+)	-2.71 V	[85]
Chloride (Cl^-)	+1.36 V	[85]
Potassium (K^+)	-2.93 V	[85]
Ammonia (NH_3)	-0.06 V	[87]
Bicarbonate (HCO_3^-)	+1.22 V	[88]
Lactate ($CH_3CHOHCOO^-$)	+0.32 V	[89]
Magnesium (Mg_2^+)	-2.37 V	[85]
Calcium (Ca_2^+)	-2.87 V	[85]

Table 4.2: Reaction voltages of common sweat constituents, relative to standard hydrogen electrode

4.7. Electrode Materials

The choice of electrode material influences the functionality of the voltammetry. Typically materials are chosen that are nonreactive. Nonreactive materials are necessary since any reaction between the electrode and the sample would skew the results [70]. Materials most commonly used in cyclic voltammetry are:

- carbon nano-tubes (CNT)
- gold (Au)
- platinum (Pt)

The differences in material also influence the voltage range in which the electrode can be used [70]. While for most common applications revolving close to 0 V solid electrodes are used, applications that require higher net voltage swings often rely on liquid-phase electrodes. These are however not feasible for applications of wearable devices for bio-essays. Between the three main materials listed above no distinction could be made from literature as to which might suit the application best. Thus tests with all electrode materials will be performed on a standardized solution to ascertain advantages and disadvantages. Concerns exist that gold might be unfeasible due to it forming Au_2Cl_6 (chemically: gold(III) chloride) complexes with the chloride.

5 Design

The theoretical exploration of physiology of sweat composition, state of the art technologies and the fundamentals of voltammetry indicate that a voltammetric sensor for the simultaneous detection of ions and charged molecules in sweat might be feasible. The proof-of-concept sensor is a transfer of the ideas elucidated in the literature research into a physical representation. The design is consciously kept simple. Proving the concept of the sensor with a simple design serves a dual purpose. Firstly, if there are fundamental issues with the measurement principle, they will be uncovered without incurring too high a cost or time investment. Secondly, if a simple design can be proven to work an adaption into a low-cost wearable sensor is feasible.

5.1. Requirements

The system needs to meet a number of high-level key functions. These functions are dictated by the overall task of the system to establish the ionic contents of the sample.
The highest level functions of the system are:

1. The system can contain a sample of an aqueous solution, i.e. hold the sample and continuously contact it with the electrodes.
2. The system can apply a voltage sweep over the sample, i.e. set the voltage between two electrodes in a predetermined manner
3. The system can measure the ionic current induced in the sample during the sweep.

This list can be broken down to identify major aspects of each high-level key functions.

5.1.1. Contain the sample

Containing the sample is important due to the liquid nature of it. In addition to serving as a reservoir the sample needs to contact the electrodes to allow measurement. As discussed in previous chapters some restrictions are put on this contact by the necessity to allow for flow of the sample. It is this sample flow that establishes a diffusion dominated behaviour which is necessary for accurate voltammetry [38]. Developing a microfluidics platform or integrating a sensor into such a platform is complex. As such the presented work did not implement the sensor into such a platform. This puts restrictions on the use cases in which the sensor will be accurate. If the sensor acts on larger quantities of sample and movement of the sample can be induced (e.g. stirring a beaker while electrodes are submerged) the flow might be neglected if the amount of ions in the sample are much larger than the quantity reduced in the sweep. When acting on smaller samples and no artificially movement is induced generally only the first sweep will be accurate. [38] et al. shows the importance of the flow in this behaviour. Eliminating the flow from the system is a conscious choice to reduce the complexity of the proof-of-concept.
If the material did interact with sweat then the sample might be altered by contact with the carrier. Thus, the material of the container should be nonreactive towards the components of sweat.

The container for the sample should be small (e.g. $200\ \mu l$ max). The sensor for which a proof-of-concept is explored here is meant to be wearable. A quick estimation using sweating rate during medium intensity exercise [90]:

$$V = 0.7\ \frac{ml}{cm^2 * min} * 0.1\ cm^2 * 1\ min = 70\ \mu l$$

shows that with even a small collection area this reservoir could be refilled within a minute allowing for a good temporal resolution.
While the flow is being neglected for the sake of simplicity the size of the sensor should be reasonably close to a possible wearable prototype. Certain effects such as the impedance of the cell or the physics of the fluid are dominated by the geometry.

5.1.2. Analyse the sample

To analyse a sample the voltage of the cell needs to be swept. A quick description of the cell itself aids in detailing this requirement.
A challenge somewhat unique to the electrochemical cell is the need for a reference electrode. This reference electrode is necessary to ensure that reactions that take place on the electrodes (notwithstanding their desired non-reactivity) do not shift the potential within the cell. The cell needs to be able to sweep the voltage between counter electrode [CE] and working electrode [WE] while nullifying any difference in potential between reference electrode [RE] and either WE or CE. The simplified setup of such a system with electrodes and the connected potentiostat can be seen in fig. 5.1.
The size of the electrode is not fixed but should be close in magnitude to a possible wearable application. Given that the size of the electrode is an influencing factor on the sensitivity of the sensor this requirement is tied to range, resolution and signal-to-noise-ratio [SNR] requirements.

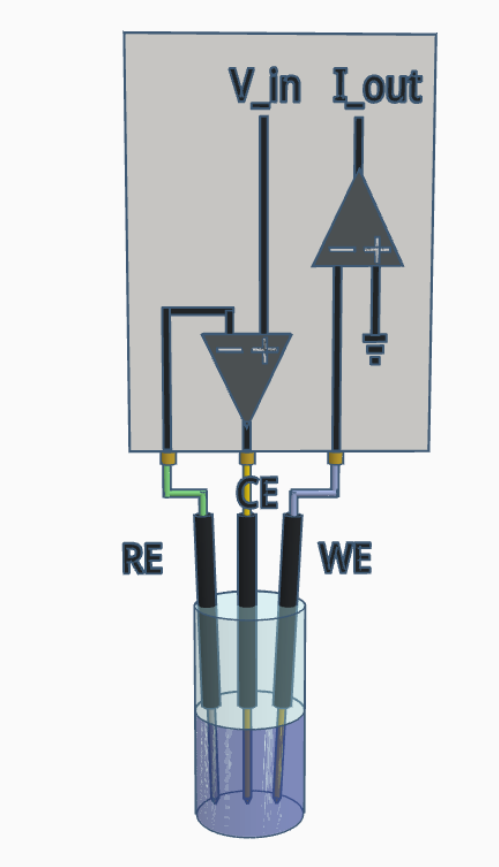

Figure 5.1: Basic setup of voltammetry with three-electrode-system submerged in sample and connected to potentiostat (electronics simplified)

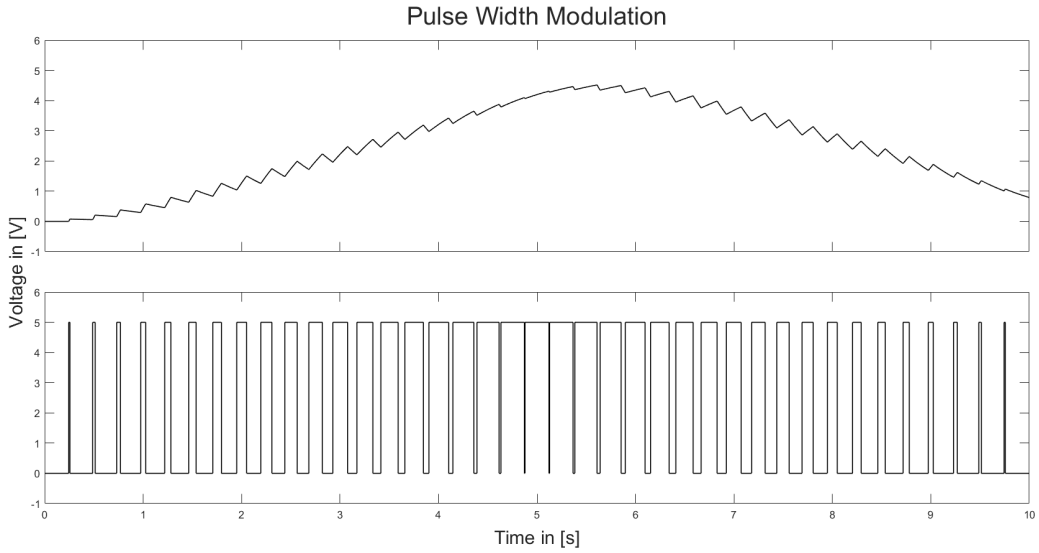

Figure 5.2: Principle of PWM with the resulting filtered signal at the top and the PWM signal at the bottom

Given that the sensitivity of the electrode is also tied to the sweep rate the system needs to be able to sweep the voltage at a variable rate. The sweep rate must be well controlled. The speed of the sweep is mainly determined by the necessity for sensitivity, the mass transport in the cell and the reversibility of the reactions. Given the relatively high concentrations of ions and charged particles the sweep rate is set between $10 - 10,000\ \frac{mV}{s}$. Higher sweep rates might cause mass transport to limit the ionic current output producing clipped results.
The system should be able to apply linear sweeps. The system should be programmable for different sweep rates, starting and final voltages. There is a trade-off in designing the system to allow for linear sweeps. To generate voltages digital-to-analog converters [DAC] or pulse-width-modulation [PWM] are commonly used. The input for both methods is discrete. Any attempt to approximate a slope using discrete signals will show a step structure in the voltage. Depending on the resolution of the DAC or PWM, the sweep rate and the ΔV the step structure is more or less pronounced. Particularly when differences between reaction voltages are small this might lead to issues in the sweep. To avoid these issues if a PWM is used, filtering will be necessary. The time constant of that filter will however not allow for changes with a high slew rate. This disallows the usage of square-wave-voltammetry [SWV] or differential-pulse-voltammetry [DPV] limiting the waveforms for an implementation of PWM. Fig. 5.2 shows a resulting filtered output voltage that can be used for linear sweep voltammetry and a PWM-signal used to generate it. The diagram is not to scale of the actual system with the PWM signal having a lower fundamental frequency and being modulated at a lower frequency. This reveals the issues of low frequencies with a considerable skew to the ideally sawtooth output signal. At the actual frequencies of $32,500\ Hz$ and 255 steps of modulation these effects are greatly reduced as can be seen from a simulation of the actual signal in 5.3. This simulation uses the real parameters of the design and a smaller deviation from the ideal triangular signal can be observed.
Voltammetric cells are (typically) three-electrode-systems [70]. A RE is necessary to avoid potential drifts caused by unwanted reactions on CE or WE. Any chemical reaction on either electrode could alter the material properties of that electrode leading to a different contact potential and a systematic error in all measurement results. While the stabilization of the potential is the main task of the electrode a current flow between RE and the other electrodes should be avoided. Any current flow over the reference might otherwise lead to measurement errors and a fast degradation of the surface and render the electrode unusable. Typical materials for reference electrodes include Ag/AgCl or saturated calomel electrodes [SCE] (chemically: mercury(I) chloride Hg_2Cl_2) [70]. To saturate the electrodes they are typically submerged in a saturated solution of KCl prior to any experiments to ensure that chloride binding sites due to material properties are used up and do not skew the result. Additionally many applications physically separate the RE from the two active electrodes via a porous diaphragm. This

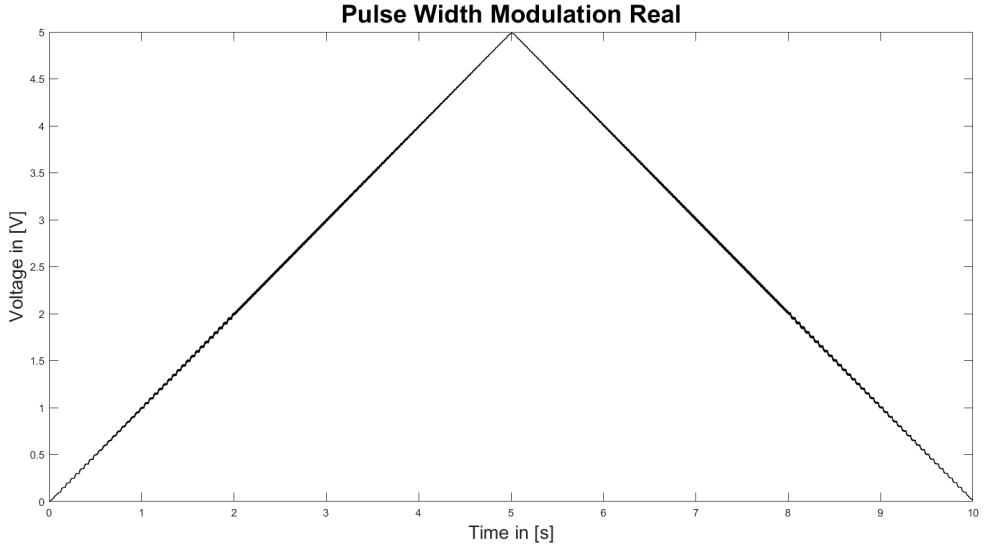

Figure 5.3: Output signal generated by PWM with real parameters used by the system

reduces contact potentials and prevents degradation of the RE as far as possible [70]. These measures, while useful in the durability of the device and the accuracy of the system are not strictly necessary as the system will be disposable.
The system shall be able to identify different peaks in ionic current at different reaction voltages. To this end the sweep needs to have a sufficient accuracy. The smallest difference between two reaction voltages in the species of interest is between Ca_2^+ and K^+ with $60\ mV$. To reliably differentiate two peaks the resolution of the voltage sweep should thus be lower than $60\ mV$.
The system must not retain an amount charge after a sweep is finished that would lead to a distortion of the current readout.

5.1.3. Measure the ionic current

The output of the voltammetric cell is the ionic current. To quantify the concentration of species in solution this ionic current needs to be measured.
We can estimate the ionic current for two different species, one with the lowest expected current and one with the highest. This allows us to establish (roughly) a desired range of the system. To this end a few assumptions are made. Firstly, the area of the electrode is approximated at $10\ mm^2$. This approximation of the area together with an assumption of the sweep rate at $1\ \frac{V}{s}$ allows to estimate the maximum current. Lastly, the temperature is set at $300\,K$ a close approximation of the temperature in a normal laboratory environment. The values that are calculated are sodium at maximum physiological concentration and magnesium at minimum physiological concentration [3]:

$$I_{p,Na} = 0.446{*}1{*}9.65{*}10^4 \frac{C}{mol}{*}10{*}10^{-6} m^2 {*} 90 \frac{mol}{m^3} * \sqrt{\frac{1 * 9.65 * 10^4\ \frac{C}{mol} * 1\ \frac{V}{s} * 1.33 * 10^{-9}\ \frac{m^2}{s}}{8.31\ \frac{J}{K*mol} * 300\ K}} = 8.79mA$$

$$I_{p,Mg} = 0.446{*}2{*}9.65{*}10^4 \frac{C}{mol}{*}10{*}10^{-6} m^2 {*} 0.2 \frac{mol}{m^3} * \sqrt{\frac{2 * 9.65 * 10^4\ \frac{C}{mol} * 1\ \frac{V}{s} * 0.704 * 10^{-9}\ \frac{m^2}{s}}{8.31\ \frac{J}{K*mol} * 300\ K}} = 4.04\mu A$$

This gives us an idea of the required resolution $I_{p,Mg} = 4.04\,\mu A$ and the range of the sensor. Given that the current can be cumulative this value is higher than the singular sodium current. The value taking all ions with significant contributions into account is $I_{max} \approx 27\ mA$. The true required value for the maximum current will be higher given the ohmic drop in the voltammetric cell and electrolysis current. Given the current limitations of many analog-to-digital converters [ADC] and operational amplifiers [OpAmp]

are in the range of $10 - 100\,mA$ and current density should be limited at any rate to avoid damage to the electrodes the maximum current for the system is set at $40\,mA$.
The excess current due to the ohmic drop and the electrolysis that is allowable is thus around $13\,mA$. While these values can be modelled reasonably in a finite element solver such as Comsol a first order approximation reveals that the currents in question can be kept to that limit relatively easily. As such no special design measures are taken and the adherence to the limit is only verified after the implementation.
The system shall be able to amplify the ionic current into a voltage that can be read out. The output range of the amplifier and with it the closed-loop-gain will be determined by the input range of the ADC.
The system must be able to convert the voltage values presented by the output amplifier into a digital signal that can be processed. This requires an ADC. Given the established ratio between resolution and range the resolution of the ADC is calculated:

$$\frac{40\,mA}{4.04\,\mu A} \approx 10,000 = 2^n \rightarrow n = log_2(10,000) = 13.3$$

The system would require at least a 14-bit ADC. In the real implementation a lower resolution ADC was chosen. This implementation was a conscious choice in the context of the sensor as a proof-of-concept. A lower resolution ADC was already implemented on the microcontroller used and thus made integration easier. Some restrictions to range and resolution are accepted, particularly considering the low importance of micronutrients in the determination of fatigue. A future prototype should use a higher resolution ADC.
The system is operating at such low frequencies that it is sensible to conceive of it as DC. The low sweep rate as well as gradual changes in current that are inherent to voltammograms allow for the simplification of not requiring an evaluation of the frequency capabilities of the components.

5.2. System Diagram

From the requirements a rough system diagram can be established (see fig.5.4). The central element of the system is a microfluidics platform. While this is technically not implemented in the current system/requirement list it is still essential to understand the overall system design. Such a microfluidics platform would include a system for the sweat collection and storage of samples not further specified at this point. The collection would have to be compatible with the other parts of the system, be non-reactive and allow for enough flow of sweat to ensure diffusion-only reactions.
The sample itself interfaces with the electrode array that is included in the microfluidics platform. Any electrode array will have to fulfil the requirements put on material and size. There are three electrodes with WE and CE from the same material and a RE made from a different material. As literature does not specify a clearly superior material for the usage in this application electrodes should be interchangeable to allow for comparative testing of materials.
The electrodes are connected to the voltage source. This source meets the specifications to produce a voltage sweep as desired. The source is connected to all three electrodes. Besides the actual sweep, the source also allows for a stabilization of the WE by nullifying the voltage between CE and RE.
The WE is additionally connected to the recording electronics. These are going to include a low-pass-filter [LPF], a low-noise trans-impedance amplifier [TIA] and an ADC. The recording electronics can read out the ionic current and turn the analog output of the sensor into a stream of digital measurement values. The components chosen and their configuration ensure adherence to the requirements put on SNR, resolution, maximum current etc. A low-noise filter is necessary to lower the bandwidth of the noise integrated by the system.
Lastly the logic and control complete the system. This block includes both the inputs to the voltage source (in the form of sweep parameters) as well as the digital signal processing [DSP] to interpret the raw stream of measurement data. While in more sophisticated systems the focus would be on miniaturization and power-consumption of this block in the present system the focus is put on ease of implementation and simple manipulation to more easily explore the space of possibility of the sensor.

5.3. Design Choices

In the following sections the requirements as well as the lessons learned from the system diagram are transformed from a set of abstract parameters into a design which can be implemented.

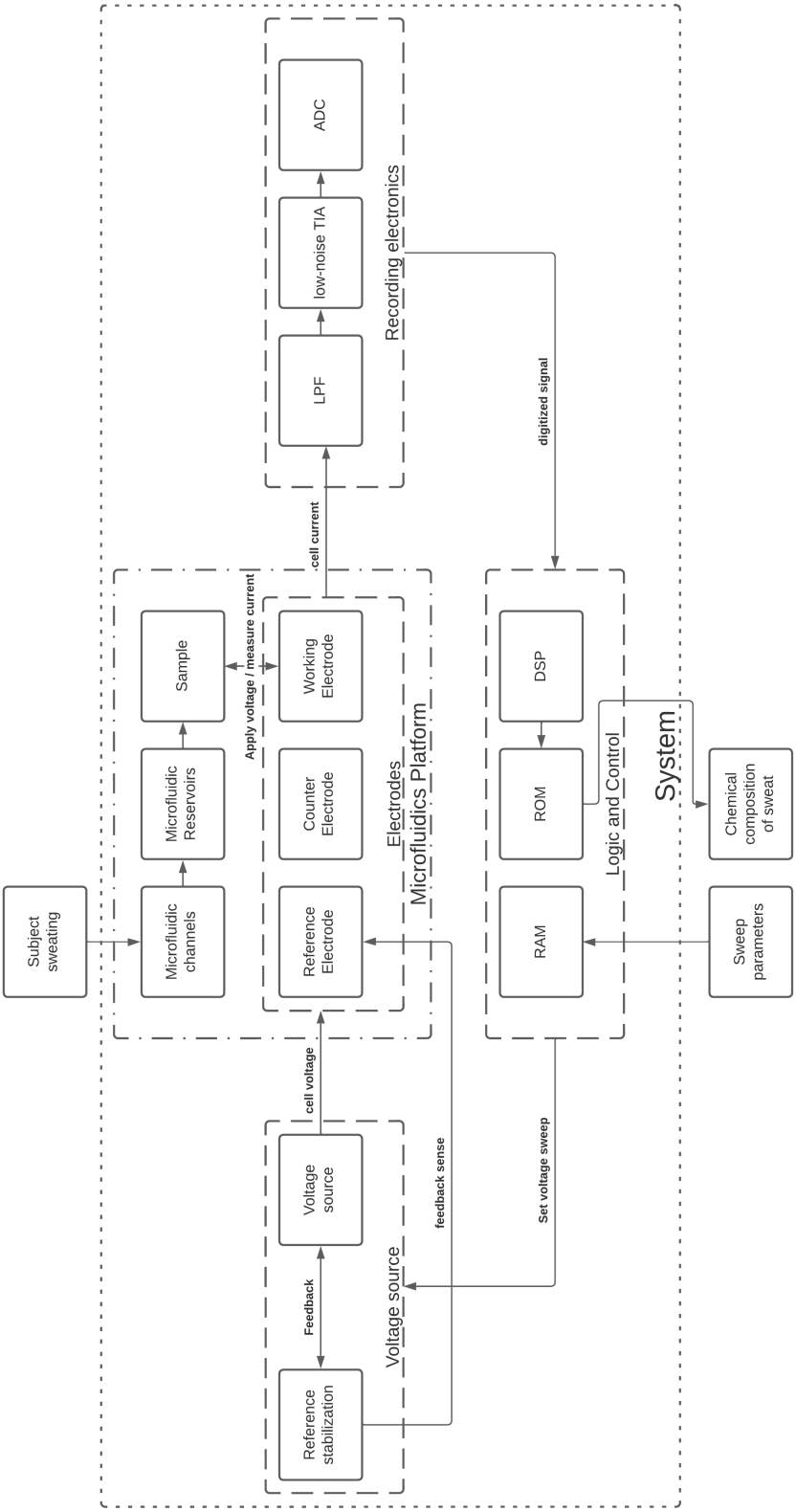

Figure 5.4: System diagram for full voltammetric sweat sensing platform

5.3.1. Electrodes

As the central element of the system the electrodes are determined first. This is necessary since any design of the output-electronics will depend on the size and material of the electrodes.
Manufacturing electrodes for use in electrochemical cells is not trivial. Rather, a well controlled process is necessary to ensure repeatable behaviour. The elements will be acquired from a professional vendor of electrochemical equipment.
Three main factors influence the choice of electrodes: size, geometry and material.

Size
No specific guideline exists for the size of the electrode size and it can be chosen (somewhat) arbitrarily. Nevertheless the size of the electrode is chosen to be larger than $10\ mm^2$ to avoid any effects caused by venturing into the realm of microelectrodes. Smaller electrodes suffer from effects such as limited mass transport that can easily be avoided by choosing a larger size. The size should be close to the $10\ mm^2$ to ensure that the output current remains limited.

Geometry
Different geometries exist for CV electrodes. Primarily these geometries are discriminated by whether they are planar or extend meaningfully into three dimensions. Intensive research has characterized these electrodes and found different relations between the diffusion coefficients and ionic currents [91], [92]. These geometries additionally influence peak separation of reversible reactions as well as the applicability of DPV [92].
The most commonly used geometries are planar discs, spheres, hemispheres, three dimensional discs and cylinders. Their common usage is owed to easy manufacturability in micro-fabrication processes. No shape of geometry has been shown to be superior in any meaningful way for the broad type of analysis performed in this thesis [91]. A wearable prototype of this sensor would be printed onto flexible substrate. This substrate could then adapt to the skin of the user. Thus a planar disc is the most logical geometry.

Material
The choice of material for the elements has two major aspects: non-reactivity to the processes in the cell and surface structure considerations.
Generally, for all purpose CV (that is to say without ion selective membranes or ligands) a non-reactive material is chosen for the active electrodes. That material often is a noble metal or, especially in the last decade, a carbon-nanotube [CNT]. The material is chosen with regards to the reactions that will take place within the electrode. In the case of sweat the main reactants have been analysed extensively in chapter 2. Of the species chloride in particular is of interest since it can have a reaction with gold (commonly used for CV WE). The formation of water soluble gold(III) chloride complexes which are produced in an acidic environment (such as the one provided by sweat) and might be redeposited on the return sweep can complicate the assertion of the effective surface area of the working electrode. Additionally to the naturally present Cl^- this effect might even be caused by the simple dissolution of Cl^- from the RE [93]. Notwithstanding, platinum, gold and CNT electrodes will be tested in the variable setup.
Besides the material choice the roughness of the electrode can have a major impact on the sensitivity of the sensor. The higher the surface roughness, the higher the effective area and subsequently the sensitivity is going to be. While this higher sensitivity might be desired it comes with the drawback of a more porous surface that is prone to adsorption of molecules (fouling) and thus degradation over time. While attempts have been made to combat this adsorption with regular crystal structure electrodes [94], these have still shown significant adsorption regardless of crystal orientation. Furthermore, affixing a crystal electrode to a carrier is more difficult than printing the material onto said carrier. Thus a screen printing method for CNT, Au and Pt active electrodes with an Ag/AgCl RE are chosen as the material.

Selected Electrodes
Given the parameters discussed above, an industry research of potential electrodes was conducted. Adherence to the requirements was taken into account with availability, delivery times and cost as additional factors. The electrodes that were finally chosen are commercialized by Metrohm (Metrohm AG, Herisau, Switzerland).

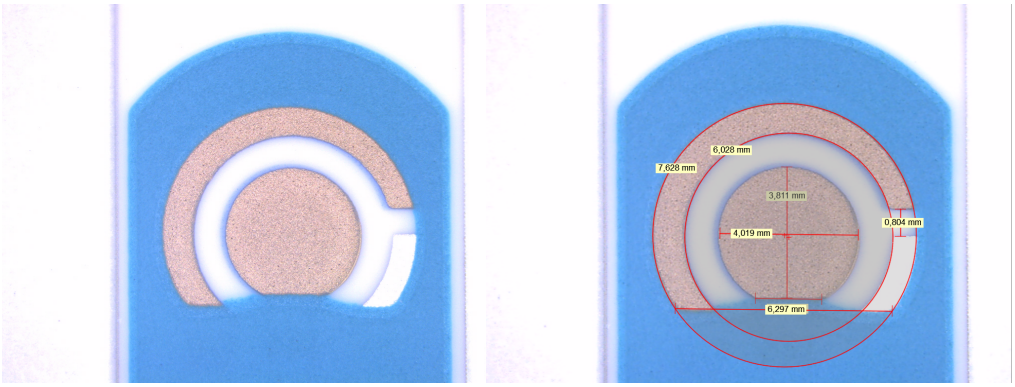

Figure 5.5: Pictures of the electrodes selected, left: without measurements, central WE with CE in ring around it (both platinum) and Ag/AgCl RE in bottom left corner; right: same electrode with detailed measurements for the accurate determination of surface area

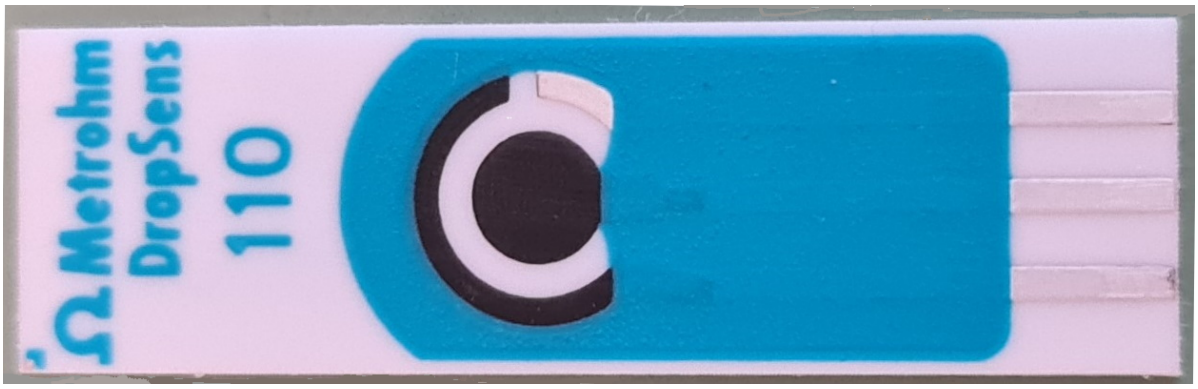

Figure 5.6: Picture of the full electrode array with substrate and connections

Fig. 5.5 shows a detail view of the electrodes. The central electrode is the WE. From measurements taken using a camera-assisted microscope the area of the WE could be calculated to $12.3\ mm^2$. This area agrees with the restrictions set on the size by the portable application discussed above. Additionally the accurate determination of the size allows for the design of the electrical components. The areas of the CE and RE were calculated to be $10.9\ mm^2$ and $3.9\ mm^2$ respectively. While their size is only of limited importance to the design it is reported here for the sake of completeness. Overall the arrangement of the electrodes with a central WE and surrounding RE and CE should aid to reduce the solution resistance as well as other contact related impedances which will be discussed later.
Fig. 5.6 shows the entire electrode. The central active area is printed on a substrate of alumina (chemically: aluminium oxide [Al_2O_3]).
The electrodes are each connected to an aluminium interconnect. This interconnect can then externally be connected to a matching cable. Each of the three electrodes can be addressed separately.
To hold the sample in place above the planar electrodes the electrode area is surrounded with a water-repellent and electrically insulating polymer sample container (3M, Saint-Paul, USA). The sample container can hold samples of up to $250\ \mu l$. This is in agreement with the requirements put on the sample container.
Electrodes were acquired with four different active electrode materials: two different gold surfaces, CNT and platinum. Surface roughness measurements were performed on all four surfaces. The acquired images can be seen in fig. 5.7. Surface roughness can be expressed using multiple different parameters. For the purposes of this thesis a simple approach is adopted in which the maximum deviation and average deviation from the height are recorded. For all materials the surface roughness is similar. The standard deviation from the average height (R_a) is less than $1\ \mu m$ for all materials while the maximum deviation (R_z) is less than $12\ \mu m$ for all measurements. A single electrode for each material was measured using a Keyence 3D-microscope (Keyence Corporation, Osaka, Japan). These initial measurements allow to evaluate the impact that measurements have on the surface of the electrodes

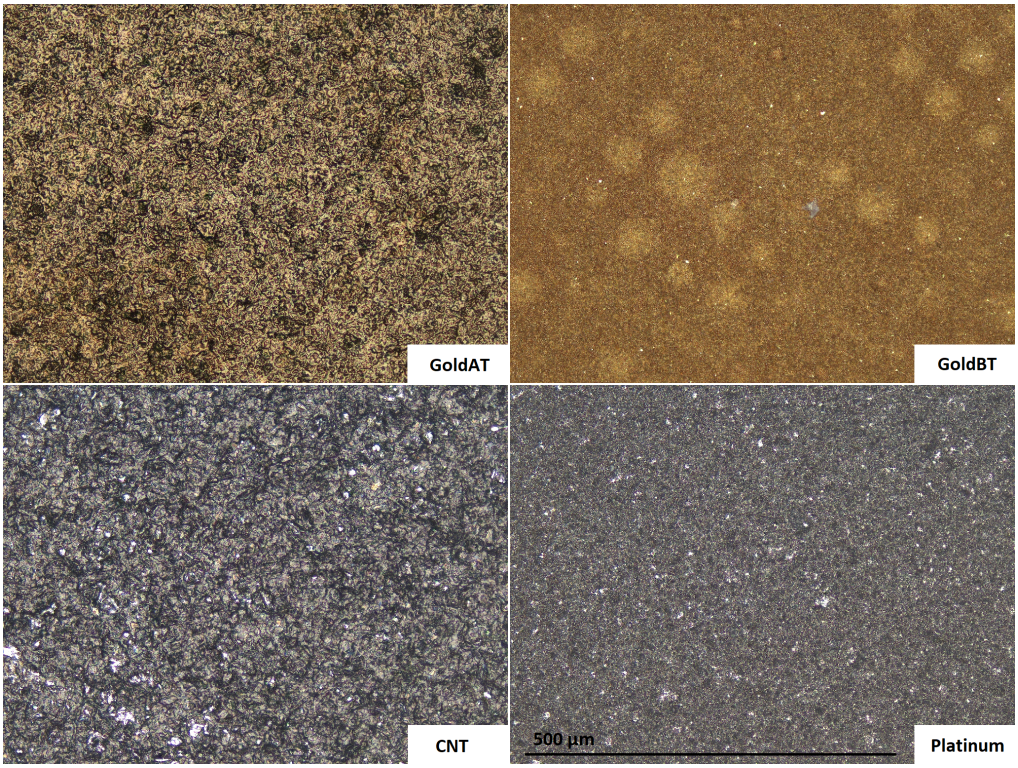

Figure 5.7: surfaces of active electrodes under 20x amplification top: two different gold surfaces; bottom left: CNT; bottom right: Pt

by performing similar measurements after a stress test (see: chap. 7.7). It should also be noted that there are no significant differences in the surface roughness between the materials suggesting a similar effective area.

Impedance Modelling

Given the selection of the electrodes the impedance of said electrodes can be modelled in detail. This model will help to predict the parasitic currents induced through ohmic drop and aid in minimizing the charge retention of the system. The modelling of the electrochemical cell will influence design choices in voltage source and recording electronics.

The model generally used to represent the electrochemical cell is the Randles Cell [95], [96]. The Randles Cell uses a combination of resistances and capacitances to approximate the response of the electrochemical cell. The model can be seen in fig. 5.8.

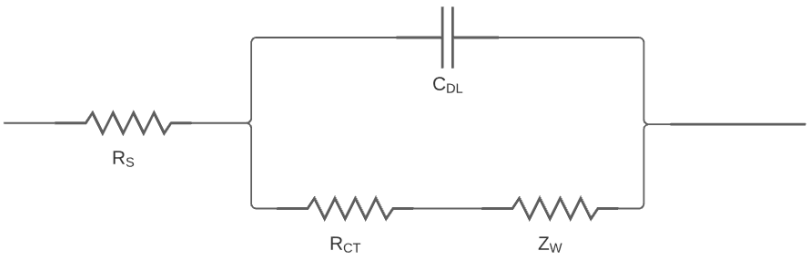

Figure 5.8: Randles Cell adapted from [95]

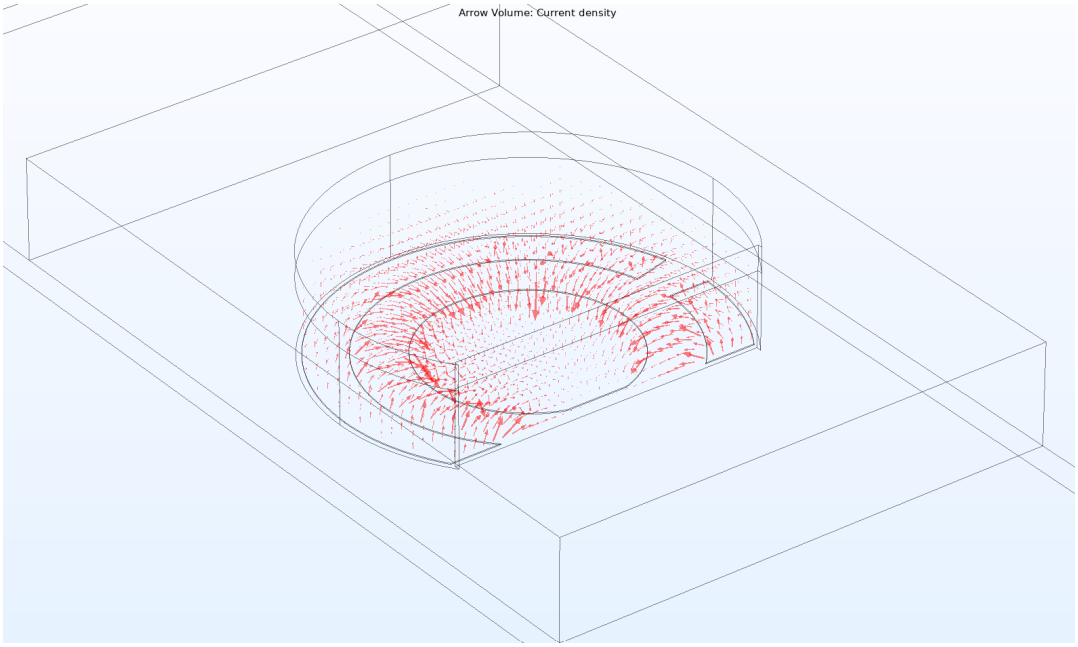

Figure 5.9: Current density after application of voltage step on CE and RE, length of arrow proportional to current density

R_s is the solution resistance. This component is influenced mainly by the conductivity of the solution and the geometry of the cell. The conductivity of the solution can be calculated based on the ionic conductivities (Λ [$S * m^2$]) and ionic concentrations (C [$\frac{mol}{m^3}$]):

$$\Lambda_{total} = \sum_{n=1}^{k} (C_n * \Lambda_n)$$

for each constituent n through k. The variations in ionic concentrations explored in chapter 2 lead to a relatively high variability in this conductivity. Plugging in values for the minimum and maximum concentration from [3] and ionic conductivities from [85] the range of conductivity can be found from $0.17 - 0.74 \frac{S}{m}$. The planar geometry complicates the calculation of the solution resistance. To model the solution resistance with reasonable accuracy the model of the electrode is passed into the finite element solver Comsol. The electrodes and carrier are modelled with their respective dimensions and materials. The sweat is replaced with a surrogate fluid with approximate conductivity. An electrostatic simulation is then performed, applying a voltage step to CE and RE relative to WE which is set as ground. The resulting current density can be seen in figure 5.9. Integrating the resulting current density over the working electrode gives an estimate of the current. Dividing the set voltage step by the current gives an estimate of the solution resistance. Depending on the conductivity of the sweat the solution resistance should vary between $306 - 1,330\,\Omega$.
The Randles cell includes in series with the solution resistance two parallel paths. One includes the double layer capacitance (C_{DL}) while the other has the charge transfer resistance (R_{CT}) in series with the Warburg impedance (Z_W).
C_{DL} models the possibility to transfer the charge from the solution into the electrode via the double layer formed at the electrode. The double layer capacitance can be estimated as:

$$C_{DL} = \frac{\epsilon_r * \epsilon_0 * A}{d}$$

with A [m^2] the area of the electrode ϵ_r [-] and ϵ_0 [$= 8.854 * 10^4 \frac{A\,s}{V\,m}$] the relative permittivity and permittivity of vacuum respectively and d [m] the thickness of the double layer commonly estimated as the inverse of the Debye length. [97] found an approximately linear relationship even in the presence

of multiple ions. The Debye length is estimated as:

$$\kappa_D^{-1} = \sqrt{\frac{\epsilon_r * k * T}{e^2 * \sum_{i=1}^{j}(n_i^2 * C_i)}}$$

with k [$= 1.38 * 10^{-23}\,\frac{J}{K}$] being the Boltzmann constant, e [$= 1.602 * 10^{-19}\,C$] the electron charge and the other parameters as introduced previously. As a matter of approximation only the three most common ions Na^+, Cl^- and K^+ are considered. Utilizing a relative permittivity of $\epsilon_r = 80$ as found by [98] and using extreme physiological levels for concentration we can calculate a range of the thickness of the double layer to be $d = 1.3 - 3.8\,nm$. This leads to an estimation of th range of $C_{DL} = 2.3 - 7\,\mu F$.
In the parallel path to C_{DL} sits the series connection of R_{CT} and Z_W. This path represents the charge-transfer complex. While R_{CT} represents the resistance of the system against the charge transfer (and is dominated by the exchange current density) the Warburg element can be understood to model the diffusion aspect of this charge transfer. R_{CT} is relatively complex in its calculation and depends on the exchange current density a parameter that is difficult to estimate a priori. [99] found a resistivity of $30\ m\Omega * cm^2$ for single CNT and $1.5\ \Omega * cm^2$ for platinum. They note however that the values are suppressed significantly by the micro-electrode nature of the setup (nm-range). As such a more conservative estimate of $1\ k\Omega$ is used as adopted by [95].
The Warburg impedance is understood to be a phase-constant element. In a Bode-plot the Warburg impedance has a slope of $-\frac{1}{2}$. It can be described as:

$$Z_W = \frac{\sigma}{\sqrt{\omega}} + \frac{\sigma}{j * \sqrt{\omega}}$$

with

$$\sigma = \frac{R * T}{n^2 * F^2 * A * \sqrt{2}} * \sum_{i=1}^{j}\left(\frac{1}{C_i * \sqrt{D_i}}\right)$$

with the symbols previously introduced. The value for σ was calculated to vary between $8.65 - 77.85\,\Omega$. To model a constant phase element with the appropriate magnitude in the circuit simulator a ladder R-C setup was used similar to [96].
Simulating a voltage over this complex impedance and sweeping over frequency reveals the Bode-plot shown in fig. 5.10. For this simulation average values of the previously calculated ranges were used.

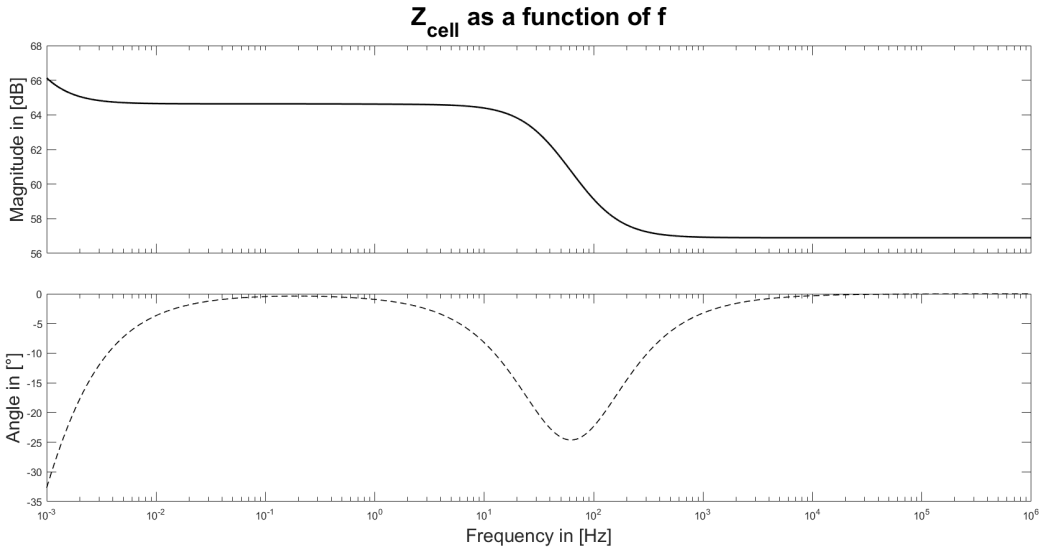

Figure 5.10: Bode plot of impedance of the electrochemical cell

In the frequency range of the voltage sweeps as defined in the previous section, $10\,mHz - 10Hz$, the impedance has a constant magnitude of $1,700\,\Omega$ while the phase delay is between $0 - (-6)°$. This

model shows that the current introduced via ohmic drop with the electrode design will remain below the required threshold even at a full scale sweep of 5 V: $\frac{5\,V}{1{,}700\,\Omega} < 5\,mA$. At higher sweep rates the ohmic drop will be higher possibly preventing sweep rates above $10\,\frac{V}{s}$. Given that these are not a requirement this is not considered a design problem but should be noted regardless.

5.3.2. Voltage Source

A voltage source is necessary to sweep the voltage and induce the electrochemical response. Additionally the voltage source needs to act as a potentiostat to allow the stabilization of the working electrode. These two functions will be treated separately from the design point of view.

Sweep Generation

The voltage sweep can be generated in several different ways. Given that this research is exploratory and not all parameters of the sweep can be determined a priori it should be flexible and programmable. To this end a generation via a PWM is chosen. This is easiest to implement while still providing reasonable accuracy and allowing for simple modification. To further ease execution and allow for the focus to be put on the electrochemical research the PWM is implemented using an Arduino. This open-source HW/SW package implementing an I/O and computation for analog and digital signals allows for quick programming in C++ with extensive existing libraries. It additionally comes with an ADC allowing for integration into the recording electronics. Some disadvantages of the Arduino include lower capabilities of the ADC (i.e. speed, resolution) and somewhat slow computation. Given that none of these parameters are critical to the project the ease of implementation of the Arduino made it an ideal candidate. The final choice of board was an Arduino Nano.

The board has a PWM with a fundamental frequency of (maximally) $62,500\,Hz$, a maximum voltage of $5\,V$ and a resolution of $\frac{5\,V}{255} = 19.6\,mV$. This allows for a sweep of the full range of reaction voltages of the components listed in chapter 4 with an adequate resolution as established earlier and a sufficiently high fundamental frequency as to not distort the output current.

Given that a PWM signal is generated by switching between the maximum value ($5\,V$) and minimum value ($0\,V$) with a duty cycle corresponding to the fraction of the maximum voltage desired an unfiltered signal would not produce the desired output. Thus the PWM signal needs to be filtered using a low-pass-filter (LPF). The time constant of this LPF needs to be much lower than the fundamental frequency of the PWM. A simple first-order RC-filter with a time constant of $50\,ms$ was implemented. This smooths out the carrier signal while still allowing the low-frequency sweeps to pass unattenuated.

The voltage source needs to be able to produce identical sweeps subsequently. This is necessary given that changes between two subsequent sweeps might be interrogated for information on the overall ionic content of the sample. A change between the sweeps can be introduced by charge being retained in the system. This ought to be avoided using appropriate methods.

WE stabilization

A two-electrode system cannot ensure that there is a stable potential between WE and CE. Any chemical reaction could alter the potential difference. Thus a RE is used to stabilize this potential. The setup of the potentiostat relies on the usage of an OpAmp. While the sweep is applied to the positive input the RE is connected to the negative input. The CE is connected to the OpAmp output and the WE is virtually grounded. If a potential difference between RE and CE occurs it is nulled via the feedback-loop containing the OpAmp. Fig. 5.11 shows the schematic of the circuitry described, adapted from [100]. Given that the OpAmp is used in open-loop configuration and the changes to the potential are expected to be both slow and low in amplitude the requirements on the OpAmp are very low and a simple off-the-shelf model can be chosen.

5.3.3. Readout-electronics

Readout-electronics are used to amplify, filter and convert the output current from the analog to the digital domain to make them machine-readable. The current, overlaid with an undesirable faradaic component, is amplified by a transimpedance amplifier (TIA), then low-pass-filtered and subsequently converted via an ADC.

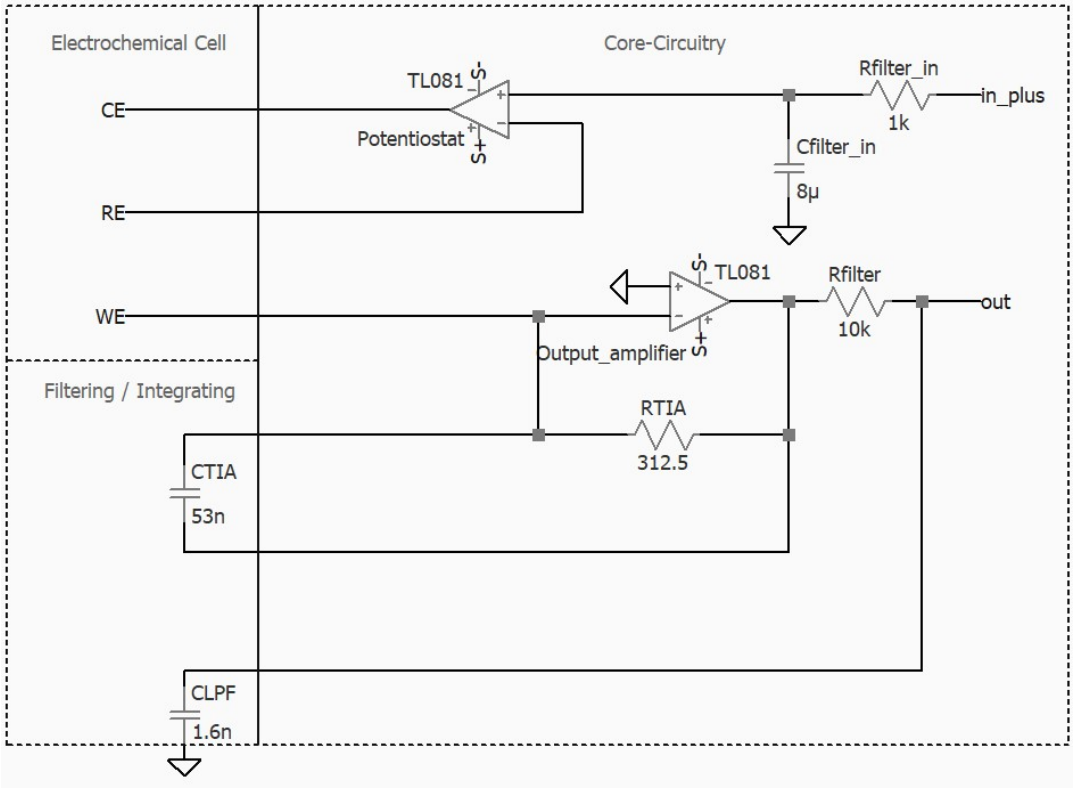

Figure 5.11: Full design of the sensor in LTSpice excluding PWM and ADC on Arduino for simulation of DR, linearity, SNR and WE stabilization

TIA

To read out a current a TIA is the most commonly applied architecture. A TIA takes in a low-signal-power current and outputs a higher-signal-power voltage. The relationship between current and voltage is ideally linear. The amplification of such an amplifier is:

$$A = \frac{V_{out}}{I_{in}} \left[\frac{V}{A}\right]$$

The gain is expressed in Ω giving the amplifier its name - transimpedance amplifier.

To meet noise requirements, slew-rate, bandwidth and open-loop-gain the OpAmp TL081 by Texas Instruments (Texas Instruments, Dallas, USA) was selected. The requirements to the OpAmp are not high leading to the selection of a relatively simple and inexpensive off-the-shelf OpAmp. In a TIA the OpAmp is set into a negative feedback configuration. The closed-loop-gain of the amplifier is determined by the passive elements in the feedback loop.

To establish the desired closed-loop-gain of the amplifier the ionic current of the species of interest at minimum and maximum physiological concentrations were estimated according to the formula presented in chapter 4. Values ranged from $4.97\ \mu A$ at the lowest concentration of Mg_2^+ to $13.4\ mA$ at the highest concentration of Na^+. The sum of currents at maximum concentration was $33.4\ mA$ while an average sample is expected to produce a sum of $19\ mA$. The ratio between the two values is higher than the $60\ dB$ set out in the requirements. Thus, either range or resolution need to be cut in order to achieve the desired performance of the other. Given that the low concentration substances (e.g. Mg_2^+ and Ca_2^+) are considered less useful markers for fatigue the resolution is restricted more than range. This additionally allows for a buffer at the higher end of the scale to take possible electrolysis-current into consideration. The maximum current that can be detected is set at $16\ mA$ allowing for a measurement of the maximum current in most cases while still allowing for the measurement of lower concentration species with reasonable accuracy. Here it should be noted that the above calculations give an envelope. The true value of the ionic current is expected to be considerably lower (by about an order of magnitude) due to influencing factors discussed in chapter 4 including but not limited to, diffusion limited transport, effective area of the electrodes and the assumption that the maximum current of

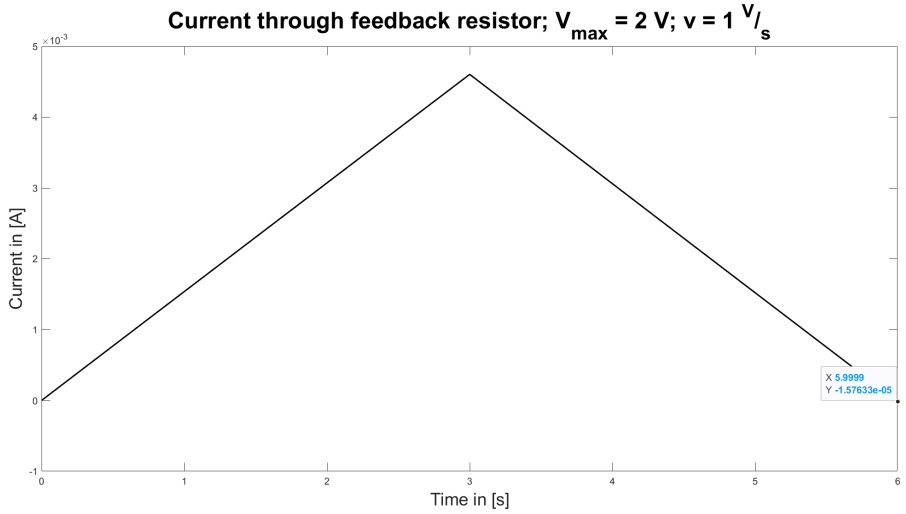

Figure 5.12: Overcurrent with purely resistive feedback after single sweep

all ions overlaps. As such these restrictions to the range are reasonable as can also be seen from the verification. Considering the full-scale value of the ADC ($5\ V$) this gives a closed loop-gain of:

$$A_{closed-loop} = \frac{5\ V}{16\ mA} = 312.5\ \Omega$$

The OpAmp requires supply voltage to output the amplified signal. Given that power consumption is not critical the supply voltage of the OpAmp is set to $\pm 12V$. The supply of the OpAmp was decoupled from the supply rails via a $100\ nF$ capacitor to minimize the influence of supply variations. Simulations in LTSpice showed a significant overcurrent at the end of the sweep as seen in fig. 5.12. The overcurrent added up over multiple sweeps and led to distortion. The current was caused by significant loading of the electrochemical cell. To minimize this current the purely resistive feedback was changed to integration with a corner frequency of $10\ kHz$. This reduced the distortion below the threshold of $\frac{1}{10}$ of the resolution of the sensor.

LPF
A low-pass-filter is placed at the output of the amplifier. This LPF aims to reduce the impact of noise on the output. The signal can, as discussed earlier, be considered DC. Out of an abundance of caution the corner frequency of the LPF is set at $10\ kHz$. The filter is implemented as a first-order R-C filter where R is defined by the trade-off between the input-impedance to the ADC and the load that needs to be driven by the OpAmp. Considering that the ADC can still convert values at maximum speed even with an input impedance of $10\ k\Omega$ and this does not load the OpAmp strongly the resistance is set at this value. Given resistance and corner frequency this sets the capacitance of the filter at:

$$C = \frac{1}{2 * \pi * 10\ k\Omega * 10\ kHz} = 1.6\ nF$$

ADC
The ADC converts the continuous signal that is amplified and then filtered into a discrete signal. Sampling frequency and resolution are set at $1kHz$ and 10 Bits respectively. The in-built ADC of the Arduino Nano meets both these requirements (a conversion generally lasts 13 clock cycles at a frequency of $200\ kHz$).

$$t_{conversion} = \frac{1}{f_{clock}} * 13 = 65\ \mu s$$

The error of the ADC is given in the data sheet as 2 least significant bits [LSB], including quantization error, non-linearity, offset-error and gain-error. The (input referred) error in concentration introduced by the inaccuracy of the ADC is thus in the current setup:

$$\epsilon_{ADC} = \frac{16\ mA}{1024} * 2 = 31.2\ \mu A$$

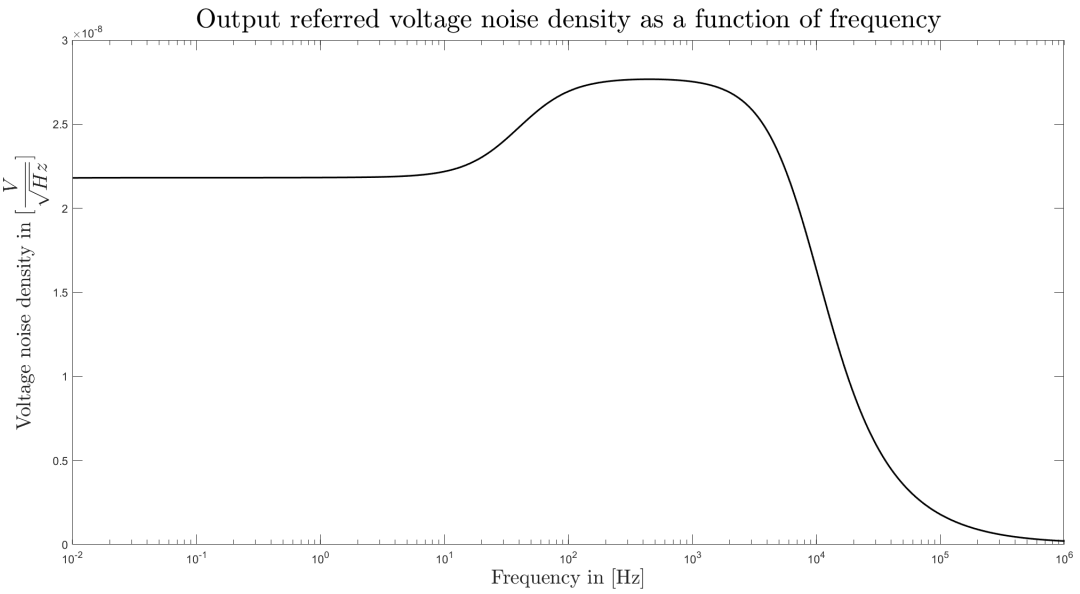

Figure 5.13: Output referred voltage noise of the system at in the frequency range between $10\ mHz - 1\ MHz$

This current transduces to different errors in different ions due to varying diffusion coefficients but is generally in the range of $.2 - .5\ \frac{mmol}{l}$ (assuming ideal ionic current, relative error is higher in practise).

5.4. Design verification

After having presented the design choices, which are rooted in the requirements previously introduced, this section aims to verify the design along the choices that were made. Some choices were already justified by information gathered from different data sheets while other design aspects will be verified either by simulation or testing.
The design of the sensor was transferred to the circuit simulator LTSpice. The resulting circuitry can be seen in fig. 5.11.
Not depicted in fig. 5.11 but implemented between the electrodes in the electrochemical cell on the top left is the model of the Randles cell (with the values previously calculated for an average sample) between each of the electrodes.

5.4.1. SNR

The noise of the system should be low enough to not change the output of the sensor. Fig. 5.13 shows the simulation of the output referred voltage noise. In the range $10\ mHz - 1\ MHz$ the integrated noise is $3.34\ \mu V$. This, even given the wider than required frequency range, still is lower than one LSB of the ADC by more than a factor of $1,000$. As expected from the relatively low requirements on the speed of the system SNR is not an issue.

5.4.2. Range and Resolution

Range and resolution requirements of the system were verified to a first order on a purely electrical level in LTSpice. Given that these are mainly bounded by the resolution of the ADC a simple simulation using the TIA was performed to establish that it limits neither.

Fig. 5.14 shows the output voltage of the TIA after a sweep of the CE voltage superimposed with an excitation of the ionic current. The voltage is swept with usual parameters while the ionic current is stepped from the minimum specified value (bottom) to the maximum specified value (top). In the output voltage a step in the voltage relative to the current input is expected. The curves show the expected behaviour with a step in the voltage of $5\ mV$ and $5\ V$ respectively. The values measured in the graph were corrected by the slope induced by the ohmic drop ($400\ \mu V$). This simulation shows that the readout-electronics does not restrict resolution and range beyond the bounds determined by the ADC.

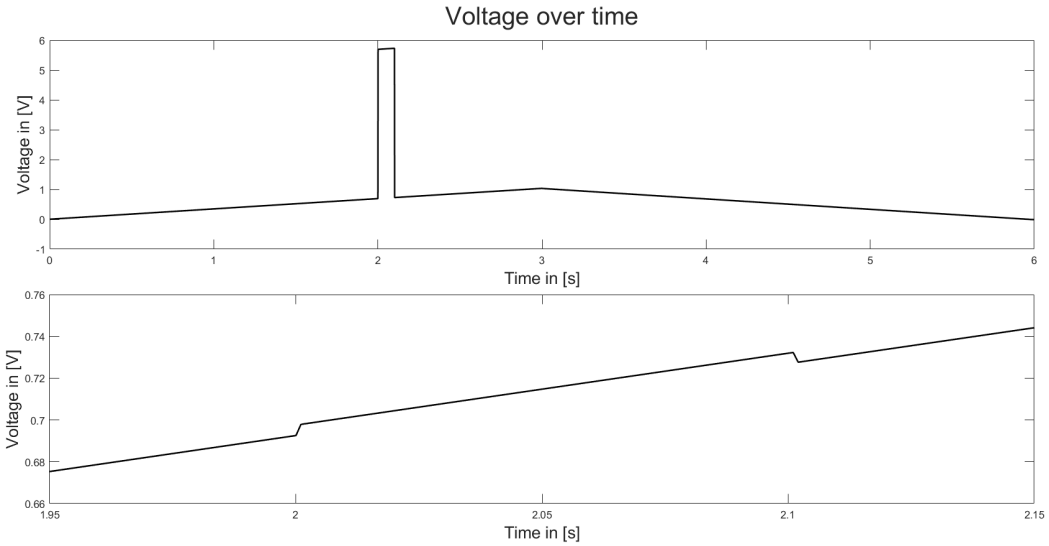

Figure 5.14: Ionic current induced between CE and WE superimposed on voltage sweep; ionic current modelled as pulse ($t_{rise} = t_{fall} = 1\ ms$, $t_{on} = 100\ ms$, $I_{on} = 16\ mA/16\ \mu A$); plotted: (a) output voltage of TIA at $I_{in} = 16\ mA$, (b) output voltage of TIA at $I_{in} = 16\ \mu A$

5.4.3. Non-linearity

Non-linearity is defined as the deviation that a target value has from an ideally linear dependence on another quantity. In this case the non-linearity between ionic current and output voltage of the TIA is researched. To interrogate this relationship the range of the sensor is swept logarithmically and the resulting output voltage is recorded. The result of that sweep along with the ideal linear relationship is plotted in fig. 5.15. The deviation from the ideal linear relationship calculated as an absolute value was found to have a maximum value of $V_{err} = 4.5\ mV$ or less than 1 least significant bit [LSB] of the ADC.

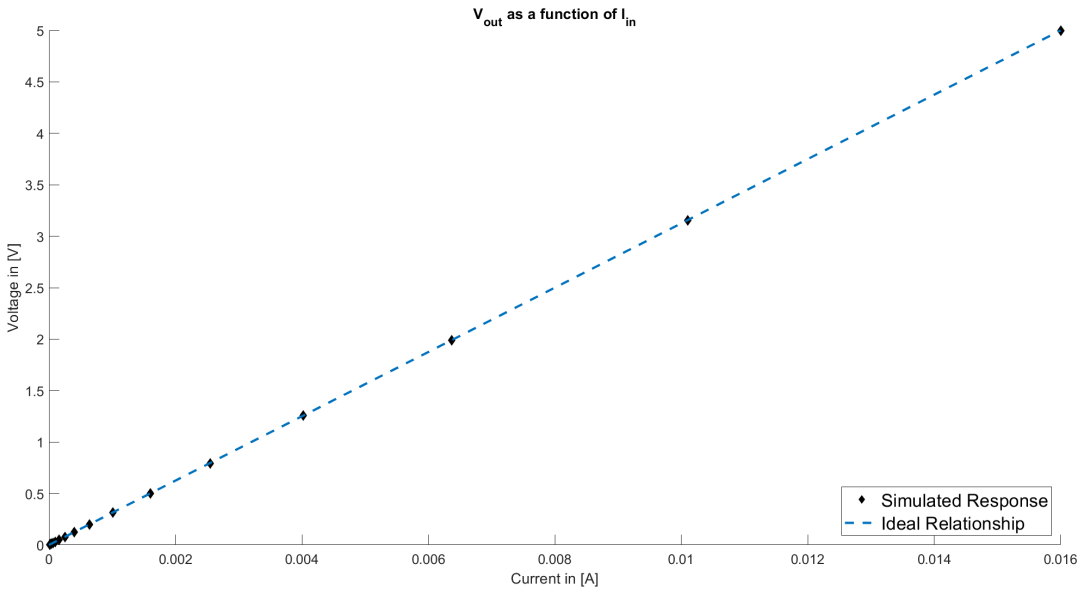

Figure 5.15: Output voltage over sweep of dynamic range of current (black) with ideal linear relationship (blue)

5.5. Lessons Learned

The low requirements to speed, accuracy and dynamic range that are necessary to measure the constituents of sweat relevant to fatigue show that a possible wearable sensor could be produced at low costs. The low requirements also indicate a strong possibility for miniaturization of the sensor. This fur-

ther allows for the sensor principle to be implemented in wearable devices. The electronics are simple and if the focus is not on ease of implementation, as in this proof-of-concept device, an implementation either on a flexible substrate or on chip is plausible. The design presented shows no issues with linearity or SNR but the range of the device could be improved by using a higher resolution ADC and removing this as a bottleneck. Furthermore the speed of the ADC and processor could be improved to allow for FSCV. Additionally while the implementation of the PWM again was easiest, replacing this component with a DAC would allow for more varied waveforms such as SWV or DPV.
The simplicity of the design presented here allows for a variety of performance improvements in a possible prototype. As a proof-of-concept the design meets the requirement of being as simple as possible.

6

Implementation

Implementation is the process of transferring the system from the sole simulation domain into the physical representation. This project has two major parts to the implementation: electronics and software.

6.1. Electronics

Electronics were built independently instead of using a prefabricated potentiostat chip. This allows for the implementation of different waveforms, voltage sweep rates and maximum voltages. Most commercial chips only allow for a limited selection of waveforms and additionally the usage of the voltammetric source in combination with the readout on the same chip allows for easier communication and coordination of the system. The implementation of the electronics from the simulation into the physical domain is relatively simple with this design. This is owed to the streamlined proof-of-concept approach. The design was done with implementation in mind and due to the low requirements on component variations and interconnect parasitics the design can be implemented on a breadboard. This allows for both an easy setup with little material costs and quick adaptability. The system can be setup in a few hours of work and can be adapted and reiterated upon easily. The adaptability is crucial to a proof-of-concept. Any unforeseen variations in influencing factors (e.g. EMI, temperature, component variations etc.) can quickly be addressed.
Any second version of this design that treats with an application closer to a working wearable sensor will necessarily be adapted onto a PCB or chip. Adaptations in the design would be necessary to allow for a change of platform.
Fig. 6.1 shows the implementation of the sensor and the general experimental setup. A quick description of the components, their function and possible issues follows:

6.1.1. Voltage Source

The voltage source is implemented as a symmetrical source. The voltage source is able to supply the $\pm 12\ V$ required by the system. The source can supply $600\ mA$. This is far above the required power of the system. The supply has a stable output voltage that allows for an equal stability of the result voltage.

6.1.2. Arduino Nano

The chosen control system for the proof-of-concept is a microcontroller. For the design at hand the microcontroller easiest to implement was chosen. The Arduino Nano is a microcontroller containing an I/O, a PWM generator and an ADC. The parameters of the Arduino meet the requirements set out by the design. The Arduino is easily accessible allowing for a more flexible software development. Changes to the software can be uploaded quickly and the Arduino allows for programming in a language similar to C++.
The accessibility and simplicity of the Arduino makes it ideal for applications in a proof-of-concept. It is however limited in its capabilities. The accuracy of the PWM and the resolution of the ADC are main limiting factors to the overall system resolution and accuracy. However if the system can be shown

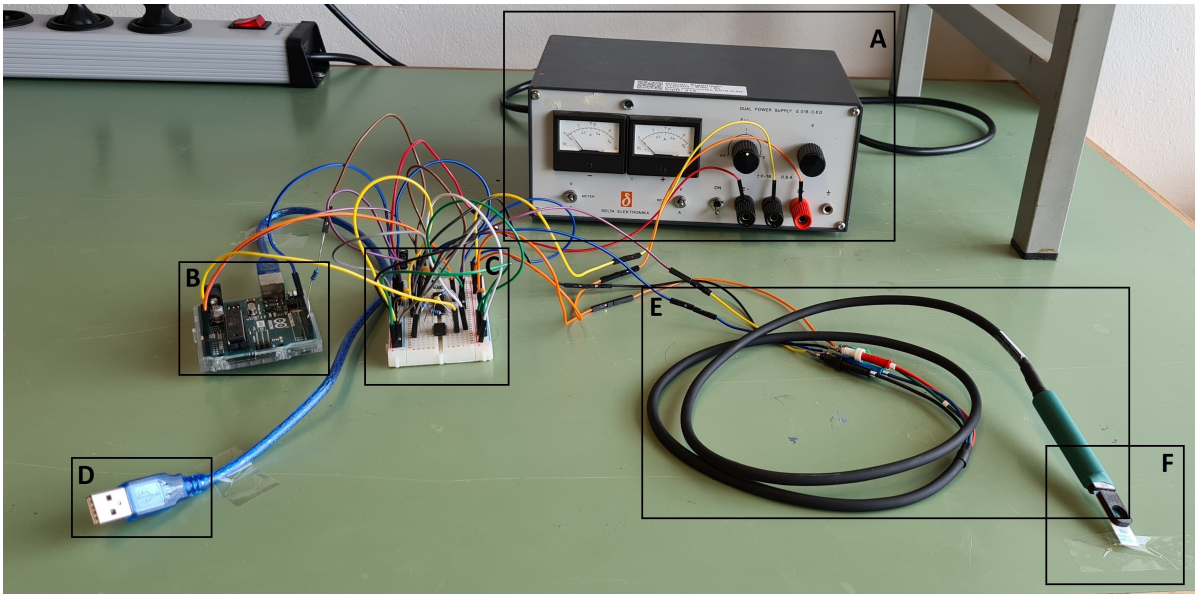

Figure 6.1: Implementation of voltammetric sweat sensor with (A) voltage source, (B) Arduino Microcontroller with ADC, (C) sensor electronics, (D) connector to laptop, (E) connector to electrode, (F) electrode

to function with these components it is likely to work with more miniaturized electronics as well. The advantages of the Arduino outweigh the disadvantages for this experiment.

6.1.3. Serial Connection

The Arduino receives its supply voltage via a USB-connector. The cable simultaneously is the data connection. That dual function both eases the implementation but also complicates the transfer somewhat. A Laptop cannot provide a very stable supply voltage given that the usage of other parts of the device and the data transfer load the voltage source. These deviations could theoretically affect the stability of the system. Practical tests show that the voltage source of the Laptop is stable enough to not introduce significant distortion.

6.1.4. Sensor Electronics

The sensor electronics are implemented as through-hole components on a simple breadboard. The advantages of the breadboard were discussed above. The particular application requires the usage of a rather high amount of cables. The setup with the breadboard and associated wiring did not give any problems with regards to electrical interference.

6.1.5. Electrodes and Connector

The connector of the electrode is a specialized cable provided by the supplier of the electrodes. The requirements and implementation of the electrodes have been discussed in the previous chapter.

6.2. Software

The software for the device is kept simple. It has two main components: the generation of the voltage sweep and the conversion, transmission and recording of the analog voltages.
The voltage sweep was, at first, as described previously, generated by a PWM-signal. The signal had to be internally set to the highest fundamental frequency. To control the sweep rate of the system the steps were timed using the theoretical value for their length. This value was calculated from the final value of the sweep, the resolution of the PWM and the desired sweep rate. The timing is then controlled in the software via a state machine. Measurements and transformations are performed synchronously every ms. Once the set number of integer ms have elapsed the system idles the remaining time and then iterates to the next voltage step. The voltage is stepped up and down at the same speed (using a 'for' loop) producing a LSV signal.

The sweep was later also implemented using a DAC with better accuracy and allowing for DPV. The DAC is addressed using a serial peripheral interface. Beside the communication with the Arduino the generation of the voltage sweep is identical with the PWM.
The second main function of the software is to convert, transmit and record the data. During each cycle three measured values are of interest:

- CE-voltage
- sweep-voltage
- output-voltage

One millisecond is too short for the ADC to perform three conversions and subsequently send four values on the serial connection (including a timestamp). The bottleneck is the relatively slow serial.println() function. To attain data with reasonable temporal resolution regardless, the values are converted every cycle and added to an array. The array is then summed every four cycles and sent to the laptop. Which value is sent each cycle is determined by an incremental data-selector. Each cycle contains three analog conversions and one serial send. The data sent via the serial port is saved to a CSV-file using a serial terminal. The full code can be found in Appendix B.

7

Experiments and Results

After design and implementation of the sensor are completed, experiments are performed to characterize the sensor. The experiments aim to verify the assumptions made in the design and determine the usability of the sensor for real-time measurements of ionic concentrations in sweat.

7.1. Experimental Planning

To achieve the goals set out for the experiments above, experimental planning is necessary. Given the complexity of the sensor with regards to influencing factors and variations in the analyte to be tested a regimen of experiments is determined. These experiments aim to atomically verify the corresponding system requirements. The tests are not exhaustive and rather defined roughly along the lines of the requirements. Additionally the experimental planning is iterated throughout the process to account for the results of previous experiments.
Preliminary experiments will verify adherence to electrical parameters such as:

- range; sweep voltage
- sweep rate
- overshoot; sweep voltage
- resolution; current measurement
- range; current measurement
- WE stabilization

After these fundamental parameters have been established first experiments with different ionic fluids can be performed. These 'wet' experiments aim to establish the ability of the system to:

- recognize the presence of certain ions
- distinguish between concentrations of these ions
- measure the ionic concentration of the ion reproducibly
- characterize differences in the response of electrode materials
- establish a calibration curve for ions

This will require analysis of different voltammograms recorded using the complete sensor. This section of experiments aims to establish the system as an electrochemical sensor.
A set of experiments with more complex ionic fluids containing multiple ions will be performed. During these experiments the capability of the sensor to discriminate ions in presence of each other will be probed. The ionic fluids will be representative sweat surrogates adhering to physiological limits. This set of experiments will reveal to what degree the measurement of ionic concentrations in sweat using cyclic voltammetry is viable for miniaturized real-time applications.
Lastly, real sweat samples will be characterized using previously acquired calibration curved.

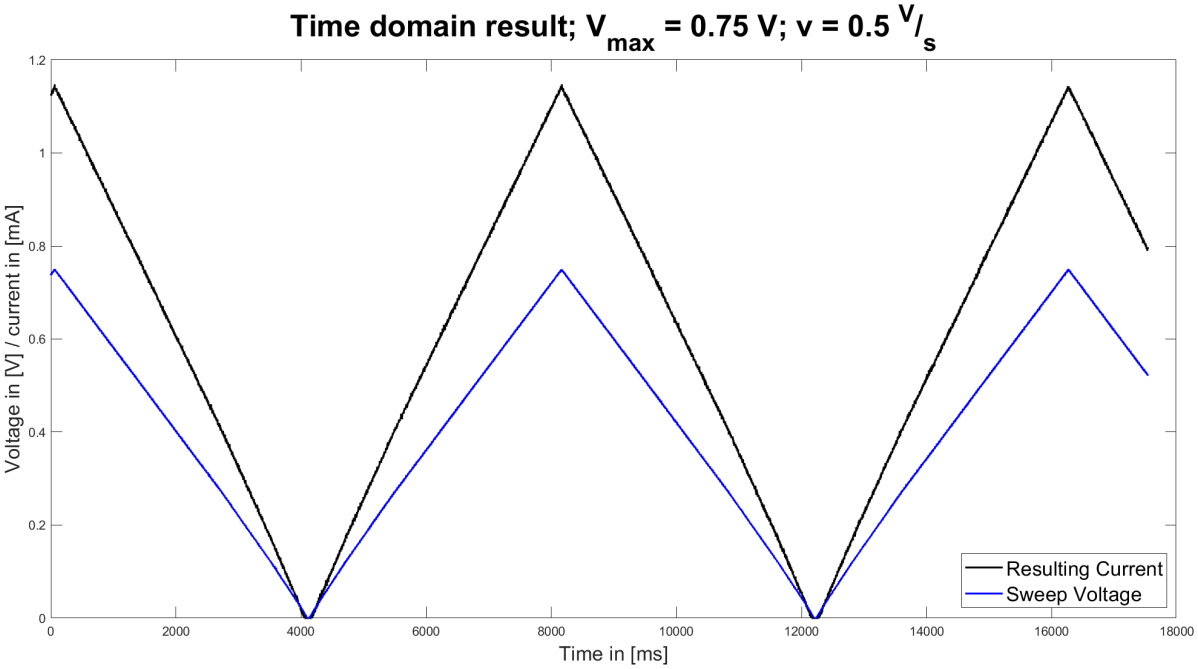

Figure 7.1: Dry test of voltage sweep with linear $1,300\ \Omega$ load, $V_{max} = 0.75\ V$ and $v = 0.5\ \frac{V}{s}$

7.2. Preliminary Experiments

Preliminary experiments are performed 'dry', that is without the addition of sweat surrogate or even the connection of the electrodes. This reduces the sensor to its fundamental components. It allows verification whether the sweep provided by the PWM is adequate with sufficient accuracy in amplitude, timing and symmetry. Furthermore, the response of the system to non-linear inputs can be tested in a well-defined environment.

The dry test necessitates the usage of equivalent impedances between the electrodes to represent the impedance of the electrochemical cell. Fig. 5.10 shows the impedance profile of the electrochemical cell over frequency. It is evident that in the frequency range of interest the impedance of the cell is relatively constant. The amplitude of the impedance is dominated by the ionic conductivity of the sweat. Assuming an average sweat sample the impedance is $\approx\ 1,300\ \Omega$ at a phase angle close to $0\ °$. Thus the electrochemical cell is represented using three $1,300\ \Omega$ resistors between each pair of electrodes.

The first dry test performed is a sweep of the voltage from an initial voltage of $0\ V$ to a final voltage of $0.75\ V$ at a sweep rate of $v = 0.5\ \frac{V}{s}$. The resulting voltage and current over time are plotted in fig. 7.1. This test and similar experiments with different V_{max} and v show that the system is able to apply voltages at the designed sweep rates and ranges. The accuracy of the dry sweep is $\approx 0.5\ \%$ in both amplitude and frequency. The measures taken in the design to avoid charging of the system were successful. The variations between the different peaks and zero-crossings of the current show no significant charging.

Having performed the first experiments on a purely linear system the load is altered. In addition to the resistors modelling the electrochemical cell diodes are clamped between CE and WE. This induces a non-linear response of the current and shows that the system is capable of measuring these. The load used in the experiment shown in fig. 7.3 is a diode in parallel with a series connection of a small resistor and another diode (see: 7.2).

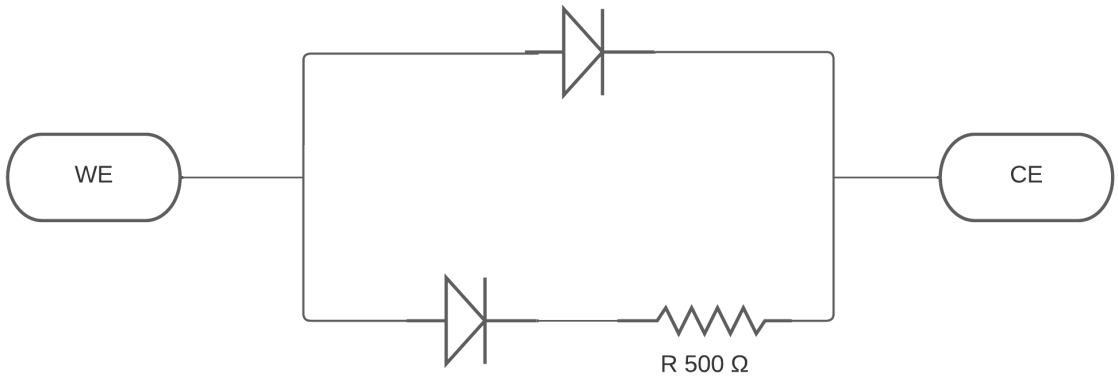

Figure 7.2: Schematic of dry test using diodes

The resulting current shown in black displays the expected characteristics with virtually no current until the built-in voltage of $0.7\,V$ of the singular diode is reached. The slope of the current changes again when the second diode starts conducting. The clipped current is reflective of the current limitations of the particular diodes used.

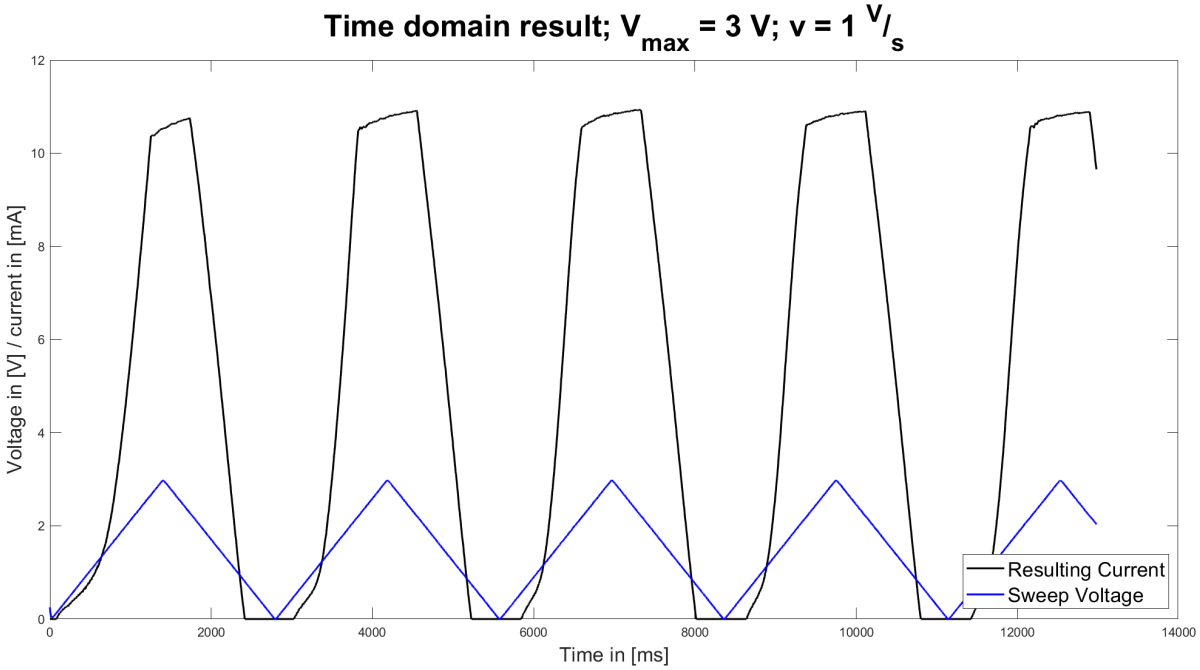

Figure 7.3: Dry test of voltage sweep with diode-load $V_{max} = 3\ V$ and $v = 1\ \frac{V}{s}$

The dry experiments additionally included tests of the WE stabilization. To this end a potential was applied to the CE relative to the RE and the voltage response of the system was tested. The tests showed that the WE stabilization is functional and can nullify differences between the two electrodes with sufficient speed.
Overall the preliminary experiments were successful and verified the design. The results of the dry experiments pave the way for further experiments and do not call for action on changing the system.

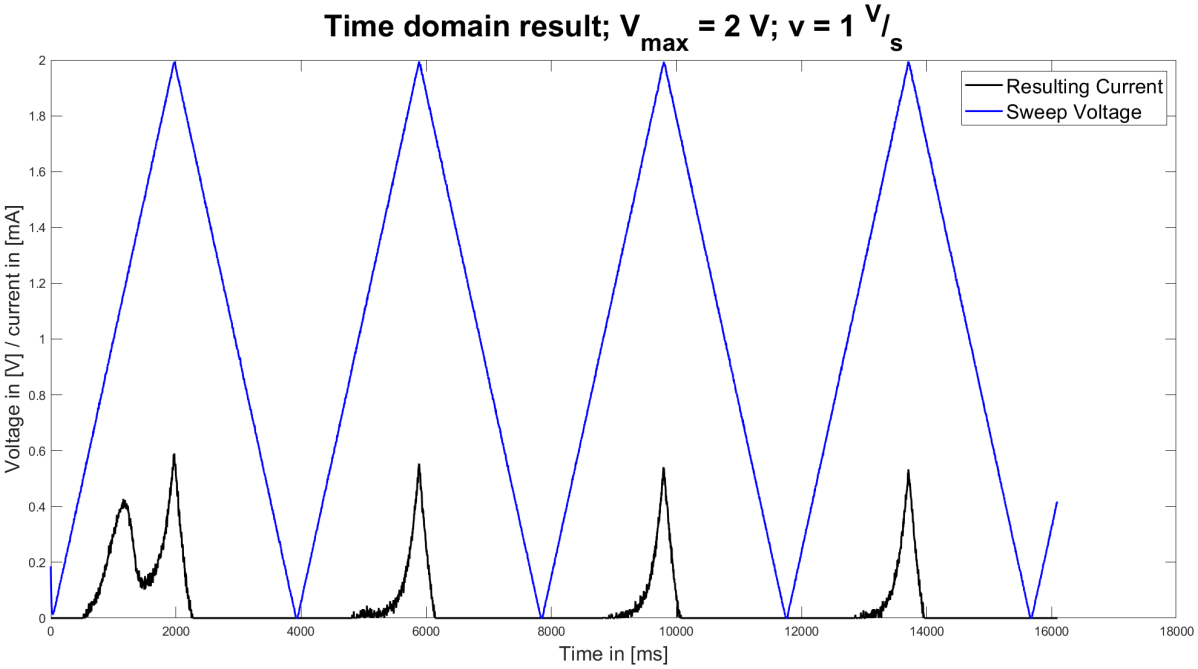

Figure 7.4: Time domain Sweep voltage and resulting ionic current of $60\ \frac{mmol}{l}$ [Na^+] swept with $V_{max} = 2\ V$ and $v = 1\ \frac{V}{s}$ using a CNT-electrode

7.3. Calibration

To establish the usability of the system as a sensor for ionic concentration it needs to be calibrated. In this process the system is presented with different known concentrations of ions and the response is recorded. A relationship between concentration and recorded ionic current is then established (also called the calibration curve). Measured currents can then be mapped to this curve to find the concentrations in unknown samples. This calibration will contain three major steps. Firstly, the response of the sensor to a generalized ionic fluid is characterized. This aims to establish the major parameters of interest. Secondly, the voltammograms is recorded for different ionic concentrations and different electrode materials. Lastly, the voltammogram is analysed, the ionic current measured and the calibration curves are generated.

7.3.1. General Ionic Fluids

To start the calibration process the impedances representing the electrochemical cell are removed. The respective nodes on the electronics are then connected via the connector cable to the electrodes. The reservoirs are then glued to the electrodes. Subsequently the reservoirs are filled with roughly $150\,\mu l$ of the fluid under test. The ionic fluids are prepared using demineralized water and NaCl ($> 99\ \%$ purity) weighing the salt with a precision scale.
Once connected to the electronics and filled with the fluid the system is powered up, starts sweeping the voltage and sending the data on CE-voltage, sweep voltage and ionic current to the laptop.
Since cations in sweat are more varied and their detection more challenging the first sweeps and the calibration were performed on such a cation, namely Na^+. This allows for data from the calibration and insights gathered during the measurement to be transferred to the analysis of multiple ions in solution. Fig. 7.4 shows the time-dependent behaviour of the electrode filled with $60\,\frac{mmol}{l}$ [Na^+]. The result gives rise to several insights. Observing the first curve of the resulting current it has a peak corresponding to the first voltage sweep. Additionally to that ohmic peak there is a secondary local maximum at around $1,200ms$. This local maximum is the ionic current. It does not occur on subsequent sweeps. Instead the following curves have an asymmetric left-sided tail. This indicates that the reaction leading to the ionic current majorly takes place during the first sweep and only remnants remain on subsequent sweeps. This effect is mainly owed to a layer forming on the electrode preventing further reactions. The lack of flow combined with the formation of NaOH leads to the formation of this layer. The existence of the

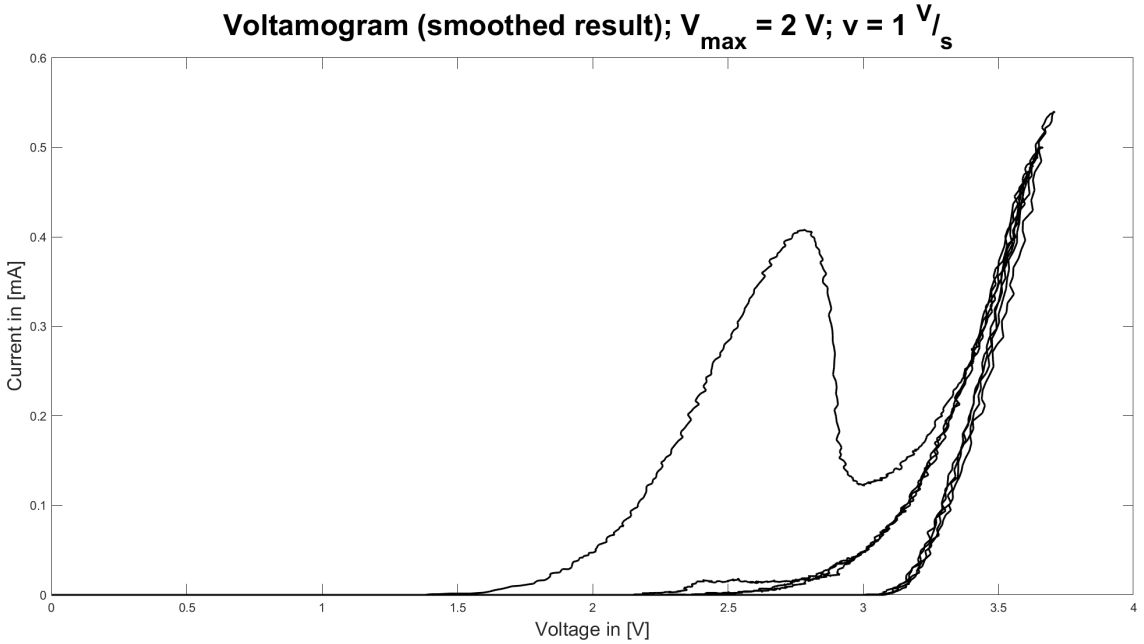

Figure 7.5: Smoothed voltammogram (time averaged over 20 ms, ionic current [mA] over CE-voltage [V]) of $60\ \frac{mmol}{l}$ [Na^+] swept with $V_{max} = 2\ V$ and $v = 1\ \frac{V}{s}$ using a CNT-electrode

layer is supported by the findings on the stress test including changes in the electrode surface and pH changes in the test-fluid. Altering the experiment by adding the electrode to a beaker and moving it leads to ionic current on subsequent sweeps. However this form of flow is too chaotic to produce repeatable results. For the purposes of this proof-of-concept only the first wave is evaluated. This does not infringe on the overall usability of the sensor. If a microfluidics platform with proper flow were implemented the existing literature indicates a semi-continuous measurement would be feasible. The fact that the peak is singular and there exists no equal and opposite peak in the return sweep indicates that the reaction is irreversible. The shape of the ionic current corresponds with theory while the height of the peak is roughly a factor 10 lower than expected at that concentration. This finding eases up on the range of the sensor compared to the design requirements while restricting the resolution below the designed value. Low concentrations of e.g. Ca_2^+ cannot be detected as intended. Apart from the chemical reaction introduced by the sodium ions the impedance of the cell appears to be real and not introduce a significant phase shift, as expected. To derive the actual ionic current of the experiment further data processing is necessary.

The next step in that data processing can be seen in fig. 7.5. This is the generation of a voltammogram. In this plot the ionic current is related to the voltage of the CE relative to the WE. The peak previously seen in the time domain result is now clearly visible. The location of that peak on the x-axis is $2.7\ V$ which corresponds with the reaction voltage of sodium. The peak of the ionic current can thus be identified as attributable to a reaction including sodium and it stands to reason that the amplitude of the ionic current is relative to the concentration of sodium in solution. The analysis of the data of the following calibration will support this statement. The asymmetry in the voltammogram with no reverse current is indicative again of the irreversibility of the reaction, while the absence of peaks on subsequent sweeps indicates the aforementioned formation of a layer on the electrode. To measure the ionic current it is not sufficient to simply record the peak height. The peak needs to instead be referred to a baseline current. The estimation of this baseline requires an extrapolation of the ionic current between the slopes before and after the peak. In more mathematically rigorous terms a linear interpolation is made between the inflection point left of the maximum and the local minimum right of the maximum. The height on the x-axis of the local maximum over the linear interpolation is the ionic current. The interpolation of the baseline can be seen visualized in fig. 7.6. An interpolation of the baseline will be necessary for each peak individually possibly complicating the data processing. With the location and amplitude of the ionic current peak the measurement is complete. A set of these measurements will constitute the calibration.

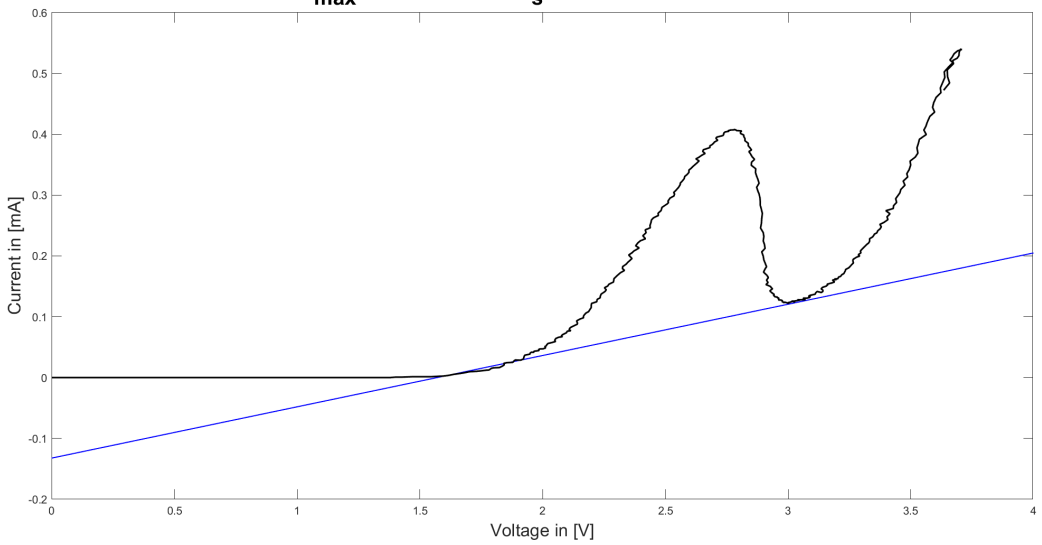

Figure 7.6: Smoothed voltammogram (time averaged over 20 ms) of $60\ \frac{mmol}{l}$ [Na^+] swept with $V_{max} = 2\ V$ and $v = 1\ \frac{V}{s}$ using a CNT-electrode, first wave with interpolation of baseline

7.3.2. Electrode Materials

The measurements of the ionic current in the course of the calibration were performed with all available electrode materials. The two different gold surfaces proved insufficient for this application. When applying any voltage larger than $1.5\ V$ a visible formation of bubbles could be observed. This bubble formation also disallowed any measurement of current with a reasonable degree of accuracy. The reaction was likely caused by the dissolution of the gold by the environment formed by water splitting. While the test fluid could not be analyzed properly after the voltammetry it is likely that Au_2Cl_6 complexes formed during the voltammetry. The platinum and CNT surfaces do not form such compounds and thus worked adequately as electrodes. All following experiments are preformed using either Pt or CNT electrodes.

A certain degradation of the electrode sensitivity could be observed but could not be approximated in a first order. The degradation is likely due to the filling of pores in the electrode surface and subsequent reduction of the effective electrode area. Measurements of the surface roughness of the electrode factory new compared to used in a number of measurements (chapter 7.7) will show the validity of this theory.

7.3.3. Calibration Results

To calibrate the sensor five different concentrations of NaCl solution were prepared. The concentrations of these solutions cover the entire physiological range between $10 - 100\ \frac{mmol}{l}$. The measurements were performed as described above with the filling of reservoirs, recording of the voltammogram and measurement of the ionic current relative to the baseline. Each of the five solutions was measured four times using both materials available for a total of 40 measurements. The measurements were scattered so that any order put to them would not influence the result (i.e. the measurements were not taken in an order high to low or vice versa). Additionally the electrodes of each material were exchanged once during the calibration to counteract the degradation. Electrodes were rinsed with demineralized water after each measurement.

The data processing of the measurements was performed using a code for the best approximation of the baseline current curve to avoid user error while calibrating. Fig. 7.7 shows the calibration data with averages and standard deviations for each concentration as well as a linear approximation of the calibration curve.

The scatter plot shows a strictly rising current for a rising concentration of Na^+ in solution. The results

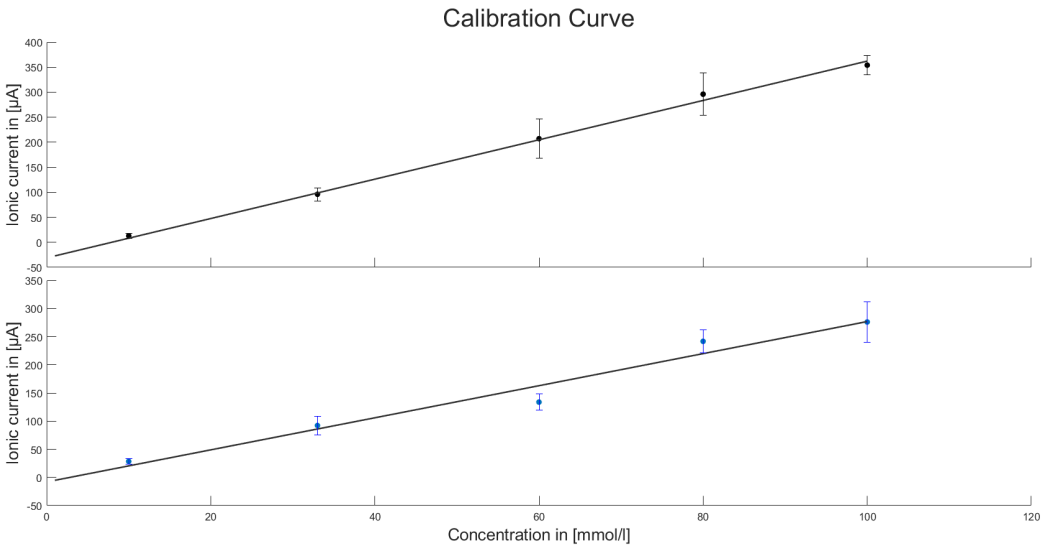

Figure 7.7: Calibration curve (linear approximation) of ionic current in [μA] over concentration of Na^+ in [$\frac{mmol}{l}$] during calibration with ionic fluids of known concentration, with CNT ($R^2 = 0.967$) in black, top and platinum ($R^2 = 0.997$) in blue, bottom

show a relatively high standard deviation. The most likely causes of this are changes to the electrode (cleaning with demineralized water notwithstanding), residual layers of fluid on the surface that are difficult to dry in this setup and variations in the determination of the baseline current. It is evident from 7.7 that while platinum shows a lower relative standard deviation, the linearity of the CNT electrodes is better.
Overall the calibration shows promising results. The sensitivity of the system to Na^+ is at $\approx 6 \frac{\mu A}{\frac{mmol}{l}}$lower than the envelope of the current by about a factor 20. Furthermore the system has a negative offset of, depending on the material, $\approx 5 - 27\,\mu A$. However the linearity of the calibration curve especially for the CNT electrode is very good. If multiple measurements are taken averaging will be able to overcome the moderate standard deviation to provide robust measurements of the concentration.

7.3.4. Sweep Rates

The sweep rate is a determining factor for the ionic current. As discussed in eq. 4.1 the ionic current rises with the square root of the sweep rate. This rise in current is owed to both a rise in the charging current as well as the faradaic current. Assuming a freely diffusing species (i.e. no adsorption of the species onto the electrode prior to sweeping) the rate of diffusion is increased when the sweep rate is increased. This in turn increases the faradaic current. The charging current is similarly increased since the higher sweep rate leads to a thinner diffusion layer and thus a higher capacitance to be charged [70]. The Randles-Sevcik equation 4.1 is thus only an approximation. The real dependence of the ionic current on the sweep rate can vary with a number of factors with the adsorption of the species onto the electrode being the most impactful one. To test the impact of the sweep rate and determine a preferred sweep rate for further experiments a sample of $100 \frac{mmol}{l}$ [Na^+] was swept using a Pt electrode at different sweep rates. The resulting voltammograms can be seen in fig. 7.8.
Between the sweep rates tested the difference in current is clearly visible. The relationship of the ionic current with the sweep rate correlates closely with the prediction made by eq. 4.1. For further testing the sweep rate is generally set at $1 \frac{V}{s}$ since this voltammogram expressed the most distinctive curve features which will be used to distinguish the presence of multiple ions in the next section.

7.4. Multiple Ions in Solution

The stated goal of this thesis is to explore the possibility of measuring the ionic concentrations in sweat using cyclic voltammetry. To this end it is not sufficient to simply measure a single ion and show that

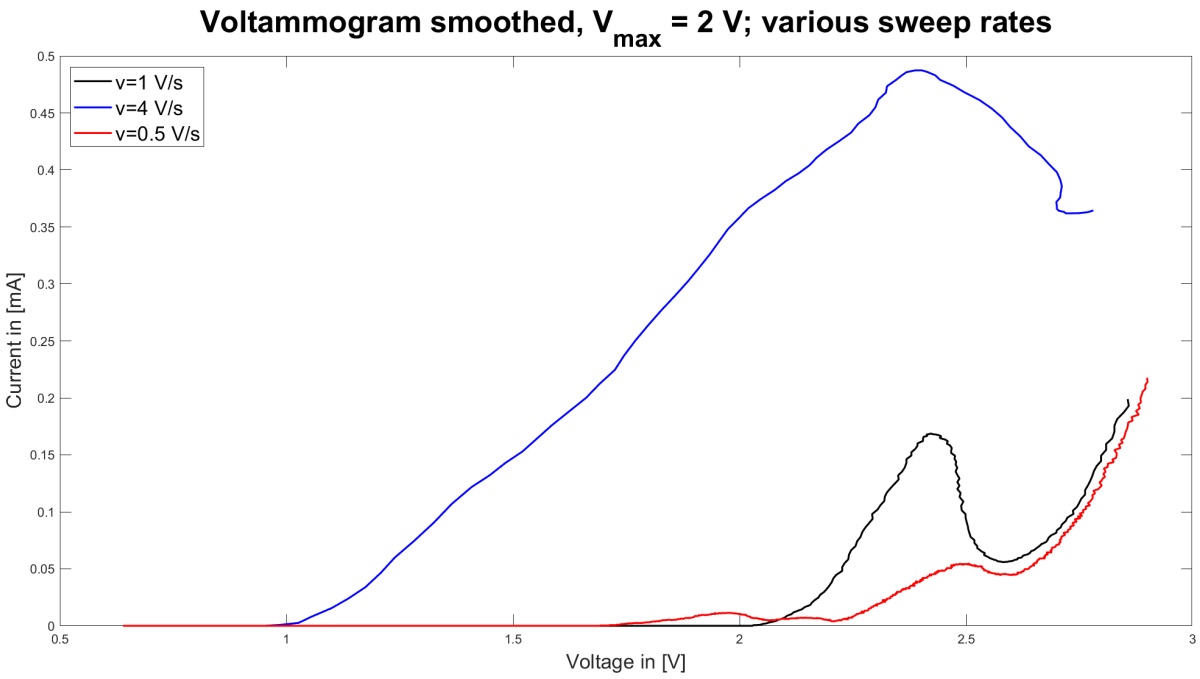

Figure 7.8: Smoothed voltammogram (time averaged over 20 ms) of $100\ \frac{mmol}{l}$ [Na^+] at different sweep rates ($v = 500\ \frac{mV}{s}; 1\ \frac{V}{s}; 4\ \frac{V}{s}$); recorded with Pt electrode

the system can create a linear relationship between the measured current and the concentration of that ion in solution. Rather it is necessary to measure the current produced by different ions in presence of each other. Ideally the system would show different peaks at the reaction voltages of different ions in solution.

To approximate the measurement of different ions in sweat a solution containing physiological levels of ions is created. A surrogate solution to test the capabilities of the system contains $100\ \frac{mmol}{l}$ [Na^+] and $10\ \frac{mmol}{l}$ [K^+]. The combination of sodium and potassium brings with it a major theoretical challenges. The value of the reaction voltages of the two ions is separated by $220\ mV$. This would lead to the separate peaks not having fully independent baseline currents. Fig. 7.9 shows that this point is moot.

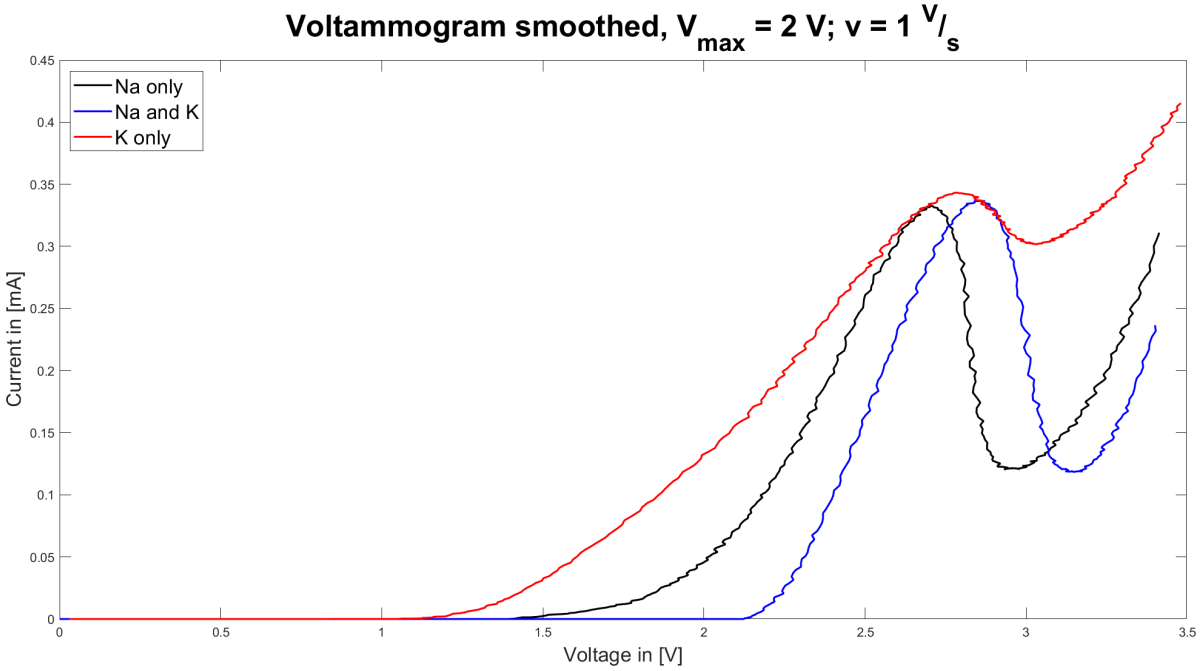

Figure 7.9: Smoothed voltammogram (time averaged over 20 ms) of linear sweep with $V_{max} = 2\,V$, $v = 1\,\frac{V}{s}$ of solutions with a concentration of $100\,\frac{mmol}{l}$ [Na^+], $10\,\frac{mmol}{l}$ [K^+] and a combination of both

Fig. 7.9 shows the voltammograms of three different solutions being linearly swept at the same sweep rate and utilizing the same maximum voltage. The solutions contain either Na^+ or K^+ in physiological levels or a combination of both. While parameters of the three curves such as the location of the peak, ionic current and location of the first current differ the overall shape of all curves is the same. There are no separate peaks in the voltammogram of the complex ionic fluid.
Given the absence of peak separation another approach to distinguishing two ions in solution is necessary. Solutions were prepared with the same concentration of Na^+ as those used in the calibration. These were supplemented with medium and high physiological concentrations of K^+ ($5 - 10\,\frac{mmol}{l}$) by adding KCl to the solution. The voltammograms of the new solution were acquired in the same procedure as the calibration. From these voltammograms a set of parameters was extracted including:

- ionic current
- absolute peak height
- peak location
- valley height
- valley location
- relative height peak / valley
- distance peak / valley
- first current location

Voltammogram, smoothed; V_{max} = 2 V; v = 1 $^{V}/_{s}$; (1st wave with linear interpolation of baseline)

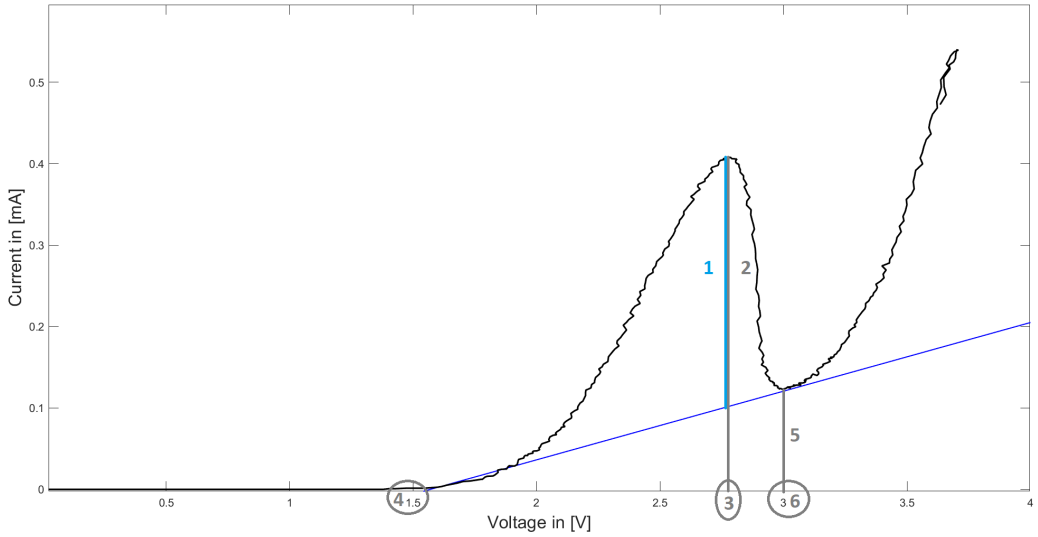

Figure 7.10: Typical voltammogram with curve features marked: (1) ionic current, (2) absolute peak height, (3) peak location, (4) first current location, (5) valley height, (6) valley location

The different parameters are marked in fig. 7.10. Beyond the parameters marked they are defined as relative height peak / valley ($(7) = \frac{(5)}{(2)}$) and distance peak / valley ($(8) = (6) - (3)$) and lastly distance first / peak ($(9) = (3) - (4)$). The same parameters were extracted from the existing calibration data. Finally these parameters describing the voltammogram were compared between the sodium-only solution and the combination of sodium and potassium. The null-hypothesis of this experiment was the existence of a set of at least two independent parameters between the two curves being statistically significantly different. If this hypothesis holds a set of equations can be found relating the parameters of the curve to the concentrations of both ions in solution.

Parameter	Value Na^+ only	Value Na^+ and K^+	p-value
peak location	2.72 V	2.81 V	0.0052
first current location	1.98 V	2.13 V	0.0493
distance first / peak	0.74 V	0.68 V	0.3286
valley location	3.01 V	3.06 V	0.046
relative height valley / peak	0.25	0.29	0.2528
ionic current	364 μA	316.5 μA	0.0042
valley height	90.28 μA	92.28 μA	0.8819

Table 7.1: Selected characteristic parameters of voltammogram between solutions of $100\ \frac{mmol}{l}$ [Na^+] and $100\ \frac{mmol}{l}$ [Na^+] & $10\ \frac{mmol}{l}$ [K^+]

Table 7.1 shows a snapshot of the data collected in the measurement of the characteristic parameters of the voltammogram. It compares the parameters such as peak current location or relative valley height directly to each other. The p-value is calculated in a double-tailed t-test between the two values with their attached standard deviations and a number of samples $n = 4$. The table shows that the difference in first current location and valley location are statistically significantly different between the two samples ($p < 0.05$). The difference in ionic current and peak current location is highly statistically significant ($p < 0.01$). Other parameters are not statistically significantly different. While valley location and peak location are correlated there is no such correlation between the other parameters leaving three parameters to be significantly different. While table 7.1 shows only the comparison between two solutions these differences appear to exist between all concentrations of sodium as long as the ratio of

sodium to potassium is not higher than 10:1

$$\frac{C_{Na^+}}{C_{K^+}} < 10 \tag{7.1}$$

[101] explored the concentrations and absolute electrolyte loss in athletes at low and moderate exercise intensity and found the ratio of the two constituents to be just below that value. Thus we might conjecture that this technique could be suitable for the simultaneous measurement of K^+ and Na^+ in sweat. More research will be necessary to establish the exact relationship between the concentrations and the shape of the voltammogram. This will aid to establish the set of equations to determine the concentrations from it. Qualitatively, the relation of concentration can likely be established from the location of the peak while the ionic current is determined by the absolute concentration of sodium minus the absolute concentration of potassium.
The peak current is determined by a subtraction of the sodium and potassium concentration. This subtraction may seem counterintuitive at first given the initial expectation of two distinctive peaks with height relative to the concentration of the individual ions. This relationship is however not present. The height of the peak, while strongly correlated with the ion in solution as shown by the calibration, is presumed to be mainly a function of the reaction between those ions and a hydroxyl-group. Both sodium and potassium compete for reaction spots with these groups. When potassium reacts less current is induced (as is observed in the lower sensitivity of the sensor to potassium).
The above discussion of multiple ions in solution shows clearly the limits of a voltammetric system for the measurement of ionic concentrations in sweat. Sodium is the most abundant cation in sweat. Any measurement of other cations will occur in a matrix of those ions with sodium. The analysis above indicates that for any ion to make a measurable impact on the voltammogram the relation of their concentration on that of sodium should be at least $1 : 10$. In a physiological sweat sample that would allow for the measurement of sodium, potassium and ammonia. Given the two independent factors described above and adding a measure for total ionic content (e.g. conductivity [before reaching any reaction voltage]), relative to the sum of all concentrations, the measurement of these three constituents seems feasible.
Further experiments were performed to define more accurately the relationships between the concentrations in solution and the peak position and ionic current. The first experiment in this series characterized the voltammogram of solutions with the same total ionic content but different ratios of concentrations of Na^+ and K^+. The data gathered from this experiment was inconclusive, showing a statistically significant difference in the parameters between the different ratios but not revealing any discernible trend. It should be noted, that these solutions were not representative of physiological sweat. Furthermore a matrix of different ionic solutions in the physiological range was measured. Solutions were prepared using 33, 60, 80 and 100 $\frac{mmol}{l}$ [Na^+] & 5 and 10 $\frac{mmol}{l}$ [K^+] respectively as well as any combination of the two ions for a total of 14 solutions. These were calibrated using a CNT as described previously. Of the curve parameters ionic current (1) and distance first-peak (9) showed the most predictable behavior. Fig. 7.11 plots the ionic current over the absolute of the difference in concentration between sodium and potassium while fig. 7.12 depicts the dependence of the distance first-peak over the sum of the ionic content. Both show a reasonably linear behavior. As it stands the variation of the experiments, while comparatively high, still allows for the creation of two independent equations describing the two different concentrations. With these equations an estimation of the concentration in an unknown sample is possible.

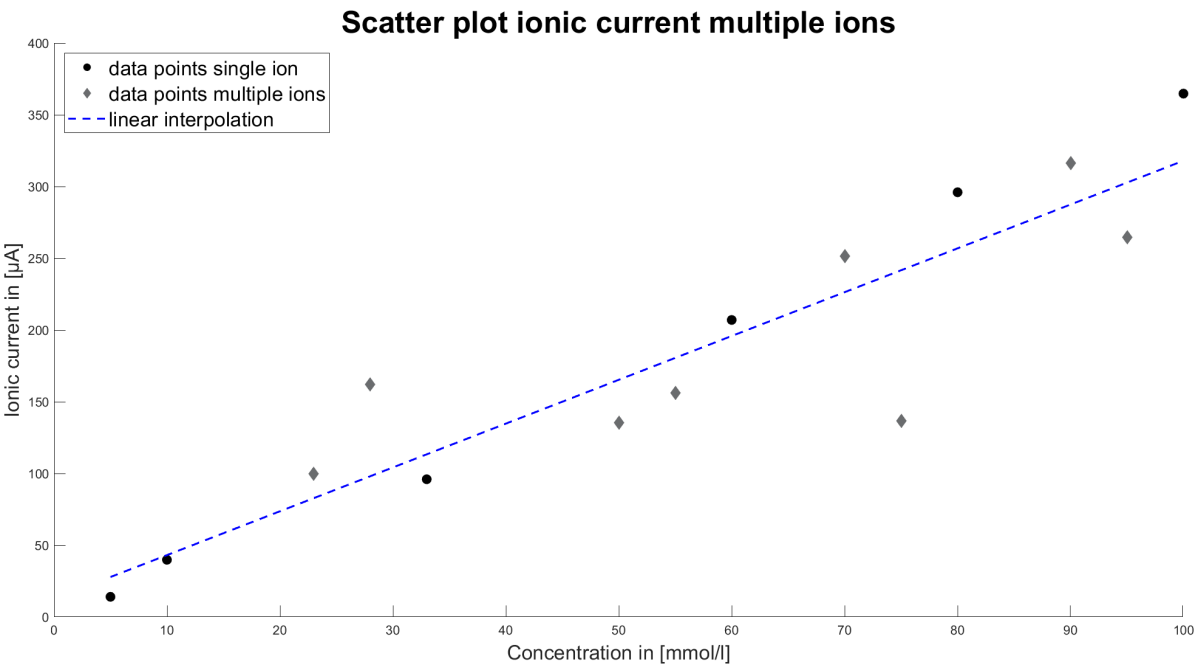

Figure 7.11: Ionic current of ionic solutions with different concentrations of sodium and potassium over the absolute difference in concentration between sodium and potassium ($R^2 = 0.83$ of the linear interpolation)

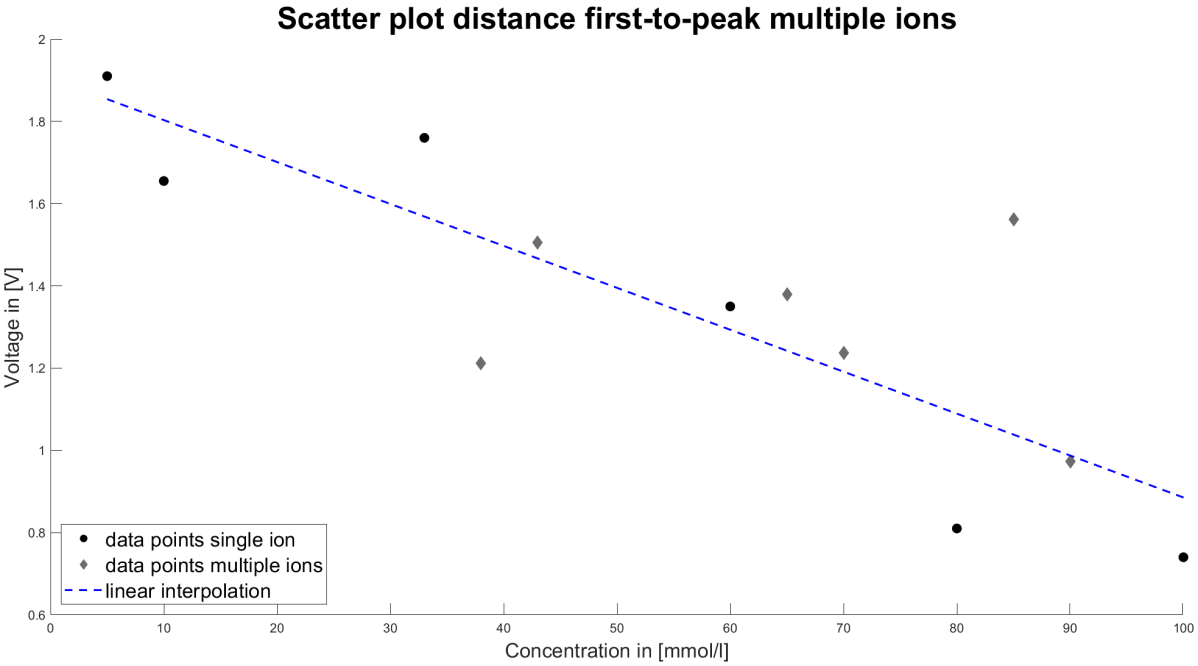

Figure 7.12: Distance between first current and peak location ionic solutions with different concentrations of sodium and potassium over the sum of concentration of sodium and potassium ($R^2 = 0.73$ of the linear interpolation)

7.5. Real Sweat

In a final step characterizing the sensor for LSV a real sweat sample was collected and the voltammogram recorded using the sensor. The sample was collected from the author during $45 min$ of medium intensity exercise using an absorbant patch. Before applying the patch the skin underneath was cleaned using demi-water. The sample was measured in the sensor without any prior preparation analogous to the calibration procedure. Sweep rate was set at $v = 1 \frac{V}{s}$ with a $V_{max} = 2\,V$. The resulting voltammo-

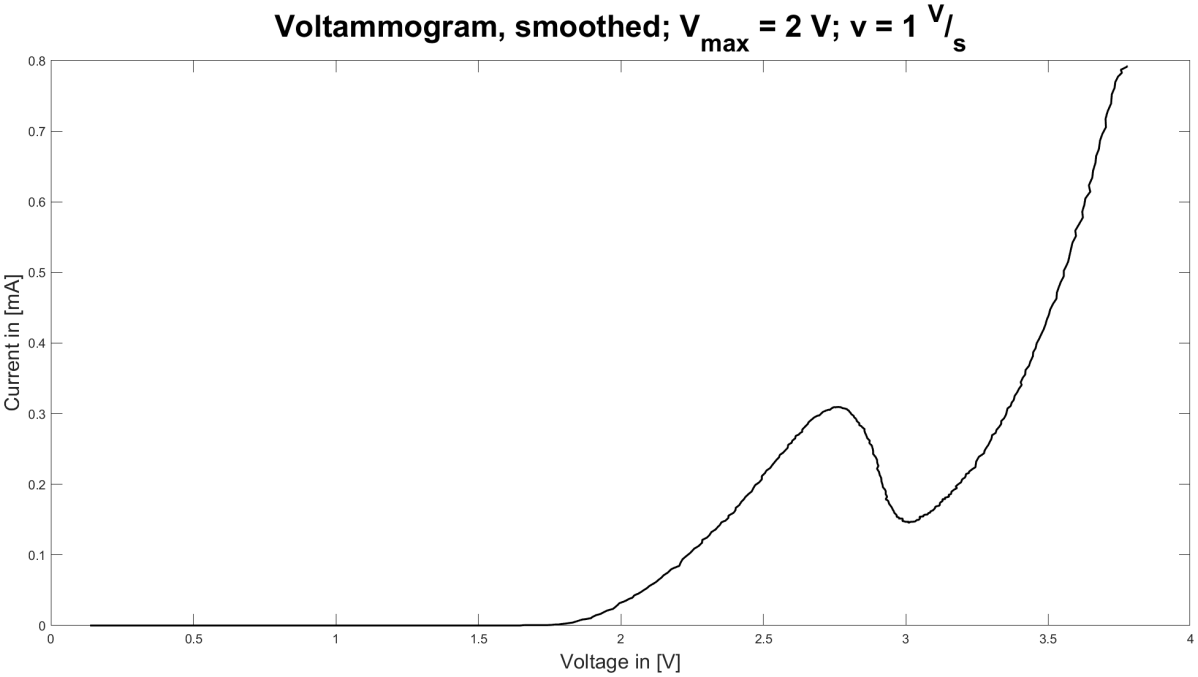

Figure 7.13: Smoothed voltammogram (time averaged over 20 ms) of real sweat collected during medium intensity exercise using CNT electrode; $v = 1\ \frac{V}{s}$ with a $V_{max} = 2\ V$

gram can be seen in fig. 7.13.

The voltammogram has a shape similar to the multiplexed solutions of sodium and potassium explored in the previous section. With $400\ \mu l$ collected during the experiment three measurements were possible. All measurements were performed using the same CNT electrode and sweep parameters. Mapping the average of the ionic current and the distance between the first current and peak-location to figs. 7.11 and 7.12 respectively indicates the sample contains $60\ \frac{mmol}{l}$ [Na^+] and $5\ \frac{mmol}{l}$ [K^+]. This is well within physiological limits. The result could not be calibrated against a standardized method such as ion chromatography due to time constraints. Nevertheless the results of this experiment support the results of the previous section and indicate the usability of the sensor for the simultaneous measurement of sodium and potassium in a single sweep.

7.6. Differential Pulse Voltammetry

Differential Pulse Voltammetry [DPV] is a waveform commonly used in tandem with LSV. Often LSV is used for more general exploration while DPV elucidates details. To be able to apply the DPV the voltage generation was changed from PWM to DAC.

The following experiments using DPV are exploratory. Given the number of parameters that can be varied during DPV (e.g. pulse height, pulse width, duty cycle) a more thorough research would be extensive. A calibration is performed following the same procedure as with LSV. Parameters are set at $V_{pulse} = 100\ mV$, $t_{pulse} = 100\ ms$ and $duty\ cycle = 50\ \%$ overlaid onto the previously used sweep of $V_{max} = 2\ V$ and $v = 1\ \frac{V}{s}$.

The current was recorded at the beginning and end of the first pulse higher than the reaction voltage of sodium. The difference between the two currents is the ionic current. Fig. 7.14 shows the calibration curve of the DPV. The data shows good linearity. Both the offset and the sensitivity of the DPV are higher than the same measurement for the LSV.

A similar calibration was performed on complex ionic solutions with both sodium and potassium in solution in physiological levels as previously described. The resulting currents did not reveal any clear correlation between the concentration of the singular ions. The sweep is however highly sensitive to the total ionic content and shows very good linearity to it with $R^2 = 0.965$.

DPV can be used in conjunction with LSV to determine ionic content. The ability of DPV to detect

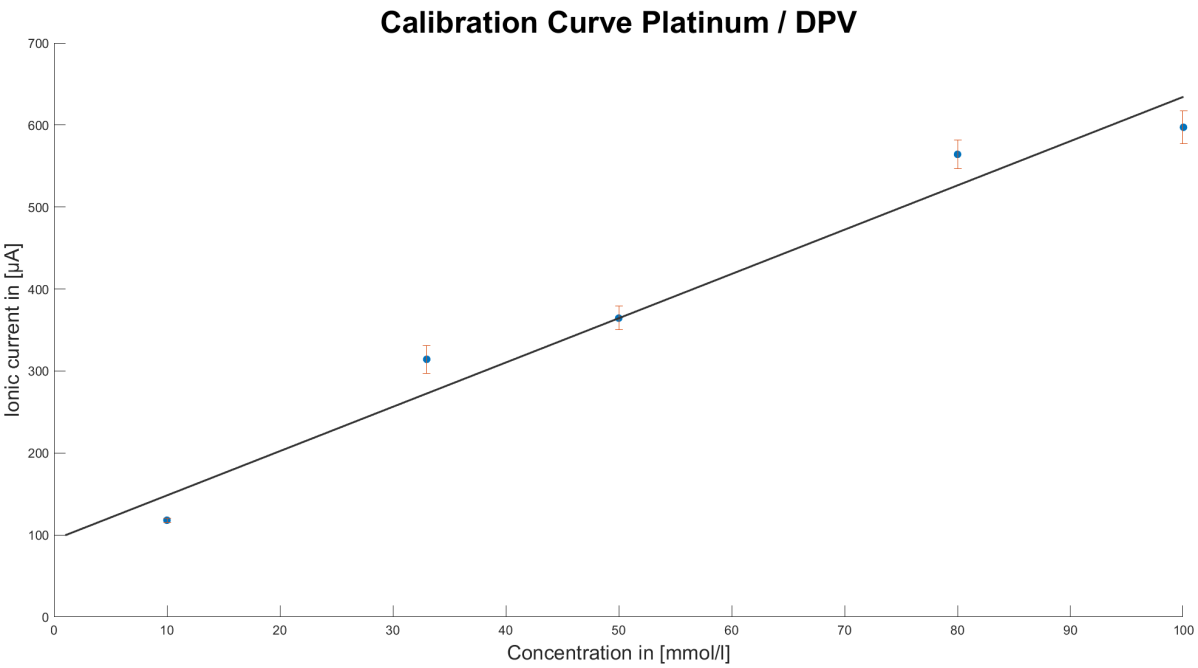

Figure 7.14: Calibration curve of DPV ($R^2 = 0.934$); $V_{pulse} = 100\ mV$, $t_{pulse} = 100\ ms$ and $duty\ cycle = 50\ \%$ overlaid onto $V_{max} = 2\ V$ and $v = 1\ \frac{V}{s}$; physiological concentrations of Na^+

the total ionic content can be paired with the analysis methods applied to the LSV voltammogram. Given that both can be implemented in the same system with a simple change to software pairing both methods seems sensible. Whether DPV can be exploited to determine singular ion concentrations is the subject of further research. There are a large number of parameters that could be varied to elucidate an adequate response. Preliminary tests with different parameters such as varying pulse voltage or duty cycle showed significant changes to the current. Whether any of these changes allows for better separation of ions is unclear.

7.7. Reliability

The voltage ranges at which the voltammetry is performed in this system have the potential to deteriorate the system. Both the function of the electrodes as catalysts for the redox-reactions and the water splitting taking place at the surface can alter the electrode surface significantly. Besides the electrodes all other parts of the proof-of-concept system do not lend themselves to a practical approximation of the reliability given how far they are removed from any prototype.

Deterioration on the electrodes can have two major effects. Formation of a layer on top of the active material can reduce the effective area and thus reduce sensitivity. Secondly, deteriorating effects if they are aggressive enough could render the electrode entirely unusable.

To test the durability of the electrodes a stress test was performed. In this test a factory new electrode from each material was submerged in $1\ \frac{mol}{l}$ [NaCl] solution. The voltage was then swept with $1\ \frac{V}{s}$ up to $2\ V$ continuously for 5 minutes. This represents an accelerated test compared to the usual application. A quick estimate of the relevant factors (i.e. typical ionic concentration $50\ \frac{mmol}{l}$ and duty cycle $20\ \%$) gives an acceleration factor of roughly 100. Multiplying this with the time tested this comes out to 500 minutes or over 8 hours. If the electrodes can maintain functionality over this time-frame their reliability over single applications will be sufficient for i.e. a long distance run or a football game.

The results for this experiment were mixed. The gold electrode tested is wholly unusable for cyclic voltammetry and the degradation of the electrode is visible with the naked eye. Fig. 7.15 shows the discoloration of the electrode from solid gold to mostly purple with some gold remaining. The electrode has lost all capability to record a proper voltammogram.

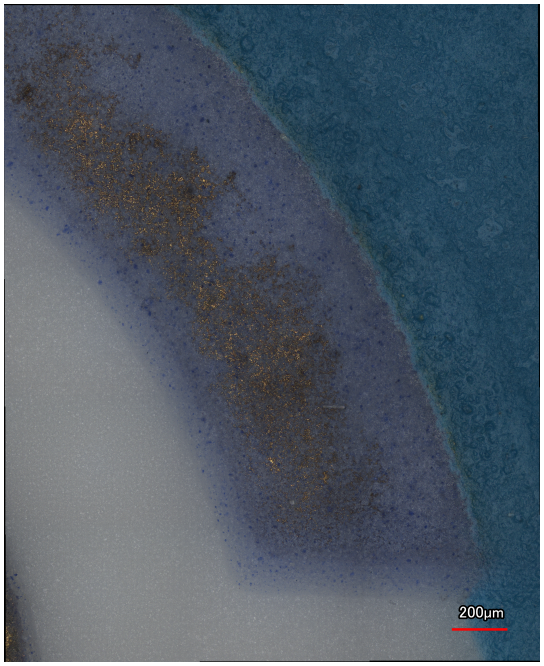

Figure 7.15: CE of gold electrode after stress test, 20x planar amplification

The platinum electrode held up better than the gold electrode with only a slight discoloration of the working electrode. The surface of the CNT electrode showed no discoloration whatsoever. However any change would be harder to detect from the black starting state. Additionally, as an objective measure, the surface roughness of the electrodes was determined and the change compared to measurements of unused electrodes.
There are three main measures of surface roughness: S_a, S_z and S_{pc}. S_a [μm] is the standard deviation of the surface height from the arithmetic average. This is a good overall measure for the change of surface roughness. S_z [μm] is the maximum difference between peaks and valleys in the surface. An increase in maximum deviation would indicate both etching of valleys and deposition on peaks. Lastly S_{pc} [$\frac{1}{mm}$] is a measure of the number of peaks of a certain height over valleys of relative height counted along a line of $1\ mm$ length.
In a general trend S_a and S_z increased for all materials with the change strongest in platinum followed by gold and CNT. The increase in CNT was roughly $+80\ \%$. S_{pc} was only increased for platinum while it stayed the same for gold and CNT.
The results show that stress increases the surface roughness, while sensitivity falls at the same time. This indicates, that a layer of material (with a thickness of hundreds of nanometers up to several micrometers) is deposited on the electrode surface. This theory is supported by the unchanged S_{pc} indicating the layer above has a similar form.
The reduction in sensitivity to the electrode induced by the stress can be quantified. For the gold electrodes the destructive processes taking place during the stress test reduces the sensitivity to zero. The platinum electrode has lost about 90 % of the sensitivity it had prior to the stress test. A calibration with a CNT electrode after the stress test with a known solution that had been calibrated for before the test revealed a statistically significant shift in the peak location and a reduction in the ionic current of 20 - 50 % (95 % confidence interval).
The fluid used for the stress test was analysed. For this purpose the fluid was evaporated. The remaining solids are presumably constituted of NaCl and NaOH (with traces of Au_2Cl_6 from the gold electrode [both auric chloride and its subjugate base are strongly water soluble]). The solids were then weighed and diluted 1/10 in demi-water. The pH of the demi-water and of the diluted stress solids was measured. Adding the solids shifted the pH from 6.6 of the demi-water to 9.0. This indicates the presence of $\approx 10\ \frac{\mu mol}{l}$ [NaOH]. Referring the amount of NaOH created to the NaCl we find that

$$\frac{C_{NaOH}}{C_{NaCl}} \approx 3.7 * 10^{-6}$$

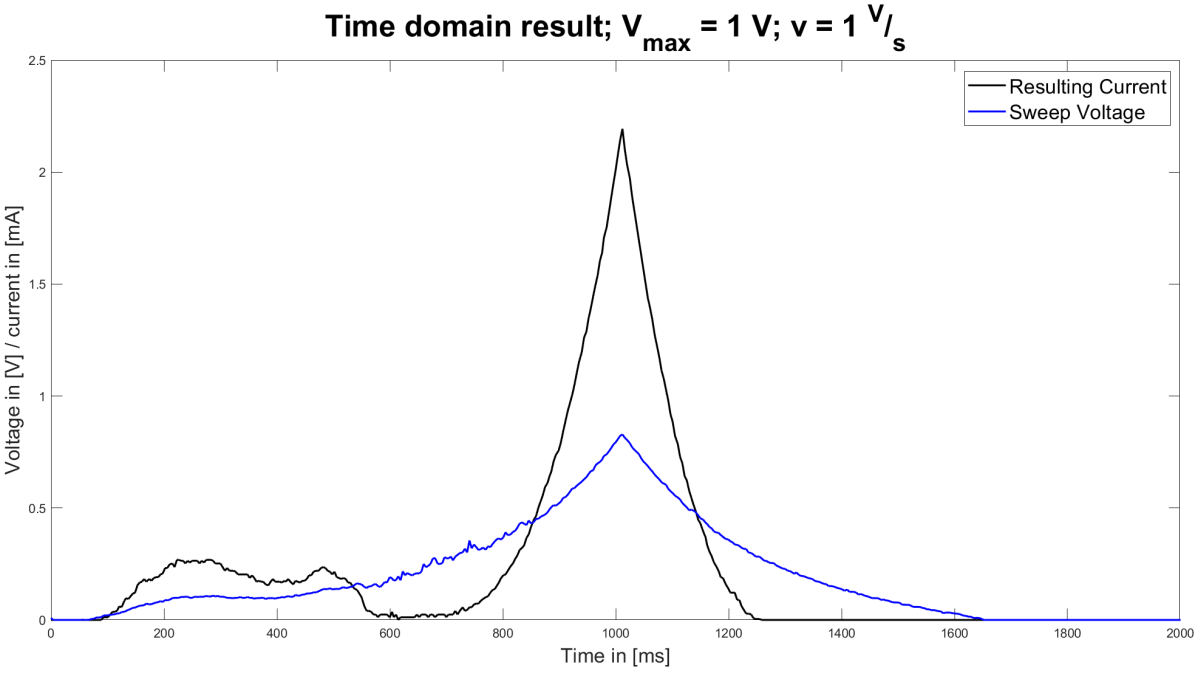

Figure 7.16: Time domain result of LSV with $V_{max} = 1\,V$ and $v = 1\,\frac{V}{s}$ of $100\,\frac{mmol}{l}$ [NaCl] and $1\,\frac{\mu mol}{l}$ [NaOH]

The ratio of NaOH created is relatively low. From the amount created during this stress test we can conclude that in a usual application the process will never be inhibited by the amount of Na in solution. Given the high concentration of NaCl in the original solution we can conjecture that the process was inhibited by the pH-change induced in the solution.

7.8. pH-Changes

Changes in the pH of the solution can change parameters of the voltammogram including ionic current, reaction voltages and the water window. The stress test indicates a change in the pH of the solution during the experiment. To further investigate this phenomenon a solution containing $100\,\frac{mmol}{l}$ [NaCl] was prepared and $1\,\frac{\mu mol}{l}$ [NaOH] was added to change the pH of the sample to 9.0. A simple LSV with $V_{max} = 1\,V$ and $v = 1\,\frac{V}{s}$ was performed. The corresponding time-domain signal is depicted in fig. 7.16. The result shows a double peak instead of the regular singular voltammetric peak. It can be hypothesized that this is due to the presence of OH^- in solution before water splitting. The first peak is attributed to the reaction of sodium with the OH^- present in solution a priori, while the secondary peak is due to the creation of hydroxide groups during water splitting and the subsequent reaction with sodium. At a pH of 9, as observed after the stress test, the ionic current and reaction voltage are significantly lower. The process is thus to a certain extent self-inhibitory. Changes in pH would only play a minor role in a prototype given the constant flow of sweat would prevent the build-up of hydroxide groups.

7.9. Discussion

The experiments performed in this chapter explore the feasibility of sweat measurement using cyclic voltammetry. A focus was set on the sensor as a proof of concept. Thus the experiments test out limiting factors for the process in an attempt to either prove its usability or find knock-out criteria. Calibration, the matrix of multiple ions in solution and the measurement of real sweat samples all aim to explore the method rather than quantify any particular element of it.

The dry experiments and initial tests on general ionic fluids show the functionality of the sensor. The different parameters such as sweep rate, resolution and range were verified and found to adhere to the requirements set out in the design. The ionic current measured during these experiments revealed the sensitivity of the system to be lower than expected within the envelope of the Randles-Sevcik equation

but usable regardless.
Subsequently the system was calibrated. Here the differences in electrode material discussed in chapter 4 were verified. The linearity of the sensor was found to be high within physiological limits and both Pt and CNT show promise as material choices. The sweep rate as an influencing factor was tested and an 'ideal' sweep rate for determination of curve parameters chosen for subsequent experiments.
Determination of concentration of multiple ions in solution using CV is complicated. There are no multiple peaks expressed by the voltammogram. Thus the concentrations needs to be determined using other curve parameters. A matrix of different concentrations of sodium and potassium were measured and two independent variables with a linear relationship to combinations of the concentrations determined. This result shows promise for the measurement of complex ionic fluids such as real sweat. The measurements performed on real sweat showed the validity of the surrogate ionic fluids. It also supports the possibility of using the sensor for the simultaneous measurement of sodium and potassium.
Given the concrete scenario of the sensor as a wearable real time monitor, reliability of the electrodes was explored. CNT as a material showed promise during this experiment to perform with little degradation during exercise.
Overall while CV appears to be usable for measurement of certain ionic concentrations in sweat care needs to be taken during the design of the sensor. There are several pitfalls such as the flow inside the sensor, electrochemical degradation of electrodes and proper measurement of the ionic current from the voltammogram. While the advantage of being able to measure several ions in a single sweep using an unmodified electrode remains, simpler methods such as colorimetric patches or ISEs retain their edge in usability. Whether CV is able to measure the ionic contents with sufficient accuracy remains to be seen. Overall the concept of CV for measurement of ionic contents in sweat was proven but the applicability in a prototype is subject of further research.

8

Conclusion and Outlook

In this project a sensor for the measurement of ionic concentrations in sweat was researched, designed, implemented and tested. The process revealed a multitude of new insights regarding CV of ionic fluids outside the water window and the applicability of new techniques for the measurement of sweat in a wearable manner. The research showed the complexity of the topic and forms a foundation for future experiments and prototypes.

The literature research explores in depth the issues of sweat secretion, state-of-the-art sweat measurement and voltammetry. These chapters give an overview of the influencing factors, opportunities and challenges facing sweat measurement in general and CV in particular.

Design of this sensor, while technically relatively simple, has to account for a large number of influencing factors. These factors were for the purpose of this thesis either neglected where possible (e.g. flow rate) or explored in depth where necessary (e.g. multiple ions in solution). The multitude of influencing factors is one of the major areas of future research.

Implementation of the sensor was simple and allowed for a variety of experiments to be performed. These experiments showed some success and revealed some issues that could not be extracted from literature. Generally the experiments served to prove the concept of the sensor while laying groundwork for future explorations.

A prototype of a wearable CV sweat sensor would be substantially different from the proof-of-concept presented here. To transform the sensor into a wearable device the electronics ought to be miniaturized. As explored in the design and implementation of this sensor such a miniaturization appears feasible. Furthermore a prototype should remove bottlenecks found in this thesis. Among these a higher resolution ADC to improve resolution of the measurement is most prominent. Additionally the author recommends the implementation of the sensor into a microfluidics platform addressing several issues relating to sample flow. Moreover the author suggests the implementation of a pH-sensor in the design to allow for the correction of the ionic current for this parameter. Finally, the author urges the exploration of DPV be pursued given its adaptability

The present thesis developed a proof-of-concept of the principle for the measurement of ionic concentration in sweat using cyclic voltammetry. The research while generally proving the concept as viable, leaves the questions of applicability and practicality to future research.

Appendix A

Ion / Molecule	Chemical formula	Concentration range in sweat ($\frac{mmol}{l}$)	Diffusion Coefficient ($10^{-9}\ \frac{m^2}{s}$)	Charge state
Sodium	Na^+	10-90	1.33	+I
Chloride	Cl^-	10-90	2.03	-I
Potassium	K^+	2-8	1.96	+I
Ammonia	NH_3	1-8	1.50	+III
Bicarbonate	HCO_3^-	0.5-5	0.92	-I
Urea	CH_4N_2O	0.2-2	1.38	—
Lactate	$CH_3CHOHCOO^-$	5-40	1.03	-I
Magnesium	Mg^{2+}	0.02-0.4	0.70	+II
Calcium	Ca^{2+}	0.2-2	0.79	+II

Table A.1: Concentrations, charge states and diffusion coefficients of sweat constituents with relevance for fatigue

B

Appendix B

```
int sweep_voltage [4] = {0, 0, 0, 0}; //initialize sweep voltage for
    ↪ measurements
int result_voltage [4] = {0, 0, 0, 0}; //initialize result voltage for
    ↪ measurements
int ce_voltage [4] = {0, 0, 0, 0}; //initialize ce voltage for measurement
int sum_sweep_voltage = 0; //initialize sweep voltage sum for transfer
int sum_result_voltage = 0; //initialize sweep voltage sum for transfer
int sum_ce_voltage = 0; //initialize ce voltage sum for trnasfer
int sweep_voltage_pin = A1; //define sweep voltage pin
int result_voltage_pin = A2; //define result voltage pin
int ce_voltage_pin = A3; //define ce voltage pin
int max_voltage_help = 102; //define help-value for max voltage (on scale
    ↪ 0 to 255 // 0 to 5 V)
int min_voltage_help = 0; //define help-value for min voltage (on scale 0
    ↪ to 255 // 0 to 5 V)
int wait_time = 19; //integer portion of the wait time in ms
int wait_time_frac_int = 906; //fractional part of the wait time in us
int output_pin = 3; //define PWM output pin
unsigned long current_micros = 0; //buffer for current time in us to time
    ↪ 1 ms cycle (overflows after 70 s!)
unsigned long previous_micros = 0; //buffer for previous time in us to
    ↪ time 1 ms cycle
unsigned long current_millis = 0; //buffer for ms (used for timestamp)
long data_selector = 0; //define global variable to determine which value
    ↪ is transmitted over the serial connection

void setup() { //setup code to be run on bootup
pinMode(output_pin, OUTPUT); //define the output pin as output
Serial.begin(115200); //setup serial connection with Baud rate of 115200
    ↪ bit/s
pinMode(3,155); //set pinMode to PWM-output with high frequency
TCCR2B = TCCR2B & B11111000 | B00000001; //write registers to increase PWM
    ↪  frequency to maximum value
}

void loop() {
for (int i = min_voltage_help; i < max_voltage_help; i++) { //for loop to
    ↪ cover a voltage sweep up
  analogWrite(output_pin, i); //write the PWM signal onto the output pin
     ↪ controlled via duty cycle
```

```
for (int j = 0; j < wait_time; j++){ //for loop for measurements on
    ↪ every sweep step
  current_micros = micros(); //write the current microsecond into the
      ↪ variable current_micros
    if(data_selector % 4 == 0){ //if data selector divides by 4 with
        ↪ rest 0 do this
      result_voltage [1] = result_voltage [0]; //shift values in voltage
          ↪ arrays, deleting oldest
      result_voltage [2] = result_voltage [1];
      result_voltage [3] = result_voltage [2];
      ce_voltage [1] = ce_voltage [0];
      ce_voltage [2] = ce_voltage [1];
      ce_voltage [3] = ce_voltage [2];
      sweep_voltage [1] = sweep_voltage [0];
      sweep_voltage [2] = sweep_voltage [1];
      sweep_voltage [3] = sweep_voltage [2];
      result_voltage [0] = analogRead(result_voltage_pin); //read and
          ↪ transform voltages into lowest position of respective array
      sweep_voltage [0] = analogRead(sweep_voltage_pin);
      ce_voltage [0] = analogRead(ce_voltage_pin);
      current_millis = millis(); //read timestamp into variable
          ↪ current_millis
      Serial.println(current_millis); //serial print of timestamp
      data_selector = data_selector + 1; //increment the data selector
    }
    else
    if(data_selector % 4 == 1){ //if data selector divides by 4 with
        ↪ rest 1 do this
      result_voltage [1] = result_voltage [0];
      result_voltage [2] = result_voltage [1];
      result_voltage [3] = result_voltage [2];
      ce_voltage [1] = ce_voltage [0];
      ce_voltage [2] = ce_voltage [1];
      ce_voltage [3] = ce_voltage [2];
      sweep_voltage [1] = sweep_voltage [0];
      sweep_voltage [2] = sweep_voltage [1];
      sweep_voltage [3] = sweep_voltage [2];
      result_voltage [0] = analogRead(result_voltage_pin);
      sweep_voltage [0] = analogRead(sweep_voltage_pin);
      ce_voltage [0] = analogRead(ce_voltage_pin);
      sum_result_voltage = result_voltage [0] + result_voltage [1] +
          ↪ result_voltage [2] + result_voltage [3];
      //sum the result voltages from the last 4 cycles
      current_millis = millis();
      Serial.println(sum_result_voltage); //serial print sum of result
          ↪ voltage
      data_selector = data_selector + 1;
    }
    else
    if(data_selector % 4 == 2){
      result_voltage [1] = result_voltage [0];
      result_voltage [2] = result_voltage [1];
      result_voltage [3] = result_voltage [2];
      ce_voltage [1] = ce_voltage [0];
      ce_voltage [2] = ce_voltage [1];
      ce_voltage [3] = ce_voltage [2];
```

```
        sweep_voltage [1] = sweep_voltage [0];
        sweep_voltage [2] = sweep_voltage [1];
        sweep_voltage [3] = sweep_voltage [2];
        result_voltage [0] = analogRead(result_voltage_pin);
        sweep_voltage [0] = analogRead(sweep_voltage_pin);
        ce_voltage [0] = analogRead(ce_voltage_pin);
        sum_sweep_voltage = sweep_voltage [0] + sweep_voltage [1] +
            ↪ sweep_voltage [2] + sweep_voltage [3];
        current_millis = millis();
        Serial.println(sum_sweep_voltage);
        data_selector = data_selector + 1;
      }
      else
      if(data_selector % 4 == 3){
        result_voltage [1] = result_voltage [0];
        result_voltage [2] = result_voltage [1];
        result_voltage [3] = result_voltage [2];
        ce_voltage [1] = ce_voltage [0];
        ce_voltage [2] = ce_voltage [1];
        ce_voltage [3] = ce_voltage [2];
        sweep_voltage [1] = sweep_voltage [0];
        sweep_voltage [2] = sweep_voltage [1];
        sweep_voltage [3] = sweep_voltage [2];
        result_voltage [0] = analogRead(result_voltage_pin);
        sweep_voltage [0] = analogRead(sweep_voltage_pin);
        ce_voltage [0] = analogRead(ce_voltage_pin);
        sum_ce_voltage = ce_voltage [0] + ce_voltage [1] + ce_voltage [2] +
            ↪  ce_voltage [3];
        current_millis = millis();
        Serial.println(sum_ce_voltage);
        data_selector = data_selector + 1;
      }
      while(current_micros - previous_micros <= 1000){ //check if 1000 us
          ↪ hasve passed
        current_micros = micros(); //only exit this loop if 1000 us have
            ↪ passed (wait 1 ms from start of this cycle)
    }
    previous_micros = micros(); //save the current us into the
        ↪ previous_micros variable
   }
      while(current_micros - previous_micros <= wait_time_frac_int){//loop
          ↪  only runs after the integer wait_time has expired
        current_micros = micros(); //wait until the microsecond reaches the
            ↪  fractional value of the wait_time
    }
    previous_micros = micros(); //save the current us into the
        ↪ previous_micros variable; necessary so the next cycle is not
        ↪ shortened
  }
for (int i = max_voltage_help; i > min_voltage_help; i--) { //for loop to
    ↪ cover a voltage sweep down
  analogWrite(output_pin, i);
   for (int j = 0; j < wait_time; j++){
    current_micros = micros();
      if(data_selector % 4 == 0){
        result_voltage [1] = result_voltage [0];
```

```
  result_voltage [2] = result_voltage [1];
  result_voltage [3] = result_voltage [2];
  ce_voltage [1] = ce_voltage [0];
  ce_voltage [2] = ce_voltage [1];
  ce_voltage [3] = ce_voltage [2];
  sweep_voltage [1] = sweep_voltage [0];
  sweep_voltage [2] = sweep_voltage [1];
  sweep_voltage [3] = sweep_voltage [2];
  result_voltage [0] = analogRead(result_voltage_pin);
  sweep_voltage [0] = analogRead(sweep_voltage_pin);
  ce_voltage [0] = analogRead(ce_voltage_pin);
  current_millis = millis();
  Serial.println(current_millis);
  data_selector = data_selector + 1;
}
else
if(data_selector % 4 == 1){
  result_voltage [1] = result_voltage [0];
  result_voltage [2] = result_voltage [1];
  result_voltage [3] = result_voltage [2];
  ce_voltage [1] = ce_voltage [0];
  ce_voltage [2] = ce_voltage [1];
  ce_voltage [3] = ce_voltage [2];
  sweep_voltage [1] = sweep_voltage [0];
  sweep_voltage [2] = sweep_voltage [1];
  sweep_voltage [3] = sweep_voltage [2];
  result_voltage [0] = analogRead(result_voltage_pin);
  sweep_voltage [0] = analogRead(sweep_voltage_pin);
  ce_voltage [0] = analogRead(ce_voltage_pin);
  sum_result_voltage = result_voltage [0] + result_voltage [1] +
     ↪ result_voltage [2] + result_voltage [3];
  current_millis = millis();
  Serial.println(sum_result_voltage);
  data_selector = data_selector + 1;
}
else
if(data_selector % 4 == 2){
  result_voltage [1] = result_voltage [0];
  result_voltage [2] = result_voltage [1];
  result_voltage [3] = result_voltage [2];
  ce_voltage [1] = ce_voltage [0];
  ce_voltage [2] = ce_voltage [1];
  ce_voltage [3] = ce_voltage [2];
  sweep_voltage [1] = sweep_voltage [0];
  sweep_voltage [2] = sweep_voltage [1];
  sweep_voltage [3] = sweep_voltage [2];
  result_voltage [0] = analogRead(result_voltage_pin);
  sweep_voltage [0] = analogRead(sweep_voltage_pin);
  ce_voltage [0] = analogRead(ce_voltage_pin);
  sum_sweep_voltage = sweep_voltage [0] + sweep_voltage [1] +
     ↪ sweep_voltage [2] + sweep_voltage [3];
  current_millis = millis();
  Serial.println(sum_sweep_voltage);
  data_selector = data_selector + 1;
}
else
```

```
      if(data_selector % 4 == 3){
        result_voltage [1] = result_voltage [0];
        result_voltage [2] = result_voltage [1];
        result_voltage [3] = result_voltage [2];
        ce_voltage [1] = ce_voltage [0];
        ce_voltage [2] = ce_voltage [1];
        ce_voltage [3] = ce_voltage [2];
        sweep_voltage [1] = sweep_voltage [0];
        sweep_voltage [2] = sweep_voltage [1];
        sweep_voltage [3] = sweep_voltage [2];
        result_voltage [0] = analogRead(result_voltage_pin);
        sweep_voltage [0] = analogRead(sweep_voltage_pin);
        ce_voltage [0] = analogRead(ce_voltage_pin);
        sum_ce_voltage = ce_voltage [0] + ce_voltage [1] + ce_voltage [2] +
            ↪  ce_voltage [3];
        current_millis = millis();
        Serial.println(sum_ce_voltage);
        data_selector = data_selector + 1;
       }
       while(current_micros - previous_micros <= 1000){
        current_micros = micros();
     }
     previous_micros = micros();
    }
       while(current_micros - previous_micros <= wait_time_frac_int){
        current_micros = micros();
     }
     previous_micros = micros();
  }
}
```

Bibliography

[1] A. Best and J. M. Kamilar, “The evolution of eccrine sweat glands in human and nonhuman primates,” *Journal of Human Evolution*, vol. 117, pp. 33–43, 2018, ISSN: 0047-2484. DOI: https://doi.org/10.1016/j.jhevol.2017.12.003. [Online]. Available: https://www.sciencedirect.com/science/article/pii/S0047248417303652.

[2] J. E. Brinkman, B. Dorius, and S. Sharma, “Physiology, body fluids,” 2018.

[3] L. B. Baker and A. S. Wolfe, “Physiological mechanisms determining eccrine sweat composition,” *Eur J Appl Physiol*, vol. 120, no. 4, pp. 719–752, 2020, Baker, Lindsay B Wolfe, Anthony S eng NA/Gatorade Sports Science Institute Review Germany 2020/03/04 Eur J Appl Physiol. 2020 Apr;120(4):719-752. doi: 10.1007/s00421-020-04323-7. Epub 2020 Mar 2., ISSN: 1439-6327 (Electronic) 1439-6319 (Linking). DOI: 10.1007/s00421-020-04323-7. [Online]. Available: https://www.ncbi.nlm.nih.gov/pubmed/32124007%20https://www.ncbi.nlm.nih.gov/pmc/articles/PMC7125257/pdf/421_2020_Article_4323.pdf.

[4] C. B. Wenger, “Heat of evaporation of sweat: Thermodynamic considerations,” *Journal of Applied Physiology*, vol. 32, no. 4, pp. 456–459, 1972. DOI: 10.1152/jappl.1972.32.4.456. [Online]. Available: https://journals.physiology.org/doi/abs/10.1152/jappl.1972.32.4.456.

[5] E. V. Karpova, A. I. Laptev, E. A. Andreev, E. E. Karyakina, and A. A. Karyakin, “Relationship between sweat and blood lactate levels during exhaustive physical exercise,” *ChemElectroChem*, vol. 7, no. 1, pp. 191–194, 2020, ISSN: 2196-0216 2196-0216. DOI: 10.1002/celc.201901703.

[6] L. Klous, C. J. de Ruiter, S. Scherrer, N. Gerrett, and H. A. M. Daanen, “The (in)dependency of blood and sweat sodium, chloride, potassium, ammonia, lactate and glucose concentrations during submaximal exercise,” *Eur J Appl Physiol*, vol. 121, no. 3, pp. 803–816, 2021, ISSN: 1439-6327 (Electronic) 1439-6319 (Linking). DOI: 10.1007/s00421-020-04562-8. [Online]. Available: https://www.ncbi.nlm.nih.gov/pubmed/33355715.

[7] A. Sharma, M. Badea, S. Tiwari, and J. L. Marty, “Wearable biosensors: An alternative and practical approach in healthcare and disease monitoring,” *Molecules*, vol. 26, no. 3, 2021, Sharma, Atul Badea, Mihaela Tiwari, Swapnil Marty, Jean Louis eng Review Switzerland 2021/02/05 Molecules. 2021 Feb 1;26(3). pii: molecules26030748. doi: 10.3390/molecules26030748., ISSN: 1420-3049 (Electronic) 1420-3049 (Linking). DOI: 10.3390/molecules26030748. [Online]. Available: https://www.ncbi.nlm.nih.gov/pubmed/33535493.

[8] K. Saga, “Structure and function of human sweat glands studied with histochemistry and cytochemistry,” *Progress in Histochemistry and Cytochemistry*, vol. 37, no. 4, pp. 323–+, 2002, 594eg Times Cited:112 Cited References Count:213, ISSN: 0079-6336. DOI: Doi10.1016/S0079-6336(02)80005-5. [Online]. Available: %3CGo%20to%20ISI%3E://WOS:000178035300001.

[9] M. Asahina, A. Poudel, and S. Hirano, “Sweating on the palm and sole: Physiological and clinical relevance,” *Clinical Autonomic Research*, vol. 25, no. 3, pp. 153–159, 2015, Ck1cf Times Cited:18 Cited References Count:52, ISSN: 0959-9851. DOI: 10.1007/s10286-015-0282-1. [Online]. Available: %3CGo%20to%20ISI%3E://WOS:000355942300003%20https://link.springer.com/content/pdf/10.1007/s10286-015-0282-1.pdf.

[10] *Nci dictionary of cancer terms*. [Online]. Available: https://www.cancer.gov/publications/dictionaries/cancer-terms/def/fatigue.

[11] J. G. Betts, K. A. Young, J. A. Wise, *et al.*, *Anatomy and physiology*. 2013.

[12] R. A. McCance, “The effect of salt deficiency in man on the volume of the extracellular fluids, and on the composition of sweat, saliva, gastric juice and cerebrospinal fluid,” *Journal of Physiology-London*, vol. 92, no. 2, pp. 208–218, 1938, V06qb Times Cited:142 Cited References Count:30, ISSN: 0022-3751. DOI: DOI10.1113/jphysiol.1938.sp003595. [Online]. Available: %3CGo%20to%20ISI%3E://WOS:000207207000008%20https://www.ncbi.nlm.nih.gov/pmc/articles/PMC1395172/pdf/jphysiol01556-0090.pdf.

[13] G. W. Cage and R. L. Dobson, “Sodium secretion and reabsorption in the human eccrine sweat gland*,” *Journal of Clinical Investigation*, vol. 44, no. 7, pp. 1270–1276, 1965, ISSN: 0021-9738. DOI: 10.1172/jci105233.

[14] D. L. Costill, “Sweating: Its composition and effects on body fluids*,” *Annals of the New York Academy of Sciences*, vol. 301, no. 1, pp. 160–174, 1977, ISSN: 0077-8923. DOI: https://doi.org/10.1111/j.1749-6632.1977.tb38195.x. [Online]. Available: https://nyaspubs.onlinelibrary.wiley.com/doi/abs/10.1111/j.1749-6632.1977.tb38195.x.

[15] E. N. Marieb and K. Hoehn, *Human Anatomy and Physiology*. Pearson, 2019, ISBN: 0-13-458099,0;

[16] K. Sato, W. Kang, K. Saga, and K. T. Sato, “Biology of sweat glands and their disorders. i. normal sweat gland function,” *J Am Acad Dermatol*, vol. 20, no. 4, pp. 537–563, 1989.

[17] M. J. Buono, K. D. Ball, and F. W. Kolkhorst, “Sodium ion concentration vs. sweat rate relationship in humans,” *Journal of Applied Physiology*, vol. 103, no. 3, pp. 990–994, 2007. DOI: 10.1152/japplphysiol.00015.2007. [Online]. Available: https://journals.physiology.org/doi/abs/10.1152/japplphysiol.00015.2007.

[18] J. R. Allan and C. Wilson, “Influence of acclimatization on sweat sodium concentration,” *Journal of Applied Physiology*, vol. 30, no. 5, pp. 708–712, 1971.

[19] L. B. Baker, “Physiology of sweat gland function: The roles of sweating and sweat composition in human health,” *Temperature*, vol. 6, no. 3, pp. 211–259, 2019, doi: 10.1080/23328940.2019.1632145, ISSN: 2332-8940. DOI: 10.1080/23328940.2019.1632145. [Online]. Available: https://doi.org/10.1080/23328940.2019.1632145.

[20] G. L. Khanna and I. Manna, “Supplementary effect of carbohydrate-electrolyte drink on sports performance, lactate removal cardiovascular response of athletes,” *Indian Journal of Medical Research*, vol. 121, no. 5, pp. 665–669, 2005, 934nj Times Cited:17 Cited References Count:29, ISSN: 0971-5916. [Online]. Available: %3CGo%20to%20ISI%3E://WOS:000229715200009.

[21] K. Gibiński, F. Kumaszka, J. Zmudziński, L. Giec, J. Waclawczyk, and J. Dosiak, “Sodium 24na and potassium 42k availability for sweat production after intravenous injection and their handling by sweat glands,” *Acta Biol Med Ger*, vol. 30, no. 5, pp. 697–708, 1973, Gibiński, K Kumaszka, F Zmudziński, J Giec, L Waclawczyk, J Dosiak, J Journal Article Germany 1973/05/01 Acta Biol Med Ger. 1973 May;30(5):697-708., ISSN: 0001-5318 (Print) 0001-5318.

[22] W. Jahnen-Dechent and M. Ketteler, “Magnesium basics,” *Clinical Kidney Journal*, vol. 5, no. Suppl$_1$, pp. i3–i14, 2012, ISSN: 2048-8505. DOI: 10.1093/ndtplus/sfr163. [Online]. Available: https://doi.org/10.1093/ndtplus/sfr163.

[23] T. D. La Count, A. Jajack, J. Heikenfeld, and G. B. Kasting, “Modeling glucose transport from systemic circulation to sweat,” *Journal of Pharmaceutical Sciences*, vol. 108, no. 1, pp. 364–371, 2019, Hj1by Times Cited:9 Cited References Count:36, ISSN: 0022-3549. DOI: 10.1016/j.xphs.2018.09.026. [Online]. Available: %3CGo%20to%20ISI%3E://WOS:000456898100055.

[24] A. M. Spehar-Deleze, S. Anastasova, and P. Vadgama, “Monitoring of lactate in interstitial fluid, saliva and sweat by electrochemical biosensor: The uncertainties of biological interpretation,” *Chemosensors*, vol. 9, no. 8, 2021, Uf9te Times Cited:0 Cited References Count:71. DOI: ARTN19510.3390/chemosensors9080195. [Online]. Available: %3CGo%20to%20ISI%3E://WOS:000688907600001%20https://mdpi-res.com/d_attachment/chemosensors/chemosensors-09-00195/article_deploy/chemosensors-09-00195.pdf.

[25] H. Okawara, T. Sawada, D. Nakashima, *et al.*, “Kinetic changes in sweat lactate following fatigue during constant workload exercise,” *Physiological Reports*, vol. 10, no. 2, 2022, Yn6zs Times Cited:0 Cited References Count:62, ISSN: 2051-817x. DOI: ARTNe1516910.14814/phy2.15169. [Online]. Available: %3CGo%20to%20ISI%3E://WOS:000747405400001%20https://physoc.onlinelibrary.wiley.com/doi/pdfdirect/10.14814/phy2.15169?download=true.

[26] D. Czarnowski, J. Gorski, J. Jozwiuk, and A. Boronkaczmarska, “Plasma ammonia is the principal source of ammonia in sweat,” *European Journal of Applied Physiology and Occupational Physiology*, vol. 65, no. 2, pp. 135–137, 1992, Jh302 Times Cited:30 Cited References Count:18, ISSN: 0301-5548. DOI: Doi10.1007/Bf00705070. [Online]. Available: %3CGo%20to%20ISI%3E://WOS:A1992JH30200007%20https://link.springer.com/content/pdf/10.1007/BF00705070.pdf.

[27] J. Gorski, K. Lerczak, and I. Wojcieszak, “Urea excretion in sweat during short-term efforts of high-intensity,” *European Journal of Applied Physiology*, vol. 54, no. 4, pp. 416–419, 1985, Asp01 Times Cited:5 Cited References Count:26, ISSN: 1439-6319. DOI: Doi10.1007/Bf02337187. [Online]. Available: %3CGo%20to%20ISI%3E://WOS:A1985ASP0100013%20https://link.springer.com/content/pdf/10.1007/BF02337187.pdf.

[28] P. W. Lemon, K. E. Yarasheski, and D. G. Dolny, “Validity/reliability of sweat analysis by whole-body washdown vs. regional collections,” *Journal of Applied Physiology*, vol. 61, no. 5, pp. 1967–1971, 1986. DOI: 10.1152/jappl.1986.61.5.1967. [Online]. Available: https://journals.physiology.org/doi/abs/10.1152/jappl.1986.61.5.1967.

[29] L. B. Baker, K. A. Barnes, B. C. Sopena, R. P. Nuccio, A. J. Reimel, and C. T. Ungaro, “Sweat sodium, potassium, and chloride concentrations analyzed same day as collection versus after 7 days storage in a range of temperatures,” *International Journal of Sport Nutrition and Exercise Metabolism*, vol. 28, no. 3, pp. 238–245, 2018, Gj7bq Times Cited:2 Cited References Count:21, ISSN: 1526-484x. DOI: 10.1123/ijsnem.2017-0199. [Online]. Available: %3CGo%20to%20ISI%3E://WOS:000435540200003%20https://journals.humankinetics.com/view/journals/ijsnem/28/3/article-p238.xml.

[30] L. B. Baker, “Sweating rate and sweat sodium concentration in athletes: A review of methodology and intra/interindividual variability,” *Sports Medicine*, vol. 47, no. 1, pp. 111–128, 2017, ISSN: 1179-2035. DOI: 10.1007/s40279-017-0691-5. [Online]. Available: https://doi.org/10.1007/s40279-017-0691-5.

[31] Y. C. Chen, S. S. Shan, Y. T. Liao, and Y. C. Liao, “Bio-inspired fractal textile device for rapid sweat collection and monitoring,” *Lab on a Chip*, vol. 21, no. 13, pp. 2524–2533, 2021, Tb3dc Times Cited:0 Cited References Count:45, ISSN: 1473-0197. DOI: 10.1039/d1lc00328c. [Online]. Available: %3CGo%20to%20ISI%3E://WOS:000658830300001%20https://pubs.rsc.org/en/content/articlepdf/2021/lc/d1lc00328c.

[32] E. Garcia-Cordero, F. Wildhaber, F. Bellando, *et al.*, “Embedded passive nano-liter micropump for sweat collection and analysis,” *2018 Ieee Micro Electro Mechanical Systems (Mems)*, pp. 1217–1220, 2018, Bk3fz Times Cited:3 Cited References Count:9 Proceedings IEEE Micro Electro Mechanical Systems, ISSN: 1084-6999. [Online]. Available: %3CGo%20to%20ISI%3E://WOS:000434960900317.

[33] A. Kusbaz, I. Gocek, G. Baysal, *et al.*, “Lactate detection by colorimetric measurement in real human sweat by microfluidic-based biosensor on flexible substrate,” *Journal of the Textile Institute*, vol. 110, no. 12, pp. 1725–1732, 2019, Iz7sz Times Cited:4 Cited References Count:30, ISSN: 0040-5000. DOI: 10.1080/00405000.2019.1616955. [Online]. Available: %3CGo%20to%20ISI%3E://WOS:000469149200001%20https://www.tandfonline.com/doi/full/10.1080/00405000.2019.1616955.

[34] J. T. Reeder, J. Choi, Y. G. Xue, *et al.*, “Waterproof, electronics-enabled, epidermal microfluidic devices for sweat collection, biomarker analysis, and thermography in aquatic settings,” *Science Advances*, vol. 5, no. 1, 2019, Hj9vr Times Cited:105 Cited References Count:50, ISSN: 2375-2548. DOI: ARTNeaau635610.1126/sciadv.aau6356. [Online]. Available: %3CGo%20to%20ISI%3E://WOS:000457547900072%20https://www.science.org/doi/10.1126/sciadv.aau6356.

[35] J. T. Reeder, Y. G. Xue, D. Franklin, *et al.*, "Resettable skin interfaced microfluidic sweat collection devices with chemesthetic hydration feedback," *Nature Communications*, vol. 10, 2019, Js7ro Times Cited:22 Cited References Count:47, ISSN: 2041-1723. DOI: ARTN551310.1038/s41467-019-13431-8. [Online]. Available: %3CGo%20to%20ISI%3E://WOS:000500501400001%20https://www.nature.com/articles/s41467-019-13431-8.pdf.

[36] A. S. M. Steijlen, J. Bastemeijer, W. A. Groen, K. M. B. Jansen, P. J. French, and A. Bossche, "Development of a microfluidic collection system to measure electrolyte variations in sweat during exercise," *42nd Annual International Conferences of the Ieee Engineering in Medicine and Biology Society: Enabling Innovative Technologies for Global Healthcare Embc'20*, pp. 4085–4088, 2020, Bq8tk Times Cited:0 Cited References Count:18 IEEE Engineering in Medicine and Biology Society Conference Proceedings, ISSN: 1557-170x. [Online]. Available: %3CGo%20to%20ISI%3E://WOS:000621592204105.

[37] Y. Zhang, H. X. Guo, S. B. Kim, *et al.*, "Passive sweat collection and colorimetric analysis of biomarkers relevant to kidney disorders using a soft microfluidic system," *Lab on a Chip*, vol. 19, no. 9, pp. 1545–1555, 2019, Hw0cj Times Cited:59 Cited References Count:68, ISSN: 1473-0197. DOI: 10.1039/c9lc00103d. [Online]. Available: %3CGo%20to%20ISI%3E://WOS:000466348200015%20https://pubs.rsc.org/en/content/articlepdf/2019/lc/c9lc00103d.

[38] B. J. Adesokan, X. Quan, A. Evgrafov, A. Heiskanen, A. Boisen, and M. P. Sorensen, "Experimentation and numerical modeling of cyclic voltammetry for electrochemical micro-sized sensors under the influence of electrolyte flow," *Journal of Electroanalytical Chemistry*, vol. 763, pp. 141–148, 2016, De2lh Times Cited:7 Cited References Count:49, ISSN: 1572-6657. DOI: 10.1016/j.jelechem.2015.12.029. [Online]. Available: %3CGo%20to%20ISI%3E://WOS:000370458300020.

[39] V. Oncescu, D. O'Dell, and D. Erickson, "Smartphone based health accessory for colorimetric detection of biomarkers in sweat and saliva," *Lab on a Chip*, vol. 13, no. 16, pp. 3232–3238, 2013, 183zu Times Cited:248 Cited References Count:26, ISSN: 1473-0197. DOI: 10.1039/c3lc50431j. [Online]. Available: %3CGo%20to%20ISI%3E://WOS:000321856800010%20https://pubs.rsc.org/en/content/articlepdf/2013/lc/c3lc50431j.

[40] J. Choi, A. J. Bandodkar, J. T. Reeder, *et al.*, "Soft, skin-integrated multifunctional microfluidic systems for accurate colorimetric analysis of sweat biomarkers and temperature," *Acs Sensors*, vol. 4, no. 2, pp. 379–388, 2019, Hm9wt Times Cited:95 Cited References Count:48, ISSN: 2379-3694. DOI: 10.1021/acssensors.8b01218. [Online]. Available: %3CGo%20to%20ISI%3E://WOS:000459836400015%20https://pubs.acs.org/doi/pdf/10.1021/acssensors.8b01218.

[41] A. Koh, D. Kang, and J. Rogers, "Wearable epidermal microfluidic systems capable of capture, storage and colorimetric sensing of sweat," *Abstracts of Papers of the American Chemical Society*, vol. 253, 2017, Gd5tc 452 Times Cited:0 Cited References Count:0, ISSN: 0065-7727. [Online]. Available: %3CGo%20to%20ISI%3E://WOS:000430568500719.

[42] K. K. Zhang, J. X. Zhang, F. F. Wang, and D. S. Kong, "Stretchable and superwettable colorimetric sensing patch for epidermal collection and analysis of sweat," *Acs Sensors*, vol. 6, no. 6, pp. 2261–2269, 2021, Tc0zu Times Cited:3 Cited References Count:60, ISSN: 2379-3694. DOI: 10.1021/acssensors.1c00316. [Online]. Available: %3CGo%20to%20ISI%3E://WOS:000668374500024%20https://pubs.acs.org/doi/pdf/10.1021/acssensors.1c00316.

[43] A. Vaquer, E. Baron, and R. de la Rica, "Detection of low glucose levels in sweat with colorimetric wearable biosensors," *Analyst*, vol. 146, no. 10, pp. 3273–3279, 2021, Sd2lf Times Cited:2 Cited References Count:31, ISSN: 0003-2654. DOI: 10.1039/d1an00283j. [Online]. Available: %3CGo%20to%20ISI%3E://WOS:000639421700001%20https://pubs.rsc.org/en/content/articlepdf/2021/an/d1an00283j.

[44] V. Jain, M. Ochoa, H. J. Jiang, R. Rahimi, and B. Ziaie, "A mass-customizable dermal patch with discrete colorimetric indicators for personalized sweat rate quantification," *Microsystems Nanoengineering*, vol. 5, 2019, Id8zl Times Cited:10 Cited References Count:43, ISSN: 2055-7434. DOI: ARTN2910.1038/s41378-019-0067-0. [Online]. Available: %3CGo%20to%20ISI%3E://WOS:000471977100001%20https://www.nature.com/articles/s41378-019-0067-0.pdf.

[45] S. B. Kim, Y. Zhang, S. M. Won, *et al.*, "Super-absorbent polymer valves and colorimetric chemistries for time-sequenced discrete sampling and chloride analysis of sweat via skin-mounted soft microfluidics," *Small*, vol. 14, no. 12, 2018, Ga5ak Times Cited:50 Cited References Count:48, ISSN: 1613-6810. DOI: ARTN170333410.1002/smll.201703334. [Online]. Available: %3CGo%20to%20ISI%3E://WOS:000428344300016%20https://onlinelibrary.wiley.com/doi/10.1002/smll.201703334.

[46] L. B. Baker, R. P. Nuccio, C. T. Ungaro, *et al.*, "Epifluidic colorimetric patch for on-skin analysis of regional sweat chloride concentration during laboratory-based exercise," *Medicine and Science in Sports and Exercise*, vol. 51, no. 6, pp. 562–562, 2019, Suppl. S Ir8ag 2070 Times Cited:0 Cited References Count:0, ISSN: 0195-9131. DOI: DOI10.1249/01.mss.0000562188.44773.7d. [Online]. Available: %3CGo%20to%20ISI%3E://WOS:000481662802191.

[47] A. Vaquer, E. Baron, and R. de la Rica, "Wearable analytical platform with enzyme-modulated dynamic range for the simultaneous colorimetric detection of sweat volume and sweat biomarkers," *Acs Sensors*, vol. 6, no. 1, pp. 130–136, 2021, Qa1zj Times Cited:4 Cited References Count:40, ISSN: 2379-3694. DOI: 10.1021/acssensors.0c01980. [Online]. Available: %3CGo%20to%20ISI%3E://WOS:000613247400015%20https://pubs.acs.org/doi/pdf/10.1021/acssensors.0c01980.

[48] J. Kim, Y. X. Wu, H. W. Luan, *et al.*, "A skin-interfaced, miniaturized microfluidic analysis and delivery system for colorimetric measurements of nutrients in sweat and supply of vitamins through the skin," *Advanced Science*, 2021, Ws4to Times Cited:0 Cited References Count:52. DOI: ARTN210333110.1002/advs.202103331. [Online]. Available: %3CGo%20to%20ISI%3E://WOS:000715175700001%20https://onlinelibrary.wiley.com/doi/10.1002/advs.202103331.

[49] L. R. Wang, T. L. Xu, X. C. He, and X. J. Zhang, "Flexible, self-healable, adhesive and wearable hydrogel patch for colorimetric sweat detection," *Journal of Materials Chemistry C*, vol. 9, no. 41, pp. 14 938–14 945, 2021, Wn8fs Times Cited:0 Cited References Count:35, ISSN: 2050-7526. DOI: 10.1039/d1tc03905a. [Online]. Available: %3CGo%20to%20ISI%3E://WOS:000706774900001%20https://pubs.rsc.org/en/content/articlepdf/2021/tc/d1tc03905a.

[50] E. Tu, P. Pearlmutter, M. Tiangco, G. Derose, L. Begdache, and A. Koh, "Comparison of colorimetric analyses to determine cortisol in human sweat," *Acs Omega*, vol. 5, no. 14, pp. 8211–8218, 2020, Ld9jr Times Cited:12 Cited References Count:50, ISSN: 2470-1343. DOI: 10.1021/acsomega.0c00498. [Online]. Available: %3CGo%20to%20ISI%3E://WOS:000526342300051%20https://www.ncbi.nlm.nih.gov/pmc/articles/PMC7161047/pdf/ao0c00498.pdf.

[51] M. Parrilla, M. Cuartero, and G. A. Crespo, "Wearable potentiometric ion sensors," *TrAC Trends in Analytical Chemistry*, vol. 110, pp. 303–320, 2019, ISSN: 01659936. DOI: 10.1016/j.trac.2018.11.024.

[52] H. M. Barbour, "Development and evaluation of the simultaneous determination of sweat sodium and chloride by ion-selective electrodes," *Annals of Clinical Biochemistry*, vol. 28, pp. 150–154, 1991, 2 Fd927 Times Cited:9 Cited References Count:10, ISSN: 0004-5632. DOI: Doi10.1177/000456329102800205. [Online]. Available: %3CGo%20to%20ISI%3E://WOS:A1991FD92700005%20https://journals.sagepub.com/doi/pdf/10.1177/000456329102800205.

[53] J. J. J. Hulstein and P. van 't Sant, "Sweat analysis using indirect ion-selective electrode on the routine chemistry analyser meets uk guidelines," *Annals of Clinical Biochemistry*, vol. 48, pp. 374–376, 2011, 4 809ye Times Cited:6 Cited References Count:5, ISSN: 0004-5632. DOI: 10.1258/acb.2011.011001. [Online]. Available: %3CGo%20to%20ISI%3E://WOS:000294091800014%20https://journals.sagepub.com/doi/pdf/10.1258/acb.2011.011001.

[54] V. Mazzaracchio, A. Serani, L. Fiore, D. Moscone, and F. Arduini, "All-solid state ion-selective carbon black-modified printed electrode for sodium detection in sweat," *Electrochimica Acta*, vol. 394, 2021, Wb1fi Times Cited:0 Cited References Count:54, ISSN: 0013-4686. DOI: ARTN13905010.1016/j.electacta.2021.139050. [Online]. Available: %3CGo%20to%20ISI%3E://WOS:000703324700003.

[55] B. Paul, S. Demuru, C. Lafaye, M. Saubade, and D. Briand, "Printed iontophoretic□integrated wearable microfluidic sweat□sensing patch for on□demand point□of□care sweat analysis," *Advanced Materials Technologies*, vol. 6, no. 4, 2021, ISSN: 2365-709X 2365-709X. DOI: 10.1002/admt.202000910. [Online]. Available: https://onlinelibrary.wiley.com/doi/10.1002/admt.202000910.

[56] N. Coppede, M. Giannetto, M. Villani, *et al.*, "Ion selective textile organic electrochemical transistor for wearable sweat monitoring," *Organic Electronics*, vol. 78, 2020, Kr9wm Times Cited:17 Cited References Count:36, ISSN: 1566-1199. DOI: ARTN10557910.1016/j.orgel.2019.105579. [Online]. Available: %3CGo%20to%20ISI%3E://WOS:000517963700034.

[57] Q. F. Zhai, L. W. Yap, R. Wang, *et al.*, "Vertically aligned gold nanowires as stretchable and wearable epidermal ion-selective electrode for noninvasive multiplexed sweat analysis," *Analytical Chemistry*, vol. 92, no. 6, pp. 4647–4655, 2020, Le2pb Times Cited:33 Cited References Count:47, ISSN: 0003-2700. DOI: 10.1021/acs.analchem.0c00274. [Online]. Available: %3CGo%20to%20ISI%3E://WOS:000526563900063%20https://pubs.acs.org/doi/pdf/10.1021/acs.analchem.0c00274.

[58] L. Possanzini, F. Decataldo, F. Mariani, *et al.*, "Textile sensors platform for the selective and simultaneous detection of chloride ion and ph in sweat," *Scientific Reports*, vol. 10, no. 1, 2020, Oh6dg Times Cited:9 Cited References Count:67, ISSN: 2045-2322. DOI: ARTN1718010.1038/s41598-020-74337-w. [Online]. Available: %3CGo%20to%20ISI%3E://WOS:000582678400010%20https://www.nature.com/articles/s41598-020-74337-w.pdf.

[59] L. L. Fan, T. T. Xu, J. J. Feng, *et al.*, "Tripodal squaramide derivative as a neutral chloride ionophore for whole blood and sweat chloride measurement," *Electroanalysis*, vol. 32, no. 4, pp. 805–811, 2020, Lb5on Times Cited:3 Cited References Count:48, ISSN: 1040-0397. DOI: 10.1002/elan.201900693. [Online]. Available: %3CGo%20to%20ISI%3E://WOS:000505889800001%20https://analyticalsciencejournals.onlinelibrary.wiley.com/doi/10.1002/elan.201900693.

[60] M. Cuartero, N. Colozza, B. M. Fernandez-Perez, and G. A. Crespo, "Why ammonium detection is particularly challenging but insightful with ionophore-based potentiometric sensors - an overview of the progress in the last 20 years," *Analyst*, vol. 145, no. 9, pp. 3188–3210, 2020, Cuartero, Maria Colozza, Noemi Fernandez-Perez, Bibiana M Crespo, Gaston A eng England 2020/04/03 Analyst. 2020 May 7;145(9):3188-3210. doi: 10.1039/d0an00327a. Epub 2020 Apr 2., ISSN: 1364-5528 (Electronic) 0003-2654 (Linking). DOI: 10.1039/d0an00327a. [Online]. Available: https://www.ncbi.nlm.nih.gov/pubmed/32239016%20https://pubs.rsc.org/en/content/articlepdf/2020/an/d0an00327a.

[61] J. Kim, J. R. Sempionatto, S. Imani, *et al.*, "Simultaneous monitoring of sweat and interstitial fluid using a single wearable biosensor platform," *Advanced Science*, vol. 5, no. 10, 2018, Gx3nr Times Cited:163 Cited References Count:40, ISSN: 2198-3844. DOI: ARTN180088010.1002/advs.201800880. [Online]. Available: %3CGo%20to%20ISI%3E://WOS:000447632000018%20https://onlinelibrary.wiley.com/doi/10.1002/advs.201800880.

[62] J. Kim, A. S. Campbell, B. E. de Avila, and J. Wang, “Wearable biosensors for healthcare monitoring,” *Nat Biotechnol*, vol. 37, no. 4, pp. 389–406, 2019, Kim, Jayoung Campbell, Alan S de Avila, Berta Esteban-Fernandez Wang, Joseph eng T32 AA013525/AA/NIAAA NIH HHS/ Research Support, N.I.H., Extramural Research Support, Non-U.S. Gov’t Review 2019/02/26 Nat Biotechnol. 2019 Apr;37(4):389-406. doi: 10.1038/s41587-019-0045-y. Epub 2019 Feb 25., ISSN: 1546-1696 (Electronic) 1087-0156 (Linking). DOI: 10.1038/s41587-019-0045-y. [Online]. Available: https://www.ncbi.nlm.nih.gov/pubmed/30804534.

[63] T. Attar, Y. Harek, and L. Larabi, “Determination of ultra trace levels of copper in whole blood by adsorptive stripping voltammetry,” *Journal of the Korean Chemical Society-Daehan Hwahak Hoe Jee*, vol. 57, no. 5, pp. 568–573, 2013, Va7mk Times Cited:4 Cited References Count:37, ISSN: 1017-2548. DOI: 10.5012/jkcs.2013.57.5.568. [Online]. Available: %3CGo%20to%20ISI%3E://WOS:000410328600006%20http://koreascience.or.kr:80/article/JAKO201332479513331.pdf.

[64] D. Kinnamon, S. Muthukumar, A. P. Selvam, and S. Prasad, “Portable chronic alcohol consumption monitor in human sweat through square-wave voltammetry,” *Slas Technology*, vol. 23, no. 2, pp. 144–153, 2018, Gc7bl Times Cited:8 Cited References Count:27, ISSN: 2472-6303. DOI: 10.1177/2472630317733255. [Online]. Available: %3CGo%20to%20ISI%3E://WOS:000429946800004%20https://journals.sagepub.com/doi/pdf/10.1177/2472630317733255.

[65] X. C. Liu, Y. C. Zhu, Z. Q. Zhu, *et al.*, “Solid phase microextraction and selective determination of cysteine in whole blood by cyclic voltammetry with silver nanoparticles modified clustered carbon fiber electrodes,” *Analytical Methods*, vol. 4, no. 10, pp. 3256–3260, 2012, 012ls Times Cited:6 Cited References Count:26, ISSN: 1759-9660. DOI: 10.1039/c2ay25369k. [Online]. Available: %3CGo%20to%20ISI%3E://WOS:000309238300029%20https://pubs.rsc.org/en/content/articlepdf/2012/ay/c2ay25369k.

[66] E. N. Nicolai, J. K. Trevathan, E. K. Ross, *et al.*, “Detection of norepinephrine in whole blood via fast scan cyclic voltammetry,” *2017 Ieee International Symposium on Medical Measurements and Applications (Memea)*, pp. 111–116, 2017, Bm4pm Times Cited:8 Cited References Count:15 IEEE International Symposium on Medical Measurements and Applications Proceedings-MeMeA. [Online]. Available: %3CGo%20to%20ISI%3E://WOS:000463744700021.

[67] M. Pohanka, H. Bandouchova, J. Sobotka, J. Sedlackova, I. Soukupova, and J. Pikula, “Ferric reducing antioxidant power and square wave voltammetry for assay of low molecular weight antioxidants in blood plasma: Performance and comparison of methods,” *Sensors*, vol. 9, no. 11, pp. 9094–9103, 2009, 525cc Times Cited:41 Cited References Count:33. DOI: 10.3390/s91109094. [Online]. Available: %3CGo%20to%20ISI%3E://WOS:000272189700043%20https://mdpi-res.com/d_attachment/sensors/sensors-09-09094/article_deploy/sensors-09-09094.pdf.

[68] E. D. Goulet, A. Asselin, J. Gosselin, and L. B. Baker, “Measurement of sodium concentration in sweat samples: Comparison of 5 analytical techniques,” *Applied Physiology, Nutrition, and Metabolism*, vol. 42, no. 8, pp. 861–868, 2017. DOI: 10.1139/apnm-2017-0059%M28407476. [Online]. Available: https://cdnsciencepub.com/doi/abs/10.1139/apnm-2017-0059.

[69] M. Ciszkowska and Z. Stojek, *Peer reviewed: Voltammetric and amperometric detection without added electrolyte*, Generic, 2000.

[70] N. Elgrishi, K. J. Rountree, B. D. McCarthy, E. S. Rountree, T. T. Eisenhart, and J. L. Dempsey, “A practical beginner’s guide to cyclic voltammetry,” *Journal of Chemical Education*, vol. 95, no. 2, pp. 197–206, 2018, Fx3zu Times Cited:778 Cited References Count:29, ISSN: 0021-9584. DOI: 10.1021/acs.jchemed.7b00361. [Online]. Available: %3CGo%20to%20ISI%3E://WOS:000426012300004%20https://pubs.acs.org/doi/pdf/10.1021/acs.jchemed.7b00361.

[71] G. Hussain and D. Silvester, “Comparison of voltammetric techniques for ammonia sensing in ionic liquids,” *Electroanalysis*, vol. 30, 2017. DOI: 10.1002/elan.201700555.

[72] B. N. Altay, J. Jourdan, V. S. Turkani, *et al.*, “Impact of substrate and process on the electrical performance of screen-printed nickel electrodes: Fundamental mechanism of ink film roughness,” *ACS Applied Energy Materials*, vol. 1, no. 12, pp. 7164–7173, 2018, doi: 10.1021/acsaem.8b01618. DOI: 10.1021/acsaem.8b01618. [Online]. Available: https://doi.org/10.1021/acsaem.8b01618.

[73] E. J. F. Dickinson and A. J. Wain, “The butler-volmer equation in electrochemical theory: Origins, value, and practical application,” *Journal of Electroanalytical Chemistry*, vol. 872, p. 114 145, 2020, ISSN: 1572-6657. DOI: https://doi.org/10.1016/j.jelechem.2020.114145. [Online]. Available: https://www.sciencedirect.com/science/article/pii/S1572665720303283.

[74] M. Chudecka and A. Lubkowska, “The use of thermal imaging to evaluate body temperature changes of athletes during training and a study on the impact of physiological and morphological factors on skin temperature,” *Human movement*, vol. 13, no. 1, pp. 33–39, 2012, ISSN: 1899-1955.

[75] A. Merla, P. A. Mattei, L. Di Donato, and G. L. Romani, “Thermal imaging of cutaneous temperature modifications in runners during graded exercise,” *Annals of Biomedical Engineering*, vol. 38, no. 1, pp. 158–163, 2010, ISSN: 1573-9686. DOI: 10.1007/s10439-009-9809-8. [Online]. Available: https://doi.org/10.1007/s10439-009-9809-8.

[76] S. Daniele, M. A. Baldo, C. Bragato, and I. Lavagnini, “Steady state voltammetry in the process of hydrogen evolution in buffer solutions,” *Analytica Chimica Acta*, vol. 361, no. 1-2, pp. 141–150, 1998, Zj521 Times Cited:22 Cited References Count:19, ISSN: 0003-2670. DOI: Doi10.1016/S0003-2670(97)00695-8. [Online]. Available: %3CGo%20to%20ISI%3E://WOS:000073224500016.

[77] M. Masui and S. Ozaki, “Anodic-oxidation of amines .5. cyclic voltammetry and controlled potential electrolysis of ephedrine and related compounds in aqueous buffer solution,” *Chemical Pharmaceutical Bulletin*, vol. 26, no. 7, pp. 2153–2159, 1978, Fl168 Times Cited:18 Cited References Count:20, ISSN: 0009-2363. [Online]. Available: %3CGo%20to%20ISI%3E://WOS:A1978FL16800029.

[78] S. R. Belding and R. G. Compton, “Cyclic voltammetry in the absence of excess supporting electrolyte: The effect of analyte charge,” *Journal of Electroanalytical Chemistry*, vol. 683, pp. 1–13, 2012, 024rm Times Cited:17 Cited References Count:34, ISSN: 1572-6657. DOI: 10.1016/j.jelechem.2012.07.023. [Online]. Available: %3CGo%20to%20ISI%3E://WOS:000310126300001.

[79] A. M. Bond and P. A. Lay, “Cyclic voltammetry at microelectrodes in the absence of added electrolyte using a platinum quasi-reference electrode,” *Journal of Electroanalytical Chemistry*, vol. 199, no. 2, pp. 285–295, 1986, A4653 Times Cited:104 Cited References Count:17, ISSN: 0022-0728. DOI: Doi10.1016/0022-0728(86)80004-3. [Online]. Available: %3CGo%20to%20ISI%3E://WOS:A1986A465300004.

[80] H. e. a. Emrich, “Sweat composition in relation to rateof sweating in patients with cystic fibrosis of the pancreas,” *Pediat. Res.*, vol. 2, no. 1968, pp. 464–478, 1968.

[81] N. A. Bohari, S. Siddiquee, K. Ampon, K. Rodrigues, and S. Saallah, “Development of glucose biosensor based on zno nanoparticles film and glucose oxidase–immobilized eggshell membrane,” *Sensing and Bio-Sensing Research*, vol. 40, 2015. DOI: 10.1016/j.sbsr.2015.03.004.

[82] C. Batchelor-McAuley, E. Katelhon, E. O. Barnes, R. G. Compton, E. Laborda, and A. Molina, “Recent advances in voltammetry,” *Chemistryopen*, vol. 4, no. 3, pp. 224–260, 2015, Cl3ao Times Cited:99 Cited References Count:308, ISSN: 2191-1363. DOI: 10.1002/open.201500042. [Online]. Available: %3CGo%20to%20ISI%3E://WOS:000356820900002%20https://www.ncbi.nlm.nih.gov/pmc/articles/PMC4522172/pdf/open0004-0224.pdf.

[83] P. Puthongkham and B. J. Venton, “Recent advances in fast-scan cyclic voltammetry,” *Analyst*, vol. 145, no. 4, pp. 1087–1102, 2020, Puthongkham, Pumidech Venton, B Jill eng R01 EB026497/EB/NIBIB NIH HHS/ R01 MH085159/MH/NIMH NIH HHS/ Review England 2020/01/11 Analyst. 2020 Feb 17;145(4):1087-1102. doi: 10.1039/c9an01925a., ISSN: 1364-5528 (Electronic) 0003-2654 (Linking). DOI: 10.1039/c9an01925a. [Online]. Available: https://www.ncbi.nlm.nih.gov/pubmed/31922162.

[84] F. R. Simões and M. G. Xavier, “6 - electrochemical sensors,” in *Nanoscience and its Applications*, A. L. Da Róz, M. Ferreira, F. de Lima Leite, and O. N. Oliveira, Eds. William Andrew Publishing, 2017, pp. 155–178, ISBN: 978-0-323-49780-0. DOI: https://doi.org/10.1016/B978-0-323-49780-0.00006-5. [Online]. Available: https://www.sciencedirect.com/science/article/pii/B9780323497800000065.

[85] W. M. Haynes, *CRC Handbook of Chemistry and Physics*, 95th ed. CRC Press, 2014.

[86] M. Ichise, Nagayana.Y, and T. Kojima, “New mode of electrolysis for voltammetry,” *Journal of Electroanalytical Chemistry*, vol. 38, no. 2, 468–, 1972, N1292 Times Cited:2 Cited References Count:1, ISSN: 0022-0728. [Online]. Available: %3CGo%20to%20ISI%3E://WOS:A1972N129200022.

[87] N. M. Adli, H. Zhang, S. Mukherjee, and G. Wu, “Ammonia oxidation electrocatalysis for hydrogen generation and fuel cells,” *Journal of The Electrochemical Society*, vol. 165, no. 15, J3130, 2018, ISSN: 1945-7111.

[88] S. Hosseini, S. Kheawhom, S. M. Soltani, and M. K. Aroua, “Electrochemical reduction of bicarbonate on carbon nanotube-supported silver oxide: An electrochemical impedance spectroscopy study,” *Journal of environmental chemical engineering*, vol. 6, no. 1, pp. 1033–1043, 2018, ISSN: 2213-3437.

[89] J. P. Baumberger, J. Jürgensen, and K. Bardwell, “The coupled redox potential of the lactate-enzyme-pyruvate system,” *The Journal of general physiology*, vol. 16, no. 6, p. 961, 1933.

[90] L. B. Baker, C. T. Ungaro, B. C. Sopeña, *et al.*, “Body map of regional vs. whole body sweating rate and sweat electrolyte concentrations in men and women during moderate exercise-heat stress,” *Journal of Applied Physiology*, vol. 124, no. 5, pp. 1304–1318, 2018. DOI: 10.1152/japplphysiol.00867.2017. [Online]. Available: https://journals.physiology.org/doi/abs/10.1152/japplphysiol.00867.2017.

[91] A. Molina, J. Gonzalez, M. C. Henstridge, and R. G. Compton, “Voltammetry of electrochemically reversible systems at electrodes of any geometry: A general, explicit analytical characterization,” *Journal of Physical Chemistry C*, vol. 115, no. 10, pp. 4054–4062, 2011, 731ng Times Cited:48 Cited References Count:36, ISSN: 1932-7447. DOI: 10.1021/jp109587b. [Online]. Available: %3CGo%20to%20ISI%3E://WOS:000288113400030%20https://pubs.acs.org/doi/pdf/10.1021/jp109587b.

[92] A. Molina, J. Gonzalez, E. Laborda, and R. G. Compton, “Additive differential double pulse voltammetry applied to the study of multistep electron transfer reactions with microelectrodes of different geometries,” *International Journal of Electrochemical Science*, vol. 7, no. 7, pp. 5765–5778, 2012, 973zp Times Cited:10 Cited References Count:34, ISSN: 1452-3981. [Online]. Available: %3CGo%20to%20ISI%3E://WOS:000306399700003.

[93] X. Xu, A. Makaraviciute, J. Pettersson, S.-L. Zhang, L. Nyholm, and Z. Zhang, “Revisiting the factors influencing gold electrodes prepared using cyclic voltammetry,” *Sensors and Actuators B: Chemical*, vol. 283, pp. 146–153, 2019, ISSN: 0925-4005. DOI: https://doi.org/10.1016/j.snb.2018.12.008. [Online]. Available: https://www.sciencedirect.com/science/article/pii/S0925400518321270.

[94] M. T. M. Koper and J. J. Lukkien, “Modeling the butterfly: Influence of lateral interactions and adsorption geometry on the voltammetry at (111) and (100) electrodes,” *Surface Science*, vol. 498, no. 1-2, pp. 105–115, 2002, 521fd Times Cited:31 Cited References Count:21, ISSN: 0039-6028. DOI: Doi10.1016/S0039-6028(01)01681-8. [Online]. Available: %3CGo%20to%20ISI%3E://WOS:000173827800017%20https://www.sciencedirect.com/science/article/pii/S0039602801016818?via%3Dihub.

[95] unknown, *Cyclic voltammetry in spore binding membranes; simulations using a finite element solver*, Manuscript, 2019.

[96] J. Valsa, P. Dvořák, and M. Friedl, “Network model of the cpe,” *Radioengineering*, vol. 20, 2011.

[97] M. M. Kohonen, M. E. Karaman, and R. M. Pashley, “Debye length in multivalent electrolyte solutions,” *Langmuir*, vol. 16, no. 13, pp. 5749–5753, 2000, doi: 10.1021/la991621c, ISSN: 0743-7463. DOI: 10.1021/la991621c. [Online]. Available: https://doi.org/10.1021/la991621c.

[98] A. R. Eldamak, S. Thorson, and E. C. Fear, “Study of the dielectric properties of artificial sweat mixtures at microwave frequencies,” *Biosensors (Basel)*, vol. 10, no. 6, 2020, 2079-6374 Eldamak, Angie R Orcid: 0000-0002-9088-7578 Thorson, Sarah Fear, Elise C Orcid: 0000-0002-9984-8188 N/A/Natural Sciences and Engineering Research Council of Canada/ N/A/Vice-President (Research) Strategic Funding at the University of Calgary/ Journal Article 2020/06/13 Biosensors (Basel). 2020 Jun 9;10(6):62. doi: 10.3390/bios10060062., ISSN: 2079-6374. DOI: 10.3390/bios10060062.

[99] B. Corso, I. Perez, T. Sheps, P. Sims, O. Gul, and P. Collins, “Electrochemical charge-transfer resistance in carbon nanotube composites,” *Nano letters*, vol. 14, 2014. DOI: 10.1021/nl404349g.

[100] M. Lambe, *Optimizing the ad5940 for electrochemical measurements*, Generic, 2019.

[101] L. B. Baker, P. J. D. De Chavez, C. T. Ungaro, *et al.*, “Exercise intensity effects on total sweat electrolyte losses and regional vs. whole-body sweat [na+], [cl−], and [k+],” *European Journal of Applied Physiology*, vol. 119, no. 2, pp. 361–375, 2019, ISSN: 1439-6327. DOI: 10.1007/s00421-018-4048-z. [Online]. Available: https://doi.org/10.1007/s00421-018-4048-z.